

ABSTRACT

WIND WAVES AND DIFFUSION IN OPEN CHANNELS

This study describes a theoretical and experimental investigation of the vertical and lateral mixing of tracer fluids in a straight, wide, open channel. WIND WAVES AND DIFFUSION IN OPEN CHANNELS

Using appropriate assumptions and simplifications, a three-dimensional vertical and lateral mixing equation suitable for any channel geometry and source distribution is first derived. The experiments were conducted in a two-ft wide wind-water tunnel with and without wind effects. Velocity fields were measured in detail in both tanks.

Evaluated vertical diffusion coefficients from the measured velocity profiles served as a first approximation to the numerical analysis of the diffusion equation. A specially designed single-electrode conductivity probe and hot-film sensor was used to measure point velocity and concentration fluctuations. The covariances of the concentration and longitudinal component of velocity were calculated to evaluate

the longitudinal diffusion coefficients. Wave data were recorded and analyzed to relate the wave surface properties with the diffusion process. Concentration profiles of the tracer were obtained in cross-sections at various distances downstream from the source. The data were used to evaluate the vertical and lateral mixing coefficients by a simulation method.

Fluid Dynamics and Diffusion Laboratory
College of Engineering
Colorado State University
Fort Collins, Colorado

May 1972



U18401 0576346

CER71-72KSS-JG47

ABSTRACT

WIND WAVES AND DIFFUSION IN OPEN CHANNELS

This study describes a theoretical and experimental investigation of the vertical and lateral mixing of tracer fluids in a straight, wide, open channel, with and without wind action on the water surface.

Using appropriate assumptions and simplifications, a three-dimensional vertical-and lateral-mixing equation suitable for any channel geometry and source distribution is first derived. The experiments were conducted in a two-ft wide wind-water tunnel with and without wind effects. Velocity fields were measured in detail in both cases. Evaluated vertical diffusion coefficients from the measured velocity profiles served as a first approximation to the numerical analysis of the diffusion equation. A specially designed single-electrode conductivity probe and hot-film sensor was used to measure point velocity and concentration fluctuations from which the covariances of the concentration and longitudinal component of velocity were calculated to evaluate the longitudinal diffusion coefficients. Wave data were recorded and analyzed to relate the water surface properties with the diffusion process. Concentration profiles of the tracer were obtained in cross-sections at various distances downstream from the source. The data were used to evaluate the vertical and lateral mixing coefficients by a simulation method.

The results indicated that the vertical mixing rates were significantly increased when waves appear on the water surface, the rate of lateral mixing was slightly decreased and the tracer plume was found

to deflect downward in the mixing process although the tracer was neutrally buoyant.

ACKNOWLEDGMENTS

The authors express their appreciation to Dr. James Esteki, Dr. Robert Maroney and Dr. Bernard Jeringer for their critical review of the manuscript.

Acknowledgment is made to Mr. Will Burt and his colleagues for their valuable assistance during the early stages of the numerical analysis. Mr. Ralph Ames and his shop staff were most helpful in maintaining and improving the experimental equipment. We are grateful to Mrs. Julie Ruppel for typing the manuscript.

The financial support for this study was provided by the U.S. Atomic Energy Commission under contract number AT(11-1)-1613. This support is greatly appreciated.

ACKNOWLEDGMENTS

The authors express their appreciation to Dr. Susumu Karaki, Dr. Robert Meroney and Dr. Bernard Jeringer for their critical review of the manuscript.

Acknowledgment is made to Mr. Will Burt and his colleagues for their valuable assistance during the early stages of the numerical analysis. Mr. Ralph Asmus and his shop staff were most helpful in maintaining and improving the experimental equipment. We are grateful to Mrs. Julie Dunning for typing the manuscript.

The financial support for this study was provided by the U.S. Atomic Energy Commission under contract number AT(11-1)-1813. This support is greatly appreciated.

2.1	Introduction	7
2.2	Vertical Diffusion	8
2.2-1	Diffusion	9
2.2-2	Solutions of the Diffusion Equations	9
2.3	Wind Waves and Diffusion	11
2.3-1	Wind Waves	11
2.3-2	Wind Produced Drift Current	12
2.3-3	Wave Produced Drift Velocity	13
2.3-4	Wind Wave Effect on Diffusion Coefficients	14
2.4	Method of Analysis for this Study	14
III	EXPERIMENTAL EQUIPMENT AND PROCEDURES	15
3.1	The Wind Tunnel Flame Combination	15
3.1-1	The Flame	15
3.1-2	Sed Roughness	16
3.2	Water Velocity Measurement	16
3.2-1	Hot-Film Sensor	16
3.2-2	Hot-Film Anemometer	17
3.3	Tracer and Injection System	17
3.3-1	Tracer	17
3.3-2	Tracer Injection System	17
3.4	Measurement of Concentrations	18
3.4-1	Single Conductivity Probe	18
3.4-2	Carrier Amplifier	18
3.5	Measurements of Water Surface Elevations	19
3.5-1	Capacitance Probe	19
3.5-2	Capacitance Bridge	19
3.6	Measurements of Air Velocity	20
3.7	Description of Experiments	21

TABLE OF CONTENTS

<u>Chapter</u>		<u>Page</u>
IV	ABSTRACT OF DISSERTATION	iii
	ACKNOWLEDGMENTS.	v
	LIST OF TABLES	viii
	LIST OF FIGURES.	ix
	PARTIAL LIST OF SYMBOLS.	xii
I	INTRODUCTION	1
II	THEORETICAL DEVELOPMENT AND LITERATURE REVIEW.	3
	2.1 The Diffusion Equation	3
	2.2 Review of Previous Work.	5
	2.2-1 Logitudinal Dispersion.	6
	2.2-2 Longitudinal Diffusion.	7
	2.2-3 Vertical Diffusion.	8
	2.2-4 Lateral Diffusion	9
	2.2-5 Solutions of the Diffusion Equations.	9
	2.3 Wind Waves and Diffusion	11
	2.3-1 Wind Waves.	11
	2.3-2 Wind Produced Drift Current	12
	2.3-3 Wave Produced Drift Velocity.	13
	2.3-4 Wind Wave Effect on Diffusion Coefficients.	14
	2.4 Method of Analysis for this Study.	14
III	EXPERIMENTAL EQUIPMENT AND PROCEDURES.	15
	3.1 The Wind Tunnel Flume Combination.	15
	3.1-1 The Flume	15
	3.1-2 Bed Roughness	16
	3.2 Water Velocity Measurement	16
	3.2-1 Hot-Film Sensor	16
	3.2-2 Hot-Film Anemometer	17
	3.3 Tracer and Injection System.	17
	3.3-1 Tracer.	17
	3.3-2 Tracer Injection System	17
	3.4 Measurement of Concentrations.	18
	3.4-1 Single Conductivity Probe	18
	3.4-2 Carrier Amplifier	18
	3.5 Measurements of Water Surface Elevations	19
	3.5-1 Capacitance Probe	19
	3.5-2 Capacitance Bridge.	19
	3.6 Measurements of Air Velocity	20
	3.7 Description of Experiments	21

TABLE OF CONTENTS - Continued

<u>Chapter</u>		<u>Page</u>
IV	NUMERICAL ANALYSIS OF THE DIFFUSION EQUATION	23
	4.1 Limitations to the Analytical Approach	23
	4.2 Necessity of Numerical Integration	23
	4.3 Formulation of the Finite Difference Equation.	24
	4.3-1 Dimensionless Diffusion Equation.	24
	4.3-2 Alternating Direction Implicit (A.D.I.) Method	24
	4.3-3 Finite Difference Equations	25
	4.3-4 Boundary Conditions	27
	a. Initial Conditions.	27
	b. Boundary Conditions	28
	c. Continuity Conditions	28
	4.3-5 Stability Analysis.	29
V	REDUCTION AND PRESENTATION OF DATA	31
	5.1 Hydraulic Conditions	31
	5.2 Velocity Measurements and Vertical Diffusion Coefficient.	33
	5.2-1 Velocity Profiles	33
	5.2-2 Evaluation of Vertical Diffusion Coefficient	34
	5.3 The Turbulence Characteristics	35
	5.3-1 The Relative Turbulence Intensity of Water Velocity	35
	5.3-2 Relative Turbulent Fluctuations of Concentration	36
	5.3-3 The Evaluation of the Longitudinal Diffusion Coefficient	37
	5.4 Presentation of the Wind Generated Waves	37
	5.5 Concentration Profiles	39
VI	DISCUSSION OF NUMERICAL RESULTS.	41
	6.1 General Considerations and Procedures.	41
	6.2 Numerical Results Without Wind Effect.	44
	6.3 Numerical Results With Wind Wave Effect.	47
	6.3-1 The Tracer Fall Velocity.	47
	6.3-2 The Concentration Profiles.	48
	6.3-3 Properties of the Water Surface	50
	6.4 Contours of Normalized Concentration	50
VII	SUMMARY AND CONCLUSIONS.	51
	7.1 Summary.	51
	7.2 Conclusions.	52
	7.3 Suggestions for Future Research.	53
	BIBLIOGRAPHY	106

LIST OF TABLES

<u>Table</u>		<u>Page</u>
1	Basic Hydraulic Parameters	32
2	Summary of Numerical Results (no wind)	45
3	Summary of Numerical Results (with wind)	49
4	Hot-Film Sensor	57
5	Calibration Curve of Hot-Film Sensor	58
6	Tracer Injector	59
7	Tracer Injector System and General Layout of the Experiment	60
8	Single-Electrode Conductivity Probe	61
9	Calibration Curve of Single-Electrode Conductivity Probe	62
10	Water Wave Capacitance Probe	63
11	Calibration Curve of Water Wave Capacitance Probe	64
12	Schematic and Block Diagram of the Capacitance Bridge	65
13	Block Diagram of the Data Collection System	66
14	Flow-Chart of the Computer Program	67
15	Non-Dimensionalized Velocity Profile (without wind)	68
16	Non-Dimensionalized Velocity Profile (with wind)	69
17	Dimensionless Vertical Diffusion Coefficients (without wind)	70
18	Dimensionless Vertical Diffusion Coefficients (with wind)	71
19	Relative Turbulent-Intensity of Water Velocity	72
20	Relative Intensity of Concentration Fluctuations, Run NWCl (vertically)	73
21	Relative Intensity of Concentration Fluctuations, Run NWCl (horizontally)	74

LIST LIST OF FIGURES

<u>Figure</u>		<u>Page</u>
1	One-Dimensional Transport, Definition Sketch.	54
2	Schematic Diagram of the C.S.U. Wind-Water Flume.	55
3	Dimensions of the Roughness Mesh.	56
4	Hot-Film Sensor	57
5	Calibration Curve of Hot-Film Sensor.	58
6	Tracer Injector	59
7	Tracer Injector System and General Layout of the Experiment.	60
8	Single-Electrode Conductivity Probe	61
9	Calibration Curve of Single-Electrode Conductivity Probe	62
10	Water Wave Capacitance Probe.	63
11	Calibration Curve of Water Wave Capacitance Probe	64
12	Schematic and Block Diagram of the Capacitance Bridge	65
13	Block Diagram of the Data Collection System	66
14	Flow-Chart of the Computer Program.	67
15	Non-Dimensionalized Velocity Profile (without wind)	68
16	Non-Dimensionalized Velocity Profile (with wind).	69
17	Dimensionless Vertical Diffusion Coefficients (without wind).	70
18	Dimensionless Vertical Diffusion Coefficients (with wind)	71
19	Relative Turbulent-Intensity of Water Velocity.	72
20	Relative Intensity of Concentration Fluctuations, Run NW1 (vertically)	73
21	Relative Intensity of Concentration Fluctuations, Run NW1 (horizontally)	74

LIST OF FIGURES - Continued

<u>Figure</u>		<u>Page</u>
22	Relative Intensity of Concentration Fluctuations, Run WC1 (vertically)	75
23	Relative Intensity of Concentration Fluctuations, Run WC1 (horizontally)	76
24	Longitudinal Mean Concentration Profiles	77
25	Profiles of Longitudinal Velocity-Concentration Covariance	78
26	Longitudinal Turbulent Diffusion Coefficients	79
27	Measured and Filtered Water Wave Data	80
28	Estimation of the Water Wave Spectrum	81
29	Measured and Numerical Results of Vertical Concentration Profiles, Case NWS1	82
30	Measured and Numerical Results of Horizontal Concentration Profiles, Case NWS1	83
31	Measured and Numerical Results of Vertical Concentration Profiles, Case NWS2	84
32	Measured and Numerical Results of Horizontal Concentration Profiles, Case NWS2	85
33	Measured and Numerical Results of Vertical Concentration Profiles, Case NWC1	86
34	Measured and Numerical Results of Horizontal Concentration Profiles, Case NWC1	87
35	Measured and Numerical Results of Vertical Concentration Profiles, Case WS1	88
36	Measured and Numerical Results of Horizontal Concentration Profiles, Case WS1	89
37	Measured and Numerical Results of Vertical Concentration Profiles, Case WS2	90
38	Measured and Numerical Results of Horizontal Concentration Profiles, Case WS2	91
39	Measured and Numerical Results of Vertical Concentration Profiles, Case WS3	92

LIST OF FIGURES - Continued

<u>Figure</u>	<u>Description</u>	<u>Page</u>
40	Measured and Numerical Results of Horizontal Concentration Profiles, Case WS3.	93
41	Measured and Numerical Results of Vertical Concentration Profiles, Case WC1.	94
42	Measured and Numerical Results of Horizontal Concentration Profiles, Case WC1.	95
43	Relations of the Vertical Diffusivity, Tracer Fall Velocity and Wind Velocity.	96
44	Relations of the Vertical Diffusivity, Tracer Fall Velocity and Dominant Frequency	97
45	Relations of the Vertical Diffusivity, Tracer Fall Velocity and Average Wave Height.	98
46	Contours of Normalized Concentration of Numerical Results, Case NWS1.	99
47	Contours of Normalized Concentration of Numerical Results, Case NWS2.	100
48	Contours of Normalized Concentration of Numerical Results, Case NWC1.	101
49	Contours of Normalized Concentration of Numerical Results, Case WS1	102
50	Contours of Normalized Concentration of Numerical Results, Case WS2	103
51	Contours of Normalized Concentration of Numerical Results, Case WS3	104
52	Contours of Normalized Concentration of Numerical Results, Case WC1	105
	Hydraulic radius	
	Reynolds number	
	The channel slope	
	Total time	
	Time	

PARTIAL LIST OF SYMBOLS

<u>Symbol</u>	<u>Description</u>	<u>Units</u>
B	Channel width	ft/sec
C	Instantaneous concentration	ft/sec
\bar{C}	Depth averaged concentration	Arbitrary
\bar{C}'	Deviation from depth averaged concentration	Arbitrary
c'	Concentration fluctuation about the mean	Arbitrary
$\sqrt{c'^2}$	Root-mean-square of concentration fluctuations	Arbitrary
D_x	Longitudinal dispersion coefficient	ft ² /sec
F_a	Dimensionless tracer fall velocity	unit-
F_R	Froude number	ft/sec
f	Friction factor	ft/sec
g	Acceleration of gravity	ft/sec ²
i	Subscript denoting direction, x, y or z	ft/sec
j	Subscript denoting direction, x, y or z	ft/sec
M	Number of mesh points in vertical direction of cross-section	ft
N	Number of mesh points in horizontal direction of cross-section	ft
n	Exponent in power law equation, also used as a subscript denoting lateral direction	ft
Q	Volume discharge of water	ft ³ /sec
Q_0	Source strength	ft ³ /sec
R_b	Hydraulic radius	ft
R_E	Reynolds number	
s	The channel slope	
T	Total time	sec
t	Time	sec
t_i	Turbulent diffusion coefficient in ith direction, x, y or z	ft ² /sec

PARTIAL LIST OF SYMBOLS - Continued

<u>Symbol</u>	<u>Description</u>	<u>Units</u>
U	Instantaneous velocity in x direction	ft/sec
\bar{U}	Time averaged local velocity in x direction	ft/sec
$\bar{\bar{U}}$	Depth averaged velocity	ft/sec
\bar{U}_{xs}	Average velocity in channel cross section	ft/sec
U_*	Shear velocity	ft/sec
u'	Longitudinal velocity fluctuation about the mean	ft/sec
$\sqrt{u'^2}$	Root-mean-square velocity fluctuation in x direction	ft/sec
$\overline{c'u'_i}$	Velocity-concentration covariance in ith direction, x, y or z	unit-ft/sec
V	Instantaneous velocity in y direction	ft/sec
\bar{V}	Time averaged local velocity in y direction	ft/sec
W	Instantaneous velocity in z direction	ft/sec
\bar{W}	Time averaged local velocity in z direction	ft/sec
x	Longitudinal coordinate or distance, also used as a subscript denoting longitudinal direction	ft
y	Vertical coordinate or distance, also used as a subscript denoting vertical direction	ft
z	Lateral coordinate or distance, also used as a subscript denoting lateral direction	ft
α	Dimensionless vertical diffusion coefficient	
$\bar{\alpha}$	Dimensionless depth averaged vertical diffusion coefficient	
β	Dimensionless lateral diffusion coefficient	
$\bar{\beta}$	Dimensionless depth averaged lateral diffusion coefficient	
ϵ	Molecular diffusion coefficient	ft ² /sec
ϵ_i	Turbulent diffusion coefficient in ith direction, x, y or z	ft ² /sec

PARTIAL LIST OF SYMBOLS - Continued

<u>Symbol</u>	<u>Description</u>	<u>Units</u>
κ	von Kármán's kappa	
μ	Correction factor	
ν	Kinematic viscosity of water	ft ² /sec
ξ	Dimensionless distance in longitudinal direction	
ρ	Mass density of water	slugs/ft ³
η	Dimensionless distance in vertical direction	
ζ	Dimensionless distance in horizontal direction	
τ	Shear stress	lbs/ft ²
τ_o	Channel bed shear stress	lbs/ft ²
τ_w	Water surface shear stress	lbs/ft ²

The wind, which acts on the water surface, substantially increases the rate of vertical mixing. One important reason is that near the water surface, an energetic and random agitation of the fluid takes place through wave action. This agitation brings about a continuous interchange of the fluid particles in the upper layer of the water and thereby greatly increases the rate of vertical diffusion. This phenomenon has hitherto been neglected by most investigators of the diffusion process.

CHAPTER I

INTRODUCTION

The continuing growth of the world population and industrial development sets growing demands on the world's water resources. The water pollution problems in natural streams, river, oceans and the ground water menaces the balance of the ecosystem on Earth. The capability of waterways to dilute and purify the contaminants is being rapidly exceeded. In order to maintain a balanced environment, effective measures for water pollution control must be applied or the supply of usable water may be sharply curtailed.

Water pollution is a very complicated problem that involves many fields in science and engineering. The importance in determining waste and water treatment requirements and associated costs makes it essential for the development of a practical method for predicting the concentration of contaminants in the flow. This requires knowledge of the mechanisms of the diffusion process. The ability to predict vertical and lateral mixing is important to water pollution control. Most effluent systems are continuous point sources as compared to the bulk volume of the natural streams.

The wind, which acts on the water surface, substantially increases the rate of vertical mixing. One important reason is that near the water surface, an energetic and random agitation of the fluid takes place through wave action. This agitation brings about a continuous interchange of the fluid particles in the upper layer of the water and thereby greatly increases the rate of vertical diffusion. This phenomenon has hitherto been neglected by most investigators of the diffusion process.

In brief, the goals of this study were to provide laboratory data and develop a practical method to predict the rate of mixing in natural streams and rivers with and without the wind blowing over the water sur-

2.1 The Diffusion Equation

In this study, working equations were developed to describe the vertical and lateral mixing phenomena for a continuous source. Experiments in straight, wide, open channels are described. The experimental and non-deformable control volumes. If the tracer has the same properties as the ambient fluid, and the fluid is incompressible with a constant molecular diffusion coefficient, this equation is given as

$$\frac{\partial c}{\partial t} + \mathbf{u} \cdot \nabla c = \epsilon \nabla^2 c + F \quad (2-1)$$

where c is the concentration by weight of dispersant, ϵ is the molecular diffusion coefficient, \mathbf{u} is the instantaneous velocity vector and F is a source which generates the dispersant.

In turbulent flow, the diffusion process is considerably more complicated. However, introducing the time-averaged and fluctuating quantities for velocity and concentration

$$c = \bar{c} + c'$$

$$u_i = \bar{u}_i + u'_i \quad (i = 1, 2, 3)$$

where

$$\bar{c} = \frac{1}{T} \int_0^T c \, dt$$

$$\bar{u}_i = \frac{1}{T} \int_0^T u_i \, dt$$

Dropping the source term and carrying out the Reynolds averaging procedure (Hinze, 1959), the diffusion equation (Eq. 2-1) becomes

$$\frac{\partial \bar{c}}{\partial t} + \frac{\partial}{\partial x_i} (\bar{u}_i \bar{c}) = - \frac{\partial}{\partial x_i} \overline{c' u'_i} + \epsilon \frac{\partial^2 \bar{c}}{\partial x_i^2} \quad (2-2)$$

In analogy to Boussinesq (1959) momentum transfer coefficient, THEORETICAL DEVELOPMENT AND LITERATURE REVIEW

time-averaged local concentration gradient and a turbulent diffusion

2.1 The Diffusion Equation

The basic diffusion equation is readily derived by applying the conservation of mass to a tracer (dispersant) in an arbitrary, fixed, and non-deformable control volume. If the tracer has the same properties

as the ambient fluid, and the fluid is incompressible with a constant molecular diffusion coefficient, this equation is given as

$$\frac{\partial c}{\partial t} + \underline{U} \cdot \nabla c = \epsilon \nabla^2 c + F \quad (2-1)$$

where c is the concentration by weight of dispersant, ϵ is the molecular diffusion coefficient, \underline{U} is the instantaneous velocity vector and F is a source which generates the dispersant.

In turbulent flow, the diffusion process is considerably more complicated. However, introducing the time-averaged and fluctuating quantities for velocity and concentration

$$c = \bar{c} + c' \quad (i = 1, 2, 3)$$

where

$$\bar{c} = \frac{1}{T} \int_0^T c \, dt \quad (2-5)$$

$$\bar{u}_i = \frac{1}{T} \int_0^T u_i \, dt$$

Dropping the source term and carrying out the Reynolds averaging procedure (Hinze, 1959), the diffusion equation (Eq. 2-1) becomes

$$\frac{\partial \bar{c}}{\partial t} + \frac{\partial}{\partial x_i} (\bar{u}_i \bar{c}) = - \frac{\partial}{\partial x_i} \overline{c' u_i'} + \epsilon \frac{\partial^2 \bar{c}}{\partial x_i^2} \quad (2-2)$$

In analogy to Boussinesq's (Hinze, 1959) momentum transfer coefficient, the covariance $\overline{c'u'_i}$ is assumed to be proportional to the time-averaged local concentration gradient and a turbulent diffusion coefficient defined as

$$\epsilon_{T_{ij}} = - \frac{\overline{c'u'_i}}{\partial \bar{c} / \partial x_j} \quad (2-3)$$

It has been pointed out by Elder (1959) and Nickelson (1960) that if the concentrations are independent of time, and the longitudinal molecular diffusion coefficient ϵ is several orders of magnitude smaller than the turbulent diffusion coefficient ϵ_T in ordinary open channel flows. Hence, introducing Eq. (2-3) into Eq. (2-2) and neglecting the molecular diffusion term,

$$\frac{\partial \bar{c}}{\partial t} + \frac{\partial}{\partial x_i} (\bar{u}_i \bar{c}) = \frac{\partial}{\partial x_i} (\epsilon_{T_{ij}} \frac{\partial \bar{c}}{\partial x_j}) \quad (2-4)$$

Equation (2-4) will now be applied to an open channel flow and the axes of the coordinate system are taken as the principle axes of the diffusion tensor, that is; the coordinate x is in the direction of primary flow, the coordinate y is normal to the channel bed, and the coordinate z is normal to the primary flow horizontally. In this case the off-diagonal terms of the diffusion tensor are zero ($\epsilon_{T_{ij}} = 0$ for $i \neq j$). Then Eq. (2-4) reduces to

$$\frac{\partial \bar{c}}{\partial t} + \frac{\partial}{\partial x_i} (\bar{u}_i \bar{c}) = \frac{\partial}{\partial x_i} (\epsilon_{T_i} \frac{\partial \bar{c}}{\partial x_i}) \quad (2-5)$$

Dropping the over bars and letting $u_1, u_2, u_3 = u, v, w$; $\epsilon_{T_1}, \epsilon_{T_2}, \epsilon_{T_3} = \epsilon_x, \epsilon_y, \epsilon_z$; and $x_1, x_2, x_3 = x, y, z$ respectively, we get

$$\frac{\partial c}{\partial t} + \frac{\partial (uc)}{\partial x} + \frac{\partial (vc)}{\partial y} + \frac{\partial (wc)}{\partial z} = \frac{\partial}{\partial x} (\epsilon_x \frac{\partial c}{\partial x}) + \frac{\partial}{\partial y} (\epsilon_y \frac{\partial c}{\partial y}) + \frac{\partial}{\partial z} (\epsilon_z \frac{\partial c}{\partial z}) \quad (2-6)$$

Consider the dispersion process for the following case: i) neutrally buoyant dispersant, ii) steady uniform open channel flow, where $v = w = 0$, iii) ϵ_x is independent of x , and iv) neglect secondary current in the flow. With these restrictions, the convection-diffusion equation reduces further to

$$\frac{\partial c}{\partial t} + u \frac{\partial c}{\partial x} = \epsilon_x \frac{\partial^2 c}{\partial x^2} + \frac{\partial}{\partial y} \left(\epsilon_y \frac{\partial c}{\partial y} \right) + \frac{\partial}{\partial z} \left(\epsilon_z \frac{\partial c}{\partial z} \right) \quad (2-7)$$

If the concentrations are independent of time, and the longitudinal concentration gradients are small in comparison to the lateral gradient,

$$u \frac{\partial c}{\partial x} = \frac{\partial}{\partial y} \left(\epsilon_y \frac{\partial c}{\partial y} \right) + \frac{\partial}{\partial z} \left(\epsilon_z \frac{\partial c}{\partial z} \right) \quad (2-8)$$

This is the diffusion equation to which most of the following discussions indicate the deviation from the depth-averaged values (see Fig. 1), and pertain.

2.2 Review of Previous Work

Since G.I. Taylor's (1922) discussion of the diffusion problem a half century ago, numerous studies have yielded remarkable results leading to better understanding of the mechanism of the diffusion process through better theoretical approaches, experimental work and numerical solutions. The main purpose, of course, is to predict the concentration distributions at various times and locations by solving the diffusion equation. However, the diffusion coefficients as functions of flow variables and space are not universally determinable. For water pollution problems most efforts have been placed on estimating the diffusion coefficients in laboratories or in the field so as to apply them to natural streams.

$$D_x = \left(\frac{0.406}{\kappa^2} + \frac{\epsilon_x}{u_*^2} \right) U_* Y_N \quad (2-13)$$

where κ is the von Kármán constant. If $\kappa = 0.41$, $D_x = 5.93 U_* Y_N$.

2.2-1 Longitudinal Dispersion

At some distance from the injection point of a dispersant after the vertical and lateral mixing have taken place, the spread of the dispersant is confined to the longitudinal direction. Mixing is dominated by variation of mean velocity in the cross section and is referred to as dispersion (Holly, 1969). The one-dimensional diffusion equation reduces to

$$\frac{\partial \bar{c}}{\partial t} + \bar{U} \frac{\partial \bar{c}}{\partial x} = \epsilon_x \frac{\partial^2 \bar{c}}{\partial x^2} \quad (2-10)$$

In the above equation, substituting $\bar{U} = \bar{\bar{U}} + \bar{U}''$ and $\bar{c} = \bar{\bar{c}} + \bar{c}''$, where the double bar values are depth averaged and the double prime values indicate the deviation from the depth-averaged values (see Fig. 1), and carrying out the same procedures used in deriving Eq. (2-2) yields

$$\frac{\partial \bar{\bar{c}}}{\partial t} + \bar{\bar{U}} \frac{\partial \bar{\bar{c}}}{\partial x} = \epsilon_x \frac{\partial^2 \bar{\bar{c}}}{\partial x^2} - \frac{\partial (\bar{U}'' \bar{c}'')}{\partial x} \quad (2-11)$$

Again the longitudinal dispersion coefficient D_x is defined as

$$D_x \frac{\partial \bar{\bar{c}}}{\partial x} = - \overline{u'' c''}$$

If the first term on the right hand side of Eq. (2-11) is small in comparison to the second term, Eq. (2-11) reduces further to

$$\frac{\partial \bar{\bar{c}}}{\partial t} + \bar{\bar{U}} \frac{\partial \bar{\bar{c}}}{\partial x} = D_x \frac{\partial^2 \bar{\bar{c}}}{\partial x^2} \quad (2-12)$$

where D_x is considered to be independent of x . Using the logarithmic law of velocity distribution and the same principle of Reynold's analogy used by Taylor (1953, 1954) to obtain ϵ_y , D_x can be expressed as (Elder, 1959)

$$D_x = \left(\frac{0.404}{\kappa^3} + \frac{\kappa}{6} \right) U_* Y_N \quad (2-13)$$

where κ is the von Kármán constant. If $\kappa = 0.41$, $D_x = 5.93 U_* Y_N$.

Elder (1959) verified this result experimentally in a wide shallow channel with a smooth boundary. Fischer (1967) adopted Taylor's (1954) convective dispersion theory and considered the lateral velocity variation to be important. He derived an equation for predicting the longitudinal dispersion coefficient in wide open channels. It requires that the channel geometry, the lateral velocity distribution, the shear velocity, and the lateral turbulent mixing coefficient ϵ_z be known. Sayre and Chang (1966) using a parabolic velocity distribution

$$\bar{U} = \bar{U} + \frac{U_*}{\kappa} \left[-\left(\frac{y}{Y_N}\right)^2 + 6\frac{y}{Y_N} - 2 \right] , \quad (2-14)$$

and an eddy diffusivity described by

$$\bar{\epsilon}_y = \frac{\kappa}{6} U_* Y_N , \quad (2-15)$$

obtained

$$D_x = \left(\frac{0.457}{\kappa^3} + \frac{\kappa}{6} \right) U_* Y_N , \quad (2-16)$$

which is approximately the same as Elder's result.

2.2-2 Longitudinal Diffusion

Because the differential convection caused by velocity variation dominates the longitudinal spreading, turbulent diffusion contributes only one percent or less to the total dispersion. There has been little experimental work concerned with the transport of dispersants at the water surface, a few notable ones are by Sayre and Chang (1968), Englund (1969) and Keefer (1971). Determination of the turbulent diffusion coefficient as defined in Eq. (2-3) has been difficult because the covariance of velocity and concentration fluctuations has been difficult to measure. Recently, however, Keefer (1971) succeeded in making such measurements to calculate covariance so as to adopt Eq. (2-3) to obtain ϵ_x . He performed a series of experiments in a one foot deep,

3.87 feet wide and 120 feet long open channel. The results he obtained for ϵ_x are about one order of magnitude greater than that obtained from Eq. (2-15). In this study the same technique developed by Keefer was adopted to explore the longitudinal diffusion coefficient.

2.2-3 Vertical Diffusion

The vertical diffusion coefficient ϵ_y in a wide open channel flow could be derived by Reynolds' analogy for the equivalence of mass and momentum transfer (Sayre, 1968). The equation gives

$$\epsilon_y = \frac{\tau_{xy}}{\rho \frac{dU}{dy}} \quad (2-17)$$

where \bar{U} is the average velocity in the channel cross section, and σ^2 is the variance of the lateral distribution of concentration.

$$\tau_{xy} = \tau_o \left(1 - \frac{y}{Y_N}\right) = \rho U_*^2 \left(1 - \frac{y}{Y_N}\right) \quad (2-18)$$

and the von Kármán-Prandtl velocity distribution may be written as

$$\bar{U} = \bar{U} + \frac{U_*}{\kappa} \left(1 + \ln \frac{y}{Y_N}\right) \quad (2-19)$$

Substituting Eqs. (2-18) and (2-19) into Eq. (2-17) the vertical diffusion coefficient may be rewritten

$$\epsilon_y = \kappa U_* y \left(1 - \frac{y}{Y_N}\right) \quad (2-20)$$

The depth averaged value is obtained by integrating the above equation with respect to y and dividing by depth Y_N

$$\bar{\epsilon}_y = \frac{\kappa}{6} U_* Y_N \quad (2-21)$$

Jobson and Sayre (1970) conducted a series of experiments in a large open channel by using a continuous line source of dissolved dye across the width of the channel. They measured the vertical distribution of the concentration at different distances from the source, then, from

the derived transfer equation, they evaluated the vertical diffusion coefficient. The experimental results have been compared to a numerical solution of the two-dimensional diffusion equation and correspondence of the results seems to verify the vertical diffusion coefficient expressed by Eq. (2-21).

2.2-4 Lateral Diffusion

Estimation of the depth averaged lateral diffusion coefficient has been proposed by Orlob (1958) as

$$\bar{\epsilon}_z = \frac{\bar{U}_{xs}}{2} \frac{d\sigma_z^2}{dx} = \bar{\beta} Y_N U_* \quad (2-22)$$

where \bar{U}_{xs} is the average velocity in the channel cross section, and σ_z^2 is the variance of the lateral distribution of concentration.

Keefer (1971) adopted Eq. (2-22) and performed experiments for smooth and rough boundaries. The non-dimensional coefficient $\bar{\beta}$ ranged from 0.09 to 0.13. In Keefer's summary of laboratory and field data obtained by several authors, $\bar{\beta}$ ranged from 0.1 to 0.7. In curved channels an average value for $\bar{\epsilon}_z$ of 1.3 was obtained by Fischer (1969). Elder's (1959) experimental result was 0.23 and has been generally accepted. Chang (1971) used experimental results and numerical solutions to estimate the lateral diffusion coefficients in meandering channels. His results were very close to that obtained by Fischer. Generally, the lateral diffusion coefficient is largely affected by channel geometry, roughness and flow conditions.

2.2-5 Solutions of the Diffusion Equations

Analytical and numerical solutions of the diffusion equations are considered. Due to the complexities and difficulties in solving the three-dimensional, second order partial differential equation

analytically, it is usually simplified to a two- or one-dimensional equation with constant coefficients. Roberts (1923) proposed a system of analytical solutions of the diffusion equations in the atmosphere. In open channels Glover's (1964) solution to Eq. (2-7) with the initial condition of instantaneous point source at $x = y = z = 0$ is given as

$$c(x,y,z,t) = s_1 f_2 f_3 \quad (2-23)$$

where

$$s_1 = \frac{Q_0}{B Y_N} \frac{e^{-\frac{(x - Ut)^2}{4 \epsilon_x t}}}{\sqrt{\pi} \sqrt{4 \epsilon_x t}} \quad (2-24)$$

$$f_2 = \frac{B}{\sqrt{\pi}} \frac{2 e^{-\frac{y^2}{4 \epsilon_y t}}}{\sqrt{4 \epsilon_y t}} \quad (2-25)$$

$$f_3 = \frac{Y_N}{\sqrt{\pi}} \frac{2 e^{-\frac{z^2}{4 \epsilon_z t}}}{\sqrt{4 \epsilon_z t}} \quad (2-26)$$

where B is the width of the channel and Q_0 is the quantity of dispersant introduced instantaneously at $t = 0$. Solutions for the steady state continuous point source can be obtained by integrating Eq. (2-23) with respect to t .

In open channel flow, the velocity distribution and the diffusion coefficients usually vary vertically as well as laterally. Analytical solutions for such complicated cases are not easy to obtain, hence, numerical solutions are introduced. Using a high speed computer and a finite difference scheme, the diffusion equation could be solved in a wider flexibility concerning actual flow conditions. Yotsukura and Fiering (1964, 1966) solved the dispersion equation numerically. Sayre (1968)

adopted Aris' (1955) moment distribution method in open channel flow and solved the moment equation numerically. Jobson and Sayre (1970) and Chang (1971) also applied a finite difference scheme to solve the diffusion equations in two dimensions and for the condition of continuous source. The results were compared to the experimental observations to adjust the diffusion coefficients used in the equations.

2.3 Wind Waves and Diffusion

Thus far studies of diffusion in open channels have ignored the wind wave effects on the surface. The waves do have significant effects on the diffusion process as pointed out by the studies of Wu (1969) and Eloubaidy (1969).

2.3-1 Wind Waves

When a wind blows over the surface of a moving or standing body of water and the velocity exceeds a certain critical value a drift current develops and waves are generated. The mechanisms of air-water interaction have been studied extensively. Several hypotheses have been proposed to explain the physical process involved in the generation of waves by wind. Each hypothesis ignores one or more aspects of the problem and attempts to describe only a certain stage of wave growth. These models

of the generation of water waves by turbulent wind, such as Jeffreys (1925) separation mechanism, Phillips (1957) uncoupled model and Miles (1957) coupled model, have contributed to a better understanding of wind water interaction. Yet, because of limitations and biased hypotheses, the efforts have met with only partial success. For example, the experiment performed by Plate, et. al., (1966, 1969) showed that the wave growth rate was not equal to that predicted by Miles (1962a), but was about twice as large. The discrepancies between their experimental

results and theoretical predictions may be attributed to the variation of shear stress acting on the waves with fetch and a drift current developed in the water. Using a specially designed self-adjusting moving probe and with the aid of a digital computer, Chang (1969) investigated the detailed structure of turbulent air flow above and between crests of progressing wind waves. He concluded that: "The observed flow configuration suggests that the well known shear flow mechanism proposed by Miles needs revising to be applicable for predicting the growth of fully developed small water waves." Although much work has been done to relate the water waves to the wind, obtaining detailed knowledge of the air-water interaction is still not in an acceptably calculable stage.

In so far as the diffusion equation (Eq. 2-8) is concerned, it is obvious that the velocity profile, the diffusion coefficient and the boundary conditions govern the solutions. Thus, the wind raised drift current, the wave raised second-order drift velocity and the increased turbulence intensity caused by the oscillating wave actions which affects the diffusion coefficients, should have marked effect on the diffusion process.

2.3-2 Wind Produced Drift Current

The turbulent shear flow in air over the water produces a drift current in the water. This drift current obviously varies with wind speed and slightly with fetch. Experimentally the drift velocity at the water surface has been measured by Plate, *et. al.*, (1969) for two different friction velocities. They observed that over short fetches the drift velocity increased roughly according to a power law, while at fetches exceeding about one meter, the ratio of drift velocity to the

free stream velocity attains a constant ratio of 0.026. Results obtained by Plate showed that fetch was not important, while the free stream air velocity was important. Unfortunately, Plate's experiment was performed with standing water, and the velocity profile in the water has been ignored. A water surface drift velocity of three percent relative to the free stream air velocity is sometimes adopted for natural streams (Wu, 1969). In this study the structure of the wind produced velocity profile in the water was measured by a hot film anemometer.

2.3-3 Wave Produced Drift Velocity

The process of the growth of wind generated waves is complicated and there is no general mathematical form for description. Yet, it is infinitely obvious that large waves are generated by high wind speed and at large fetch. Stokes (1851) first showed that in a water wave the particles of fluid process, apart from their orbital motion, a steady second-order drift velocity (usually called the mass-transport velocity). Longuet-Higgins (1953) pointed out that experiments indicated that the mass-transport velocity can be very different from that indicated by Stokes on the assumption of a perfect, non-viscous fluid. Taking account of the viscosity and boundary conditions, he derived a formula for calculating the mass transport velocity both for standing and progressive sinusoidal waves. His results gave a strong forward velocity close to the surface and near the bottom while between the surface and bottom boundary layers a weak backward velocity was found. His theoretical velocity and experimental observations performed with standing water and mechanical sinusoidal progressive waves gave excellent agreement. Dubreil-Jacotin (1934) showed that a wave motion may be superimposed upon a steady stream having an arbitrary velocity

distribution. The wind wave effect on the water velocity profile was measured in this study.

2.3-4 Wind Wave Effect on Diffusion Coefficients

The experiments were carried out in the wind-water flume at the Fluid Dynamics and Diffusion Laboratory of Colorado State University. The experiment by Eloubaidy (1969) showed that the water reaeration rates were significantly increased when wind waves appeared on the surface. The main objective of the study was to determine the wind wave effect on the diffusion coefficients in open channel flow, by comparing computed vertical and lateral mixing with data obtained from the laboratory flume. Wu (1969) pointed out that the longitudinal dispersion coefficients were largely increased with downstream wind blowing on the channel surface when compared to those without wind or with upstream wind. Obviously, the vertical and lateral diffusion coefficients would be effected by the system; the devices for measuring salt water concentration, water velocity and their fluctuations and the water surface displacement gauge.

2.4 Method of Analysis for this Study

In the present studies, vertical and lateral diffusion coefficients were determined by a simulation method (Chang, 1971). The method involves

a step-by-step numerical representation of the mixing process (Yotsukura, et.al., 1970). It is a trial-and-error method for selecting the mixing coefficient which yields the best agreement between calculated concentration distributions and observed data. A detailed discussion of experimental and numerical analyses will be presented in the next two chapters.

The inlet section, where the water enters the facility, consists of honeycomb screens which serve as diffusers for the incoming water and at the same time act as wave dissipating beaches. The water is circulated into the channel by a three-speed pump, and returns to a 12-foot by 12-foot by 15-foot sump located under the channel. The water exits from the channel through a honeycomb beach and returns to the sump through a metering orifice which has been calibrated in place. The pinch valve located in the supply pipe is used to control the water flow.

CHAPTER III

EXPERIMENTAL EQUIPMENT AND PROCEDURES

The experiments were carried out in the wind-water flume at the Fluid Dynamics and Diffusion Laboratory of Colorado State University. The main objective of the study was to determine the wind wave effect on the diffusion coefficients in open channel flow, by comparing computed vertical and lateral mixing with data obtained from the laboratory flume. The equipment consisted of the basic flume; the salt water injection system; the devices for measuring salt water concentration, water velocity and their fluctuations and the water surface displacement gauge.

3.1 The Wind Tunnel Flume Combination

3.1-1 The Flume

The wind-water flume is shown in Fig. 2. It consists of a truss-supported plexiglass channel with a test section about 52-feet long. The cross-sectional dimension is two-feet wide by 2.5-feet high. The truss can be rotated around a central pivot by means of a screw driven support at the end of the facility to establish a desired channel slope. The inlet section, where the water enters the facility, consists of honeycomb screens which serve as diffusers for the incoming water and at the same time act as wave dissipating beaches. The water is circulated into the channel by a three-speed pump, and returns to a 12-feet by 12-feet by 15-feet sump located under the channel. The water exits from the channel through a honeycomb beach and returns to the sump through a metering orifice which has been calibrated in place. The pinch valve located in the supply pipe is used to control the water flow.

Another valve in the return pipe serves to control the depth of water in the flume. A controlled by-pass line maintains the pump with a stable operating load.

An axial fan draws air through a bell-shaped fiberglass circular inlet and two screens, into a contraction section and then smoothly enters the rectangular test section through a honeycomb screen. Downstream from the test section is a fan section, where the air is led through a honeycomb and passes into the fan through a diffuser in which the duct cross section is changed from square to round.

The air and water flows are essentially three-dimensional. However, in order to maintain water flow as nearly two-dimensional as possible, the ratio of the channel width to the water depth was kept large (to a maximum of six), and the bottom of the channel was roughened.

3.1-2 Bed Roughness

In order to provide a uniformly rough surface for generation of turbulence, the channel bed was roughened by putting sheets of expanded metal lath, as shown in Fig. 3. The meshes, which were screwed to the plexiglass bottom of the channel, were made of aluminum and coated with

lacquer to prevent oxidation. The observed value of the Darcy-Weisbach resistance coefficient for the bottom roughness was about 0.069 for a flow depth of 0.285-foot with an average water velocity of 1.02 fps. The side walls of the channel were smooth plexiglass.

3.2 Water Velocity Measurement

3.2-1 Hot-Film Sensor

As shown in Fig. 4, a parabolic-shaped hot film probe was used to measure the water mean velocity and its fluctuations. This shape was

chosen because of its durability and resistance to contamination by water-borne particles. When contaminated it was usually cleaned by a small artist paint brush. The sensor was aligned so that the longitudinal axis of the sensing element was parallel to the direction of flow and parallel to the bottom of the flume. A calibration curve of voltage output versus fluid velocity is shown in Fig. 5. The probe was calibrated against a pitot static tube. During the experiment, the water temperature in the flume was kept at 71°F, the same temperature at which the probe was calibrated.

3.2-2 Hot-Film Anemometer

The hot-film anemometer was a constant temperature compensated unit with a reasonably undistorted frequency response range of from 0 Hz to 1 K Hz. The hot-film probe and anemometer were manufactured by Thermo-Systems Inc. of St. Paul, Minnesota. In the experiment the anemometer had a signal output of eight to 15 volts, which was conditioned approximately for a tape recorder, a rms meter and other peripheral instruments.

3.3 Tracer and Injection System

3.3-1 Tracer

The dispersant used for these experiments was a mixture of laboratory quality sodium chloride and water. A certain amount of methanol was added to reduce the density until the density of the mixture was the same as that for water. The concentration of the tracer used in these experiments was about 20,000 parts per million (ppm).

3.3-2 Tracer Injection System

The salt solution was injected at ambient velocity into the flow through a 1/8-inch brass tube. As shown in Fig. 6, the brass tube was

bent at right angles with a short arm two-inches long at the end of a 13-inch long tube. The bend was smoothed to reduce turbulence at the end of the short arm where the tracer was ejected. The tracer injector was mounted on a carriage across the channel and connected to a constant head tank with an overflow hole. The salt water in the tank was supplied by a nearby tank. A sketch of the tracer injection system and general layout of the experiment is shown in Fig. 7.

other instruments.

3.4 Measurement of Concentrations

3.4-1 Single Conductivity Probe

The probe used was patterned after those of Keeler (1964) and Keefer (1971). The theory for probe operation was discussed by Gibson and Schwarz (1964). A construction detail of the probe is shown in Fig. 8. The probe consisted of a piece of 0.04-inch fine hollow glass tubing sharpened at one end, two pieces of 1/8-inch brass tubing and a 18-inch long, 3/16-inch brass tube bent at a right angle two-inches from one end. A two-inch long, 0.001-inch platinum wire was sealed in the glass tubing and connected to a hook-up wire about 20-inches long. All the brass tubings were insulated by heat shrinkable tubing. The end of the 22-gauge wire and the long end of the brass tubing were connected to the coaxial cable with a BNC connector. The probe output voltage was 0-15 volts. The response was linear within ± 1.5 percent, hence it was not necessary to run elaborate calibrations during measurement. A typical linear calibration curve for a probe is shown in Fig. 9.

3.4-2 Carrier Amplifier

The bridge unit used to operate the probes in this study was a type 3C66 carrier amplifier manufactured by Tektronix Corporation, Beaverton,

Oregon. This was a plug-in model which operates with a type 561 oscilloscope to produce a trace deflection proportional to the change in resistance across the bridge. The bridge was an a-c unit with a carrier frequency of 25 K Hz. It had a rise time of 70 micro-seconds and a band width of d-c to 5 K Hz. The bridge had a signal output jack with three volts DC for each cm deflection of oscilloscope trace. The unit was used to drive chart recorders, rms meters, tape recorders and other instruments.

3.5 Measurements of Water Surface Elevations

3.5-1 Capacitance Probe

The capacitance probe was used to continuously measure the water surface displacement at a given fetch as a function of time. It consisted of a 32 gauge Nyclad insulated copper wire stretched vertically across insulated ends of a probe as shown in Fig. 10. The copper wire and the water act as two condensor plates with the insulation coating as the dielectric medium. The bare end of the positive conductor was completely insulated from water. The probe was calibrated before and after each series of experiments. The wetting effects caused by absorption of water by the wire insulation, changed the calibration curve slightly. The effect was practically eliminated by submerging the wire in water for a period of about 24 hours. A linear relationship between water depth and the output voltage of the capacitance bridge was obtained as shown in Fig. 11.

3.5-2 Capacitance Bridge

The difference in capacitance due to the water depth was measured by a capacitance bridge developed at the Engineering Research Laboratory

at Colorado State University. The bridge was a solid state instrument with a varying DC voltage output proportional to water level. The DC level and the AC gain which control the sensitivity were controlled by

3.7 Description of Experiments
 two ten turn dial potentiometers on the front panel. The schematics and block diagrams of the capacitance bridge are shown in Fig. 12. The surveyor's level. The water pump was turned on at a medium speed. The output of the Wien bridge oscillator was fed to the input of the zero bypass valve and the supply and return valves were adjusted until a uniform flow was established with a desired hydraulic condition. The signal from the probe was applied to a low impedance transformer. The resulting signal was applied by an AC amplifier (#A.5) and was then rectified by the diode and capacitor network which was put across the channel and the signal was moved along the work of the filter and suppression board. The resulting DC voltage was amplified by the DC amplifier (#A.6) and fed through a low pass filter, the output of which was used as the output of the capacitance gauge.

3.6 Measurements of Air Velocity

The average air velocity was measured by a Dawyer 1/8-inch OD pitot-static tube fixed in space in conjunction with a Transonics Equibar Type 120 electronic micromanometer which had been calibrated against a standard water manometer. The probe was placed about 10-feet from the upstream end of the channel test section and about 15-inches above the channel bottom. The mean air velocities measured at this location were used as reference velocities.

Besides the above instrumentation, auxiliary equipment used in this experiment included: an attenuator to attenuate the output voltages from the hot-film anemometer and carrier amplifier to a suitable range (± 1.4 volts) for FM magnetic tape recorders; a strip chart recorder for recording the mean output voltage; a true rms meter for obtaining the voltage fluctuations; and a FM magnetic tape recorder for recording the voltage

fluctuations. A block diagram for the electronic hookup of velocity, concentration and water wave measurement is shown in Fig. 13.

3.7 Description of Experiments

The flume was first adjusted to a desired slope by using a surveyor's level. The water pump was turned on at a medium speed. The bypass valve and the supply and return valves were adjusted until a uniform flow was established with a desired hydraulic condition. The uniform flow condition was constantly checked by a point gauge mounted on an electrode conductivity probe in a special holder which held them within a carrier which was put across the channel and could be moved along the flume.

After a uniform flow condition was established, velocity profiles were taken at a cross-section at the centerline and midway between centerline and the walls. The difference between the velocity profiles measured at the above locations were not significant, thus only centerline profiles were measured thereafter. Two thermometers were attached to the channel side wall near the downstream end of the flume, one for measuring the air temperature and the other for that of water. The water temperature was kept at 71°F. A tracer injector was placed at the centerline of the flume 26-feet from the entrance. The source was positioned at mid-depth or near the water surface. Downstream from the source the vertical concentration profiles at the centerline and the horizontal concentration profiles near the same height as the source were measured at four different sections for each case.

When the wind wave effect on the diffusion coefficients were considered, the air fan was turned on after the normal flow of a desired hydraulic condition was obtained. The pitch of the fan was adjusted to

obtain a desired ambient air flow. The same procedures as stated above were applied to obtain the vertical and horizontal concentration profiles, except that a capacitance probe was used to record the water waves.

As described in section 2.1, the longitudinal diffusion coefficients can be related to the longitudinal velocity concentration covariance, $u'c'$, and the mean concentration. Measurements for this calculation were carried out by placing the parabolic hot-film sensor and the single electrode conductivity probe in a special holder which held them within 1/16-inch of each other. This space gave an accurate correlation (written communication, McQuivey and Keefer, 1971), and there was no significant interaction found between the hot-film and the conductivity probe. The velocity and concentration fluctuations were recorded simultaneously 11 to 12 points longitudinally downstream from the source.

After two sets of experiments, all the water in the sump and flume was drained out and replaced by fresh water. If the nutrient-rich methanol-salt solution was left in the flume for several days, organic activities introduced contaminants and at high temperatures objectionable odors were produced.

Although numerical integration of differential equations has had a long history of use, it was not popularly adopted before the advent of high speed computers. It is now one of the most popular methods in solving linear or non-linear problems with complicated initial and boundary conditions. The stability condition for the numerical solution, which is an important and difficult analysis especially for time dependent equations, can easily be analyzed for the particular case of the steady, three-dimensional diffusion equation (Eq. 2-8) applied to a

rectangular cross-section and CHAPTER IV open channel flow. In order to
render the so NUMERICAL ANALYSIS OF THE DIFFUSION EQUATION

4.1 Limitations to the Analytical Approach

No analytical solutions in closed form has ever been obtained directly for the non-linear partial differential diffusion equations. Even for linearized diffusion equations with complicated velocity and diffusivity distributions, the analytical solutions are difficult to obtain. Because of the complexities and difficulties, the analytical solutions to the diffusion equation are usually provided for simplified one- or two-dimensional equations with constant diffusion coefficients or velocities. Solutions of such simplified equations are practically not applicable because the velocity vectors and diffusion coefficients in natural streams are usually functions of position. For example, the solution to the one-dimensional Fickian diffusion equation with an initial condition of uniformly distributed instantaneous plane source in an open channel showed poor agreement with experimental observations for the early stage of the diffusion process (Sayre, 1968).

4.2 Necessity of Numerical Integration

Although numerical integration of differential equations has had a long history of use, it was not popularly adopted before the advent of high speed computers. It is now one of the most popular methods in solving linear or non-linear problems with complicated initial and boundary conditions. The stability condition for the numerical solution, which is an important and difficult analysis especially for time dependent equations, can easily be analyzed for the particular case of the steady, three-dimensional diffusion equation (Eq. 2-8) applied to a

rectangular cross-section and a straight open channel flow. In order to render the solution of the diffusion equation more applicable to natural streams and in the interest of conserving effort in solving the diffusion equation, the numerical method was adopted.

4.3 Formulation of the Finite Difference Equation

4.3-1 Dimensionless Diffusion Equation

To reduce the number of variables in the problem and to make a systematic analysis according to the related parameters, the diffusion equation may be first transformed into dimensionless form. Introducing the dimensionless parameters (Jobson, 1970)

$$\left. \begin{aligned} \xi &= \frac{x}{Y_N} & , & & \phi(y) &= \frac{U}{U_*} \\ \eta &= \frac{y}{Y_N} & , & & \alpha(y) &= \frac{\epsilon y}{U_* Y_N} \\ \zeta &= \frac{z}{Y_N} & , & & \bar{\beta} &= \frac{\epsilon z}{U_* Y_N} \end{aligned} \right\} \quad (4-1)$$

The dimensionless form of Eq. (2-8) becomes

$$\phi(y) \frac{\partial c}{\partial \xi} = \frac{\partial}{\partial \eta} \left(\alpha(y) \frac{\partial c}{\partial \eta} \right) + \bar{\beta} \frac{\partial^2 c}{\partial \zeta^2} \quad (4-2)$$

4.3-2 Alternating Direction Implicit (A.D.I.) Method

Peaceman and Rachford (1955) first introduced the A.D.I. method in solving the parabolic heat equation and the Laplace equation for a three-dimensional regime. This technique has proven to be an efficient method for rectangular regions. As shown by the authors with a typical problem, it involved about 1/25 less work than the explicit method and 1/7 less work than the Crank-Nicolson method. Discussion of the general concept and procedure of this method follows (Smith, 1965).

Referring to Eq. (4-2), assume the solution on the cross-section $\xi = n\Delta\xi$ is known, the mesh size on each cross-section is $\Delta\eta = \Delta\zeta$ and mesh points in the vertical and lateral directions are M and N respectively. The method consists of replacing only one of the second derivatives $\partial^2 c / \partial \eta^2$ say, by an implicit difference approximation in terms of unknown pivotal values of c from the $(n+1)$ th distance-level, the other second-order derivative, $\partial^2 c / \partial \zeta^2$, being replaced by an explicit finite-difference approximation. Application of the corresponding finite-difference equation to each of the M mesh points along a column parallel to the vertical direction, then given M equations for the N unknown values of c at these mesh points for distance $\xi = (n+1)\Delta\xi$. When there are N columns parallel to y , the advancement of the solution over the whole rectangle to the $(n+1)$ th distance-step involves the solution of N independent systems of equations, each system containing M unknowns. The solution of these systems is much easier than the solution of the MN equations associated with the fully implicit method. The advancement of the solution to the $(n+2)$ th distance-level is then achieved by replacing $\partial^2 c / \partial \zeta^2$ by an implicit finite-difference approximation and $\partial^2 c / \partial \eta^2$ by an explicit one and expressing a finite difference equation corresponding to each mesh point along rows parallel to the lateral direction. This gives M independent systems of equations each system involving N unknowns. The distance interval $\Delta\xi$ must be the same for each advancement.

4.3-3 Finite Difference Equations

Thus, two difference equations are used, one for the first distance step, the other for the second distance step. Putting Eq. (4-2) in a

finite difference form using a forward differencing scheme then yields

$$(c_{j,k}^{n+1} - c_{j,k}^n) \frac{\phi_j}{\Delta \xi} = \frac{1}{(\Delta \eta)^2} \{ \alpha_{j+1} (c_{j+1,k}^{n+1} - c_{j,k}^{n+1}) - \alpha_j (c_{j,k}^{n+1} - c_{j-1,k}^{n+1}) \} \quad (4-7)$$

$$+ \frac{\bar{\beta}}{(\Delta \zeta)^2} \{ c_{j,k+1}^n - 2c_{j,k}^n + c_{j,k-1}^n \} \quad (4-3)$$

$$(c_{j,k}^{n+2} - c_{j,k}^{n+1}) \frac{\phi_j}{\Delta \xi} = \frac{1}{(\Delta \eta)^2} \{ \alpha_{j+1} (c_{j+1,k}^{n+1} - c_{j,k}^{n+1}) - \alpha_j (c_{j,k}^{n+1} - c_{j-1,k}^{n+1}) \}$$

$$+ \frac{\bar{\beta}}{(\Delta \zeta)^2} \{ c_{j,k+1}^{n+2} - 2c_{j,k}^{n+2} + c_{j,k-1}^{n+2} \} \quad (4-4)$$

where j , k , and n are the indices at y , z , and x direction respectively. Equation (4-3) is implicit in the y -direction and explicit in the z -direction, while Eq. (4-4) is implicit in the z -direction and explicit in the y -direction.

The above equations may be rearranged in the following form which is more suitable for calculation

$$- \frac{\alpha_j}{(\Delta \eta)^2} c_{j-1,k}^{n+1} + \left[\frac{\alpha_j}{(\Delta \eta)^2} + \frac{\alpha_{j+1}}{(\Delta \eta)^2} + \frac{\phi_j}{\Delta \xi} \right] c_{j,k}^{n+1} - \frac{\alpha_{j+1}}{(\Delta \eta)^2} c_{j+1,k}^{n+1} \quad (4-5)$$

$$= \frac{\bar{\beta}}{(\Delta \zeta)^2} [c_{j,k+1}^n - 2c_{j,k}^n + c_{j,k-1}^n] + \frac{\phi_j}{\Delta \xi} c_{j,k}^n \quad (4-5)$$

$$- \frac{\bar{\beta}}{(\Delta \zeta)^2} c_{j,k-1}^{n+2} + \left[\frac{2\bar{\beta}}{(\Delta \zeta)^2} + \frac{\phi_j}{\Delta \xi} \right] c_{j,k}^{n+2} - \frac{\bar{\beta}}{(\Delta \zeta)^2} c_{j,k+1}^{n+2}$$

$$= \frac{\alpha_j}{(\Delta \eta)^2} [c_{j+1,k}^{n+1} - c_{j,k}^{n+1}] - \frac{\alpha_j}{(\Delta \eta)^2} (c_{j,k}^{n+1} - c_{j-1,k}^{n+1})$$

$$+ \frac{\phi_j}{\Delta \xi} c_{j,k}^{n+1} \quad (4-6)$$

where j , k vary from one to M and N respectively. Use of Eqs. (4-5) and (4-6) at each distance step leads to M (or N) sets of N (or M) simultaneous equations of the form

If the source coordinate is (x_0, y_0, z_0) and the nearby velocity and

and diffusivity U and ϵ_y respectively make no significant change, then Hino's equation gives

$$c(x,y,z) = \frac{Q_0 \exp(-(y-y_0)^2 \sqrt{2Y^2(x)})}{2\pi U(x_0, y_0, z_0) (Y^2(x) \cdot Z^2(x))^{1/2}} \times [\exp\{-(z-z_0)^2 \sqrt{2Z^2(x)}\} + \exp\{-(z+z_0)^2 \sqrt{2Z^2(x)}\}] \quad (4-9)$$

where

$$\left. \begin{aligned} \overline{Y^2(x)} &= 2 \epsilon_y (x_0, y_0, z_0) (x-x_0) / U(x_0, y_0, z_0) \\ \overline{Z^2(x)} &= 2 \epsilon_z (x_0, y_0, z_0) (x-x_0) / U(x_0, y_0, z_0) \end{aligned} \right\} \quad (4-10)$$

and Q_0 is the source discharge.

b. Boundary Conditions - The reflection boundary conditions can be stated as $\epsilon_i \partial c / \partial n' = 0$ at all boundaries including the water surface, where n' is normal to the boundary. Referring to the difference equations (Eqs. 4-3 and 4-4), the boundary conditions become

$$\left. \begin{aligned} j = 1 &, \quad \frac{\alpha_j}{(\Delta n)} (c_{j,k}^{n+1} - c_{j-1,k}^{n+1}) = 0 \\ j = M &, \quad \frac{\alpha_j}{(\Delta n)} (c_{j+1,k}^{n+1} - c_{j,k}^{n+1}) = 0 \\ k = 1 &, \quad \frac{\bar{\beta}}{(\Delta \zeta)} (c_{j,k}^{n+2} - c_{j,k-1}^{n+2}) = 0 \\ k = N &, \quad \frac{\bar{\beta}}{(\Delta \zeta)} (c_{j,k+1}^{n+2} - c_{j,k}^{n+2}) = 0 \end{aligned} \right\} \quad (4-11)$$

c. Continuity Conditions - Since there is no generation of dispersant in the flow during the dispersion process, the discharge of the total dispersant on each calculated cross-section should be a constant and equal to the discharge of the source. Let $c_{j,k}^{n+2}$ be the solutions of Eqs. (4-5) and (4-6), then the ratio between the source discharge and the solution would be

$$\mu^{n+2} = Q_0 / (\sum_j \sum_k U_j c_{j,k}^{n+2} \Delta\eta \Delta\zeta) \quad (4-12)$$

where Q_0 is the source strength. In each step of the calculation, μ^{n+2} served as a correction factor, that is, the corrected value on each mesh point is $\mu^{n+2} c_{j,k}^{n+2}$, which is then the known value for the next step of calculation.

4.3-5 Stability Analysis

To obtain a reasonably approximated solution to the original differential equation, a stability analysis is an important and fundamental requirement. The total error, which is the amount the numerical solution of the finite difference equations differs from an exact solution of the partial differential equation, consists in part of "truncation error" and "round off error." During numerical integration, the computations are restricted to a finite number of decimal places which introduce round off error and the difference equations carry the truncation errors forward in the computation. Numerical studies indicate that the truncation errors are dominant in a stable and convergent process (Smith, 1965). If a stability criterion is not satisfied, errors may accumulate as integration proceeds and cause errors in the solutions to become unreasonably large. Mathematical descriptions of stability requires the total error to be bounded after an infinite number of integration steps when space grid increments are fixed.

In Eqs. (4-5) and (4-6), if the mesh is chosen so that $\Delta\eta = \Delta\zeta$, and define $\rho = (\Delta\eta)^2/\Delta\xi = (\Delta\zeta)^2/\Delta\xi$, then a stability analysis gives the amplification factor for the two-step procedure to be (Peaceman and Rachford, 1955)

$$\frac{A_{p,q,2n+2}}{A_{p,q,2n}} = \frac{\rho - 4 \sin^2 (\beta_p \Delta\xi/2)}{\rho + 4 \sin^2 (\beta_p \Delta\xi/2)} \times \frac{\rho - 4 \sin^2 (\beta_q \Delta\eta/2)}{\rho + 4 \sin^2 (\beta_q \Delta\eta/2)} \quad (4-13)$$

where $\beta_p = (2p + 1)\pi/2$, and $\beta_q = (2q + 1)\pi/2$; p, q varies from zero to $N - 1$ and $M - 1$ respectively.

For stability, the ratio in Eq. (4-13) must have an absolute value less than or equal to unity for all p and q . By examining the above equation, it is easy to determine that the ratio has an absolute value of less than unity for all p , q and ρ , in the case where ρ , and, therefore $\Delta\xi$ are the same for two distance steps. In the early stage of integration, $\Delta\xi$ was chosen smaller, as compared to that in the latter stages of calculation

5.1 Hydraulic Conditions

Seven different flow conditions were studied in the experiments. The hydraulic parameters for each test are summarized in Table 1. For identification, the test runs are coded and are indicated in column one. The letters N and W in the first or second character denote that there was either no wind or wind blowing on the water surface respectively. The letters S and C denote source location, either near the water surface or near the mid-depth respectively. Column three gives the uniform flow depth which was measured along the centerline of the flume and was determined to be the distance from the water surface to half of the height of the screen mesh on the channel bed. With wind blowing over the water surface, a small set-up was noted, but the depth change was very small in comparison to the total depth and was

CHAPTER V

REDUCTION AND PRESENTATION OF DATA

The experimental results are presented in this chapter. The results express the essential hydraulic and turbulent characteristics of the flow and concentration field, and the wave properties which disturb the water surface and renders measurable effect on the diffusion process. They are: the hydraulic conditions; velocity profiles and evaluation of vertical diffusion coefficients; the velocity-concentration covariance and estimation of longitudinal diffusion coefficients. Properties of the water surface were measured, the spectrum and average wave height are also presented. The measured concentration profiles at four different cross-sections downstream from the source are included in the last section.

5.1 Hydraulic Conditions

Seven different flow conditions were studied in the experiments. The hydraulic parameters for each test are summarized in Table 1. For identification, the test runs are coded and are indicated in column one. The letters N and W in the first or second character denote that there was either no wind or wind blowing on the water surface respectively. The letters S and C denote source location, either near the water surface or near the mid-depth respectively. Column three gives the uniform flow depth which was measured along the centerline of the flume and was determined to be the distance from the water surface to half of the height of the screen mesh on the channel bed. With wind blowing over the water surface, a small set-up was noted, but the depth change was very small in comparison to the total depth and was

Table 1. Basic Hydraulic Parameters.

Run Designation	Flow Conditions	Normal Depth Y_N (ft)	Depth Ratio B/Y_N	Slope $S \times 10^3$	Average Velocity \bar{U}_{xs} (ft/sec)	Hydraulic Radius $R_b = A_b/Y_{N_b}$ (ft)	Shear Velocity $U_* = \sqrt{gRS}$ (ft/sec)	Friction Factor $f = 8(\frac{U_*}{\bar{U}})^2$	Reynolds Number $R_E \times 10^4 = \frac{\bar{U}R}{\nu}$	Froude Number $F_R = \frac{\bar{U}}{\sqrt{gY_N}}$
(1)	(2)	(3)	(4)	(5)	(6)	(7)	(8)	(9)	(10)	(11)
NWS1	no wind, source near water surface	0.349	5.73	0.641	0.822	0.313	0.080	0.077	2.724	0.245
NWS2	no wind, source near water surface	0.348	5.75	0.881	1.178	0.300	0.092	0.049	3.893	0.352
NWC1	no wind, source near mid-depth	0.346	5.78	0.881	1.166	0.299	0.092	0.050	3.830	0.349
WS1	with wind (16.5 ft/sec) source near water surface	0.351	5.70	0.881	1.125	0.305	0.096	0.055	3.747	0.335
WS2	with wind (26.3 ft/sec) source near water surface	0.355	5.63	0.881	1.232	0.303	0.102	0.045	4.151	0.364
WS3	with wind (39.8 ft/sec) source near water surface	0.353	5.67	1.088	1.356	0.301	0.131	0.046	4.544	0.402
WC1	with wind (27.5 ft/sec) source near mid-depth	0.357	5.60	0.881	1.241	0.304	0.104	0.045	4.208	0.366

neglected in the present study. The slope of the energy grade line or the bed slope is given in column five. This was determined by using an engineer's level. The average velocity given in column six was calculated from the observed value of discharge, Q , average depth, Y_N , and the width, B , by the use of the continuity equation,

$$\bar{U} = \frac{Q}{B \cdot Y_N} \quad (5-1)$$

Column seven gives the hydraulic radius using the sidewall correction procedure suggested by Einstein (1942). The shear velocity in column eight is defined as $\sqrt{gR_b S}$ or $\sqrt{\tau_o/\rho}$, where g is the gravitational acceleration, R_b and S were obtained from columns seven and five respectively. Column nine gives the friction factor defined as $\frac{8(U_*'/\bar{U})^2}{\rho}$. The Reynolds number and Froude number are shown in columns ten and 11 respectively.

5.2 Velocity Measurements and Vertical Diffusion Coefficient

5.2-1 Velocity Profiles

The local mean velocity profiles were measured by a hot-film probe and anemometer as described in Chapter III. For the straight wide open channel with smooth walls, the variation of velocity in the lateral direction was small as compared to the vertical velocity profile. Furthermore, all the measurements were taken near the central plane of the flume, hence only the vertical mean velocity profiles were measured in this investigation. With the wind blowing over the water surface, waves were generated. This caused difficulties in measuring the mean velocity near the water surface. Because of the physical limitation of obtaining meaningful velocity measurements near the surface with a fixed probe, the proximity of the probe near the surface was limited. Surface

velocities were estimated to be three percent of the wind velocity (Plate, et. al., 1969, Wu, 1969) and the profile between the closest measured position and the surface was estimated to provide a continuous velocity distribution by a process similar to that indicated by Drake (1967). For longer fetches, the dominant frequency of a wave was smaller, the wave height was larger, and the water velocity profile varied with fetch, particularly near the water surface. Because this study was concerned principally with the diffusion cones, which were short in comparison to the channel length, particularly with waves on the surface, a constant velocity profile measured near the middle of the test section was used. For example, the concentration profiles with a wind speed of 39.8 fps were measured between 1.1 ft and 3.5 ft downstream from the source, and the wave height changed very slightly in this distance as will be seen later.

For the purpose of numerical analysis, each measured velocity profile was non-dimensionalized by the corresponding shear velocity. The results are shown in Figs. 15 and 16 for the cases with and without wind.

5.2-2 Evaluation of Vertical Diffusion Coefficients

The vertical diffusion coefficient can be evaluated through Eq. (2-17). Assuming the pressure to be hydrostatic $\partial\tau/\partial y$ is constant so that the resulting shear stress τ at any depth can be obtained by (Wu, 1969):

$$\tau(y) = \tau_0 \left(1 - \frac{y}{Y_N}\right) + \tau_w \left(\frac{y}{Y_N}\right) \quad (5-2)$$

where τ_0 is the bed shear stress defined as $\tau_0 = (f/8) \rho \bar{U}^2$, where f is the friction factor from column nine of Table 1, ρ is the density

of the water and \bar{U} is the average water velocity. The wind shear at the water surface τ_w is expressed as $\tau_w = c_1 \rho_a U_a^2$, where c_1 is the wind stress coefficient given by Wu (1969), ρ_a is the density of air and U_a is the wind velocity. For no wind, $\tau_w = 0$. The vertical velocity gradient du/dy was obtained by expressing the velocity profile as a power law and superimposing the wind produced drift velocity. The form of the velocity profile is given as

$$u(y) = U_m \left(\frac{y}{Y_N}\right)^n + V_s \left(\frac{y'}{Y_N'}\right) \quad (5-3)$$

where u is the velocity at various depths y , n is the power obtained from a least square fitting of measured data, U_m is the measured maximum water velocity, V_s is the wind produced drift velocity on the water surface, y' is a variable which represents the distance from the highest measured point to the mean water surface, and Y_N' is a constant representing the distance between the highest measured point to the mean water surface. The derivative of Eq. (5-3) with respect to y gives the velocity gradient. The vertical diffusion coefficient was obtained in accordance with Eq. (2-17). Results of the dimensionless vertical diffusivities are shown in Figs. 17 and 18 for the cases of no wind and with wind wave effect. The depth averaged values are also indicated in the figures.

5.3 The Turbulence Characteristics

5.3-1 The Relative Turbulence Intensity of Water Velocity

The longitudinal turbulence intensity is the root-mean-square value of the deviations of the longitudinal velocity from its local mean value. Since the calibration curve of the hot-film probe was not linear, technically the turbulence intensity should be calculated by converting the

voltage output from the hot film to the actual velocity according to the calibration curve from which the variance may be calculated to obtain the turbulence intensity. However, in this study, since the velocity fluctuations with respect to the mean were small, the turbulence intensity was evaluated by playing back the analog F.M. record through a RMS meter to obtain the standard deviation of the voltage output. This value was then multiplied by the gradient of the calibration curve at the mean velocity. Usually the turbulence intensity is non-dimensionalized as relative intensity with respect to the local mean velocity, the cross-section average velocity, or the shear velocity. These ratios give indication of the relative strengths of the turbulent diffusive transport comparison to the mean convective transport at any point in the flow (Keefer, 1971). Typical results of the turbulence intensity to the cross-section average velocity is shown in Fig. 19.

5.3-2 Relative Turbulent Fluctuations of Concentration

The calibration curve of the single conductivity probe was linear, so that turbulent phenomena can easily be obtained by measurement of the rms voltage. The relative fluctuations were obtained by dividing by the maximum concentration of a section closest to the source. The relative intensity of the concentration indicates the homogeneity of the mixing of the tracer. Several selected cases of the relative turbulent fluctuations are shown in Figs 20 through 23. As indicated in the figures, the relative intensity was higher at the position close to the source. Near the boundary at the farthest downstream measuring station the values were rather small which means that mixing had taken place homogeneously particularly near the reflection boundary.

5.3-3 The Evaluation of the Longitudinal Diffusion Coefficient

The longitudinal diffusion coefficient can be related to the longitudinal velocity-concentration covariance $\overline{u'c'}$ and the mean concentration gradient. Measurements were made in accordance with the procedure described in section 3.7. Simultaneous records of the output from both hot-film and single-conductivity probes were made on F.M. magnetic tape. These records were then digitized. The sample rate was 1000 samples per second. The digital data were then computer analyzed to evaluate the velocity-concentration covariance. The voltage outputs were converted to velocity and concentration according to the corresponding calibration curves, the covariance was then calculated as a discrete time series in accordance with

$$\overline{u'c'} = \frac{1}{N} \sum_{i=1}^N u_i' c_i' \quad (5-4)$$

where N is the total number of data points each separated by fixed Δt . The longitudinal concentration profiles were also evaluated. Experimental results of the above two profiles are shown in Figs. 24 and 25. In order to avoid large fluctuations in the evaluated longitudinal diffusion coefficients, the experimental results of $\overline{u'c'}$ and \bar{c} were fitted to curves of polynomial of degree three or four, and the longitudinal diffusion coefficients were obtained according to the fitted equation, and by $\epsilon_x = -\overline{u'c'}/(\partial c/\partial x)$. Results of five tests are shown in Fig. 26.

5.4 Presentation of the Wind Generated Waves

When the wind wave effect on the diffusion process was considered, wave height measurements were also recorded on the analog F.M. tape.

The capacitance wave gauge was located in the axial plane of the flume, about ten measurements were taken for each condition at different fetches downstream from the point source. The wave records were also digitized with a sampling rate of 100 samples per second. Due to the unsteadiness of the capacitance gauge calibration, (a constant shifting of the output voltage and environmental and manual effects in opening the flume covers) a low frequency trend appeared on the wave records particularly for high frequency low amplitude waves. The analysis of the wave data proceeded as follows:

First the low frequency trend was removed from the original wave record. This was done with a digital high pass filter. The properties of the wind generated waves were then determined. The second step was the spectrum estimation of the wind wave. This was done by the Blackman-Tukey Fourier transform method. From the spectrum estimation, the dominant frequency (f_m) of the wave was determined which will be related to the diffusion coefficient later. Then a lowpass digital filter with cutoff frequency at $3/2 (f_m)$ and a band pass filter with central frequency at f_m and band width $1/3 (f_m)$ were used to analyze the data (Su, 1969, 1971). After the filtering process the waves had a smooth regular pattern, yet retained the energy content and amplitude. Finally, the average wave height was calculated, which will also be related to the diffusion coefficients. Figure 27a-c shows the original wave record, trend removed wave record, band pass filtered waves for the case of wind velocity of 39.8 fpm. Figure 28 shows the water wave spectrum estimations at several different fetches. a) closest to the source. On each individual cross-section, the maximum concentration also occurred at the section nearest the source which decreased horizontally and laterally,

5.5 Concentration Profiles

Measurements of the concentration profiles at four different stations downstream from the source were made. The source was located in the axial plane of the flume and was 22 ft from the entrance. Seven different tests, as shown in Table 1, were made. In each test, four sections of vertical concentration profiles in the axial plane of the flume and horizontal concentration profiles near the same depth as the source were taken. The relation between section numbers and distance downstream from the source are as follows:

Sect. No.	1	2	3	4	5	6	7	8	9
Dist. (ft)	0.78	1.11	1.61	2.36	2.95	3.53	4.20	4.86	5.53
Sect. No.	10	11	12	13					
Dist. (ft)	6.28	7.03	7.78	8.53					

The data were recorded on the analog F.M. tape, then played back on a strip chart recorder at twice the recorded speed. A low pass analog filter was used to attenuate the high frequency fluctuations, and average voltage was determined from the strip chart record. This value was then converted to the concentration by the linear calibration curve of the single-conductivity probe. The measured vertical and horizontal concentration profiles were normalized by the corresponding maximum values of the vertical and horizontal profiles of the first measured section closest to the source for easier comparison. The experimental results of the concentration profiles of the seven tests are shown in Figs 29 through 42. It is seen that the maximum concentration always occurred in the section (two or three) closest to the source. On each individual cross-section, the maximum concentration also occurred at the section nearest the source which decreased horizontally and laterally,

except for the cases of higher wind velocity which will be explained in the next paragraph. After release from the source, the plume spread out three dimensionally toward the reflection boundaries of the water sur-

face and the channel bed. After reaching the boundaries the tracer was reflected back and mixed with downstream spreading, thus the concentrations near the boundaries were increased and profiles tended to show a peak near the bed after a certain distance from the source. This phenomena is particularly seen on Figs. 39 and 41.

With the wind generated waves, the mixing process was tremendously increased. If compared to the data without wind, it is seen that the mixing took place in a much shorter distance. An interesting phenomenon can be seen in that the tracer tended to deflect downward. This was strongly shown in the cases of medium and high wind velocities. This downward deflection was considered to be a tracer "fall velocity" in the numerical analysis.

the mesh size and the increment of distance Δx was of concern. Large mesh size and increment of distance lowered minimal computing time, however, from the mathematical and engineering point of view, smaller mesh size and increment of distance yield the results closer to the exact solution.

Considering these two factors, a test program with two different mesh sizes, one 26 by 46 and the other 41 by 73, was set up. The calculations were made in the same domain downstream from the source, with the same distance increment. Comparison of concentration profiles showed them to be almost identical, particularly after being normalized by the local maximum values. The central process time of the computer for the larger mesh points was almost five times larger than that using

CHAPTER VI

DISCUSSION OF NUMERICAL RESULTS

This chapter presents the general considerations, procedures and the results of the numerical analysis of the diffusion equation. It is divided mainly into two parts: first, the cases of no wind, and second, the conditions with wind. From the results of the latter, the diffusion coefficients were related to the wind velocity, dominant frequencies of the water waves and the wave heights.

6.1 General Considerations and Procedures

As stated in chapter IV, the numerical integration of the dimensionless diffusion equation (Eq. 4-2) involves the solution of two sets of simultaneous finite difference equations (Eqs. 4-5 and 4-6). Stability analysis showed the ADI method to be stable for the rectangular cross-section with the dimensionless mesh size $\Delta\eta = \Delta\zeta$. Thus, only the mesh size and the increment of distance step $\Delta\xi$ was of concern. Large mesh size and increment of distance involve minimal computing time, however, from the mathematical and engineering point of view, smaller mesh size and increment of distance yield the results closer to the exact solution.

Considering these two factors, a test program with two different mesh sizes, one 26 by 46 and the other 41 by 73, was set up. The calculations were made in the same domain downstream from the source, with the same distance increment. Comparison of concentration profiles showed them to be almost identical, particularly after being normalized by the local maximum values. The central process time of the computer for the larger mesh points was almost five times larger than that using

smaller mesh points. The smaller mesh points were thus used for the numerical analysis. With 26 mesh points in 0.35 ft depth of water, the dimensionless mesh size was 0.04 and the actual mesh size was about 0.013 ft or about one-sixth of an inch.

Since the source was located in the axial plane of the flume and the flow was assumed to be two-dimensional with no velocity variation on the lateral direction, it was anticipated that the horizontal concentration profiles should be symmetric about the axial plane. In order to save further on computer time, the numerical analysis was done for the right half of the cross-section. Boundary conditions were the same except that symmetry at the center line was used in the computational domain. The systems of the finite difference equations were rewritten at the center line to deal with the imaginary boundary. The boundary conditions on Eq. (4-11) for $k = 1$ were invalid, and Eqs. (4-5) and (4-6) were rewritten to be

$$-\frac{\alpha_j}{(\Delta\eta)^2} c_{j-1,1}^{n+1} + \left[\frac{\alpha_j}{(\Delta\eta)^2} + \frac{\alpha_j}{(\Delta\eta)^2} + \frac{\phi_j}{\Delta\xi} \right] c_{j,1}^{n+1} - \frac{\alpha_{j+1}}{(\Delta\eta)^2} c_{j+1,1}^{n+1} \\ = \frac{2\bar{\beta}}{(\Delta\xi)^2} [c_{j,2}^n - c_{j,1}^n] + \frac{\phi_j}{\Delta\xi} c_{j,1}^n \quad (6-1)$$

$$-\frac{2\bar{\beta}}{(\Delta\xi)^2} c_{j,2}^{n+2} + \left[\frac{2\bar{\beta}}{(\Delta\xi)^2} + \frac{\phi_j}{\Delta\xi} \right] c_{j,1}^{n+2} = \frac{\alpha_j}{(\Delta\eta)^2} [c_{j+1,1}^{n+1} - c_{j,1}^{n+1}] \\ - \frac{\alpha_j}{(\Delta\eta)^2} (c_{j,1}^{n+1} - c_{j-1,1}^{n+1}) + \frac{\phi_j}{\Delta\xi} c_{j,1}^{n+1} \quad (6-2)$$

Furthermore, at the beginning stages of the mixing process, the tracer occupied only a small region of the cross-section, and it was not necessary to make the numerical integration of the diffusion equation for the whole cross-section. Thus, at the beginning stage, a smaller number of mesh points, usually 9 by 11, were used with imaginary

reflection boundaries at the surface, right side and the bottom. After each step of calculation, the values on those three boundaries were noted. If the ratio of these values to the maximum values, which always occurred at the center line, were greater than 0.001, the number of mesh points were automatically increased by two in each direction until the maximum number of 26 in the vertical direction was reached, then the same procedure was applied to the horizontal direction only. The computing time was greatly reduced in this way, particularly at the initial stages. The initial value of the dimensionless increment of the distance step was taken as 0.02, after 40 to 50 steps of calculation, it was increased to 0.05, then to 0.08, 0.10, 0.20 and to a maximum value of 0.30 corresponding to a physical length of about 0.1 ft. small.

As stated in section 2.4, the present analysis was a semi-empirical step-by-step, trial-and-error method. That is, the mixing coefficients were selected to yield the best agreement between calculated concentration distributions and observed data. In the beginning, the dimensionless vertical diffusion coefficient evaluated from section 5.2-2 together with a dimensionless lateral diffusion coefficient of 0.1 was used in the numerical analysis of the diffusion equation. When the calculation proceeded to the first section where the concentration profiles were measured as shown in section 5.5, the predicted normalized concentration profiles were compared with the observed profiles both horizontally and vertically. If the agreement was unsatisfactory, then the diffusivities were adjusted and the same procedure was repeated until satisfactory agreement was obtained. It was observed that the calculations were sensitive to the diffusivities. A slight change in the diffusivity and vertical dimensionless coefficients are summarized in Table 2. The would cause noticeable change of the concentration profiles. The

interaction effect between the horizontal and vertical concentration profiles were not as sensitive as expected. This made the adjustment of the diffusivities easier, however, a number (five to eight) of trials were needed for each case to obtain satisfactory agreement at the first section. The output for the first cross-sectional concentration calculations became the initial conditions for calculation to the second cross-section, the same diffusivities from the first cross-section were used. If the comparison between the observed profiles and numerical results was satisfactory, calculations proceeded to the fourth cross-section. Results also showed that the longitudinal variation of the diffusivities was small, even under 27 fps of wind wave effect. The reason being that the distances from the source were small.

6.2 Numerical Results Without Wind Effects

The best agreement of the concentration profiles between the numerical results and the laboratory observations are shown by the solid line in Figs. 29 through 34 for the cases of NWS1, NWS2 and NWC1. In each case, the numerical results and the laboratory observations compare reasonably, particularly at the first cross-section which was nearest the source. The differences become larger for the downstream stations, especially near the boundaries where the concentrations approach zero. The horizontal concentration profiles from the experimental results show them to be almost symmetric with respect to the axial plane, where $B/Y_N = 0$ on the figures. The skewness from the center line was very small.

From the numerical results, the estimated depth-averaged horizontal and vertical dimensionless coefficients are summarized in Table 2. The

Table 2. Summary of Numerical Results (no wind).

Run Number	Section Number	Dist. From Source (ft)	Dist. Between Adj. Sect. (ft)	Estimated $\bar{\alpha}$	Estimated $\bar{\beta}$	Averaged $\bar{\alpha}$	Averaged $\bar{\beta}$
(1)	(2)	(3)	(4)	(5)	(6)	(7)	(8)
NWS1	3	1.61	1.61	0.033	0.111		
	5	2.95	1.34	0.033	0.111	0.0342	0.111
	7	4.20	1.25	0.033	0.111		
	11	7.03	2.83	0.036	0.111		
NWS2	3	1.61	1.61	0.052	0.110		
	5	2.95	1.34	0.052	0.110	0.0535	0.1295
	8	4.86	1.91	0.052	0.142		
	11	7.03	2.17	0.057	0.142		
NWC1	3	1.61	1.61	0.073	0.115		
	4	2.36	0.75	0.092	0.135	0.0835	0.1284
	6	3.53	1.17	0.092	0.135		
	8	4.86	1.33	0.101	0.135		

are about constant for all runs, the average was about 0.123, which is very close to Prych (1970) and Keefer's (1971) results. Also $\bar{\beta}$'s were much larger than $\bar{\alpha}$'s, the ratio ranged from 3.2 to 1.5, again comparing favorably to Keefer's results. Smallest $\bar{\alpha}$ was observed for the case of NWS1, which involved the smallest discharge. Under the same hydraulic conditions, $\bar{\alpha}$ of NWC1 was much larger than that of NWS2. This discrepancy might be caused by the source position. As shown in Fig. 17 and by several authors, the maximum vertical diffusivities usually occur at the mid-depth of the flow. Hence, if the source is at that position the vertical mixing is greater than would be the case if the source were near the water surface or near the channel bed. Thus, for source releases near the surface, a longer distance was required for vertical mixing as compared to source releases near mid-depth. For example the distance required for mixing for Runs NWS1 and NWS2 was about seven feet, while for Run NWC1 the distance was 4.9 feet.

eight columns present respectively: (1) the run designation; (2) the section number; (3) distance from the source; (4) the distance between the adjacent section; (5) the estimated dimensionless vertical diffusion coefficient ($\bar{\alpha}$); (6) the estimated dimensionless horizontal diffusion coefficients ($\bar{\beta}$); (7) and (8) are the averaged value of columns (5) and (6) respectively which were obtained by summing the four stations in the multiplication of column (4) by column (5) and then dividing by the distance from the farthest stations to the source.

Discrepancies among $\bar{\alpha}$'s in each section and among $\bar{\beta}$'s were very small for the same run. There was a tendency for $\bar{\alpha}$'s and $\bar{\beta}$'s to become larger in the downstream direction. It is seen that for $\bar{\beta}$'s are almost constant for all runs, the average was about 0.123, which is very close to Prych (1970) and Keefer's (1971) results. Also $\bar{\beta}$'s were much larger than $\bar{\alpha}$'s, the ratio ranges from 3.2 to 1.5, again comparing favorably to Keefer's results. Smallest $\bar{\alpha}$ was observed for the case of NWS1, which involved the smallest discharge. Under the same hydraulic conditions, $\bar{\alpha}$ of NWC1 was much larger than that of NWS2. This discrepancy might be caused by the source position. As shown in Fig. 17 and by several authors, the maximum vertical diffusivities usually occur at the mid-depth of the flow. Hence, if the source is at that position the vertical mixing is greater than would be the case if the source were near the water surface or near the channel bed. Thus, for source releases near the surface, a longer distance was required for vertical mixing as compared to source releases near mid-depth. For example the distance required for mixing for Runs NWS1 and NWS2 was about seven feet, while for Run NWC1 the distance was 4.9 feet.

With the same hydraulic conditions, the average $\bar{\alpha}$ of runs NWS2 and NWC1 was 0.0685, while the depth-averaged $\bar{\alpha}$ was 0.067 as stated in section 2.2-3, the former being only two percent larger than the latter.

Reasons for the particularly small $\bar{\alpha}$ for run NWS1 are: (1) the source position which was near the water surface where the vertical diffusivity was small; (2) the small Reynolds number, and (3) less turbulence.

6.3 Numerical Results with Wind Wave Effects

6.3-1 The Tracer Fall Velocity

With wind blowing over the water surface, waves developed. This oscillating wave action significantly changed the pattern of the vertical diffusivities and the mixing process. From the experimental results, it was observed that the wind waves had the effect of forcing the tracer downward. In the beginning of the numerical analysis no tracer fall velocity was considered and the comparison of the concentration profiles between numerical and experimental results was poor, until a reasonable fall velocity was considered in Eq. (2-8) in accordance with the following:

$$u \frac{\partial c}{\partial x} = \frac{\partial}{\partial y} (\epsilon_y \frac{\partial c}{\partial y}) + \frac{\partial}{\partial z} (\epsilon_z \frac{\partial c}{\partial z}) + V_S \frac{\partial c}{\partial y} \quad (6-3)$$

where V_S is the tracer fall velocity and is positive in the downward direction. The dimensionless form becomes

$$\phi(y) \frac{\partial c}{\partial \xi} = \frac{\partial}{\partial \eta} (\alpha(y) \frac{\partial c}{\partial \eta} + F_a c) + \bar{\beta} \frac{\partial^2 c}{\partial \tau^2} \quad (6-4)$$

in which $F_a = V_S/U_*$, the dimensionless tracer fall velocity. The boundary conditions at the water surface and at the bed becomes

$$\alpha(y) \frac{\partial c}{\partial \eta} + F_a c = 0 \quad (6-5)$$

6.3-2 The Concentration Profiles

The numerical results of the concentration profiles of runs WS1, WS2, WS3 and WC1 are shown by the solid line in Figs. 35 through 42. Pertinent information and results of this study are summarized in Table 3. In addition to values tabulated in Table 2, several additional columns are included, they are: column (5) the wind velocity, (6) the average wave height, (7) the dominant frequency of the waves, (10) the estimated dimensionless fall velocity F_a , and (13) the averaged F_a . Estimation of the diffusivities and tracer fall velocities were more complex than those without wind effect, because of the unknown parameter F_a involved in the diffusion equation (Eq. 6-2). The agreement of the concentration profiles between experimental and numerical results is not as favorable as those without wind. The position of the maximum concentration at successive stations for the same run was lower. The horizontal concentration profiles were symmetric about the axial plane of the channel since the water wave action in the rectangular straight channel was substantially two-dimensional.

From Table 3, it is seen that under any condition of wind velocity and/or source position, the $\bar{\beta}$'s are almost the same and close to the values in Table 2, being perhaps slightly smaller. Variation of the $\bar{\alpha}$'s and the fall velocities largely depends on the wind velocity. Values of $\bar{\alpha}$'s tend to increase downstream but the variations are small. Smallest $\bar{\alpha}$ was observed for run WS1, which has the smallest Reynolds number and wind velocity. Obviously, larger wind velocity yielded larger $\bar{\alpha}$'s which was slightly affected by the source position. This phenomenon can be explained by the shape of the evaluated vertical

Table 3. Summary of Numerical Results (with wind).

Run No.	Sect. No.	Dist. From Source (ft)	Dist. Between Adj. Sect. (ft)	Wind Velocity (ft/sec)	Av. Wave Height (inch)	Dominant Frequency (Hz)	Estimated $\bar{\alpha}$	Estimated $\bar{\beta}$	Estimated F_a	Average $\bar{\alpha}$	Average $\bar{\beta}$	Average F_a
(1)	(2)	(3)	(4)	(5)	(6)	(7)	(8)	(9)	(10)	(11)	(12)	(13)
WSI	3	1.61	1.61				0.045	0.100	0.002			
	5	2.95	1.34	16.5	0.041	9.00	0.045	0.100	0.002	0.045	0.106	0.002
	8	4.86	1.91				0.045	0.100	0.002			
	11	7.03	2.17				0.045	0.120	0.002			
WS2	3	1.61	1.61				0.076	0.110	0.095			
	5	2.95	1.34	26.3			0.076	0.110	0.098	0.078	0.114	0.129
	7	4.20	1.25				0.076	0.110	0.135			
	9	5.53	1.33				0.083	0.125	0.195			
WS3	2	1.11	1.11				0.134	0.095	0.615			
	3	1.61	0.50	39.8	0.610	5.00	0.134	0.095	0.615	0.136	0.107	0.644
	4	2.36	0.75				0.134	0.095	0.625			
WC1	6	3.53	1.17				0.140	0.130	0.695			
	3	1.61	1.61				0.073	0.110	0.092			
	4	2.36	0.75	27.5	0.202	7.40	0.073	0.110	0.092	0.074	0.110	0.120
	6	3.53	1.17				0.075	0.110	0.115			
	8	4.86	1.33				0.075	0.110	0.175			

diffusivities (Fig. 18) where $\bar{\alpha}$'s near the water surface and the mid-depth are not much different.

6.3-3 Properties of the Water Surface

The characteristics of the water surface should be an important factor affecting the diffusion process. The source was always kept at a constant fetch, and the measurements were made at a short distance downstream from the source (maximum eight ft). Over this short range, variations of the wave height and dominant frequency were small and were considered to be negligible. For the same wind velocity, it was difficult to detect variations for the $\bar{\alpha}$'s, F_a and the fetches, wave heights and dominant frequencies. Figures 43 through 45 show the variations between the dimensionless vertical diffusivities, tracer fall velocities and the wind velocities, wave height and dominant frequencies respectively, at nearly the same fetch but different wind conditions.

6.4 Contours of Normalized Concentration

The numerical results of the contours of normalized concentration profiles on four cross-sections of each case are shown in Fig. 46 through 52. From these figures it is easier to see how the tracer diffuses vertically and laterally. The wind wave effect on the diffusion process can also be seen in that the tracer always occupied a larger region in a shorter distance when the wind was blowing over the water surface. Two cells symmetric to the axial-plane appeared on Figs 50 and 51 for the cases of medium and high wind velocity. This phenomena might be caused by tracer fall velocity considered in the numerical analysis. None was observed when F_a was considered zero.

The results of this SUMMARY AND CONCLUSIONS

7.1 Summary

This study concerned the mixing process with and without wind wave phenomena in straight, wide, open channels.

effect. A dimensionless diffusion equation for the two-dimensional,

rectangular, wide open channel was established and a numerical integra-

tion of the partial differential equation by the Alternating-Direction-implicit method was performed.

The experimental arrangements and procedures were described in

Chapter III. Experiments were performed in a straight, rectangular,

wind-water tunnel without wind effect and with the wind blowing over the

water surface. Significant effect on diffusion was observed with wind

position. Large depth-averaged mixing coefficients were found when the

source was near the mid-depth of the water. This observation supports

the Reynolds analogy of equivalence of mass and momentum transfer.

vertical diffusion coefficient was evaluated from measured velocities.

Results showed that the longitudinal mixing coefficient was ten (no wind)

to 20 (with wind) times greater than the vertical diffusion coefficient.

The longitudinal concentration gradients were found to be about several

hundreds smaller than those in the vertical and horizontal directions.

Hence, the longitudinal diffusion term in the diffusion equation (Eq.

2-7) may be neglected and the numerical solution of Eq. (2-8) should

closely approximate the solution of Eq. (2-7).

The wind effect on the diffusion process was considered and

depth. This phenomena can be explained by the profiles of the verti-

cal diffusivities. As shown in Fig. 16, the variations of the diffusiv-

ities at the upper half of the water depth were small.

7.2 Conclusions

The results of this study lead to several conclusions:

1. The three-dimensional diffusion equation without the longitudinal mixing term is adequate for analyzing the vertical and lateral mixing phenomena in straight, wide, open channels.

2. Mixing with no wind:

A. The dimensionless lateral mixing coefficients are nearly a constant and independent of the hydraulic conditions. The values obtained from these studies are in reasonable agreement with those reported by previous investigators.

B. The vertical mixing coefficients are largely affected by the hydraulic conditions, particularly the Reynolds number and the source position. Large depth-averaged mixing coefficients were found when the source was near the mid-depth of the water. This observation supports the Reynolds analogy of equivalence of mass and momentum transfer.

3. Mixing with wind:

A. Vertical mixing rates were significantly increased when waves appeared on the water surface. The dimensionless lateral diffusion coefficients were slightly decreased. The phenomenon was also reported by Chang (1971) that dimensionless lateral dispersion coefficients were found to decrease with increase of bed roughness.

B. At a certain wind velocity (i.e., 27 fps for runs WS2 and WC1), the vertical mixing rate was only slightly affected by the source position, particularly when located at the upper half of the water depth. This phenomenon can be explained by the profiles of the vertical diffusivities. As shown in Fig. 18, the variations of the diffusivities at the upper half of the water depth were small.

C. When the wind was blowing over the water surface, although the tracer was neutrally buoyant, a continuous interchange of the fluid particles occurred through the wave action in the upper layer of the water which was convected by the wind produced drift velocity near the water surface. Hence, the cross-sectional maximum concentration occurred at successively lower depths in the longitudinal direction giving rise to an apparent tracer "fall velocity."

7.3 Suggestions for Future Research

1. Additional experiments could include the effect of bed roughness on mixing rates.

2. Further experiments are suggested to understand more completely the phenomena of the apparent fall velocity.

3. More experiments under the same wind velocity but different fetches of source position are considered an important next step.

4. The ability to predict the mixing process beyond the diffusion cone (vertically and laterally) is important to water pollution control, it might directly affect the location and design of the effluent system. Further experiments are needed.

5. Further experiments on the upstream wind effect, the source position effect and the overall effect of the position-dependent vertical and lateral mixing coefficients on the diffusion process are needed to learn more about the mixing phenomena.

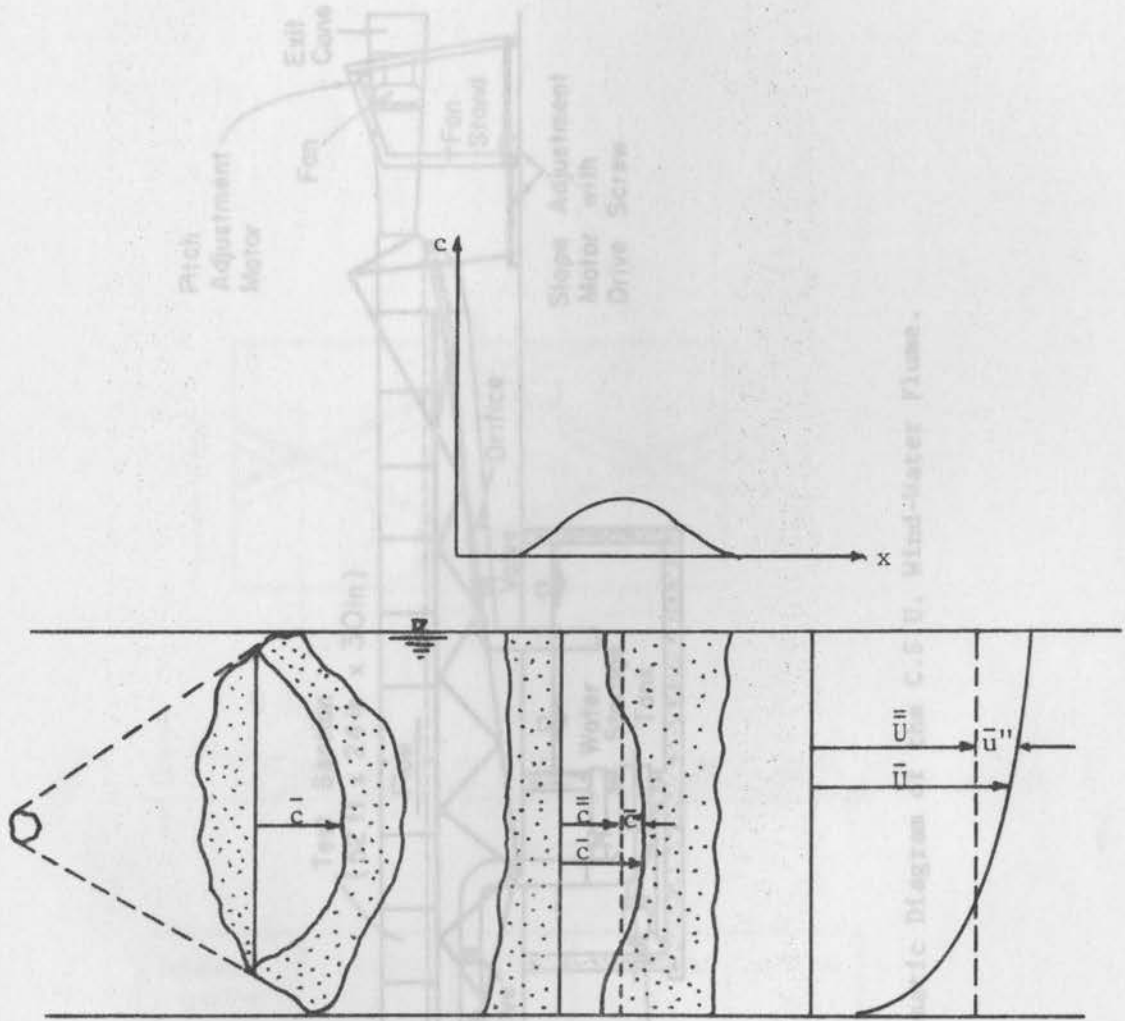


Fig. 1. One-Dimensional Transport, Definition Sketch.

Fig. Schematic Diagram C.S.F.U. Wind-Water Pump.

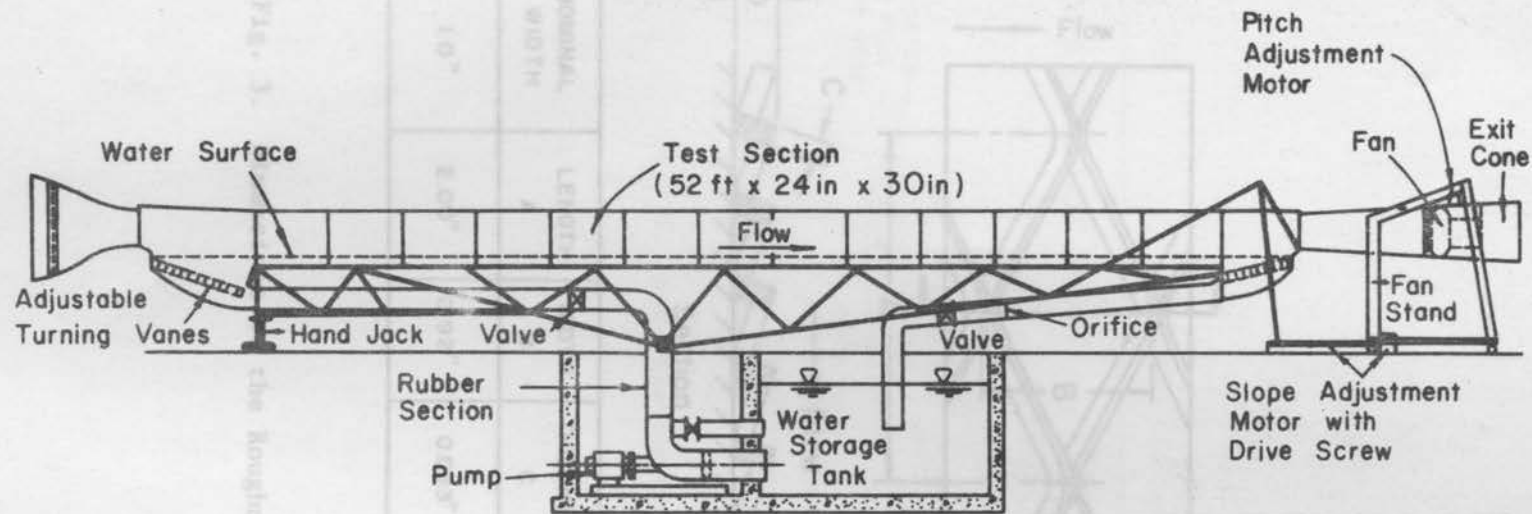


Fig. 2. Schematic Diagram of the C.S.U. Wind-Water Flume.

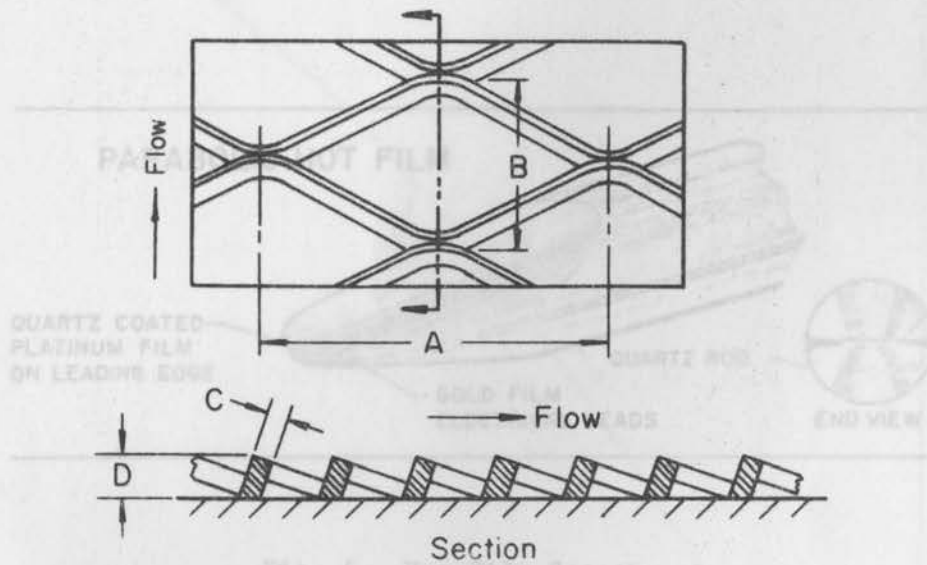


Fig. 4. Wheatstone Sensor.

NOMINAL WIDTH	LENGTH A	WIDTH B	THICKNESS C	DEPTH D
1.0"	2.00"	0.92"	0.093"	0.197"

Fig. 3. Dimensions of the Roughness Mesh.

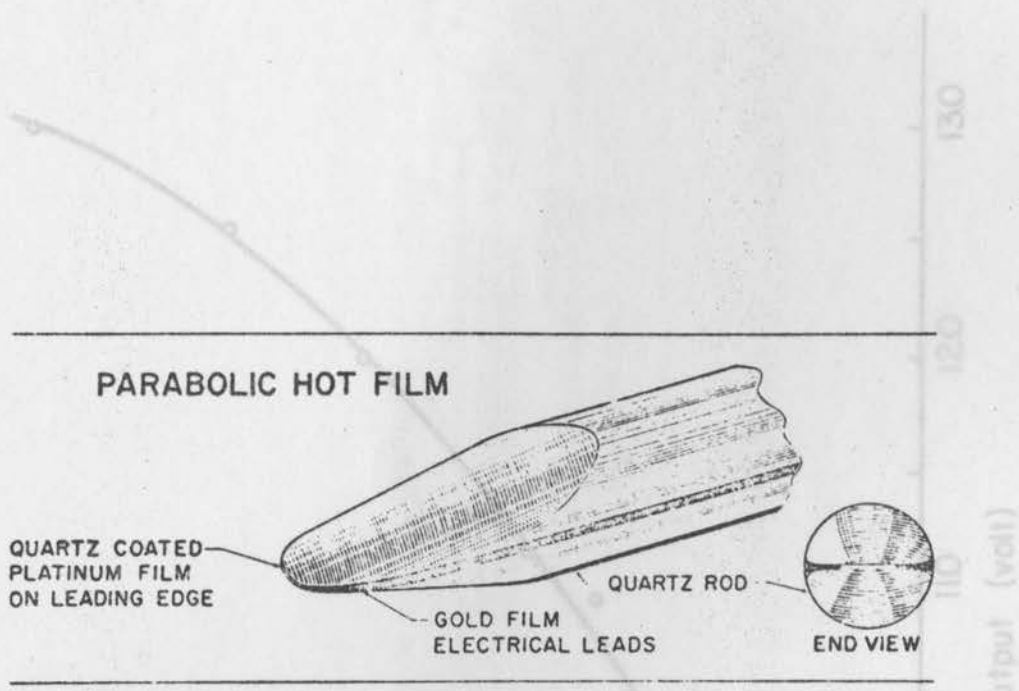


Fig. 4. Hot-Film Sensor.

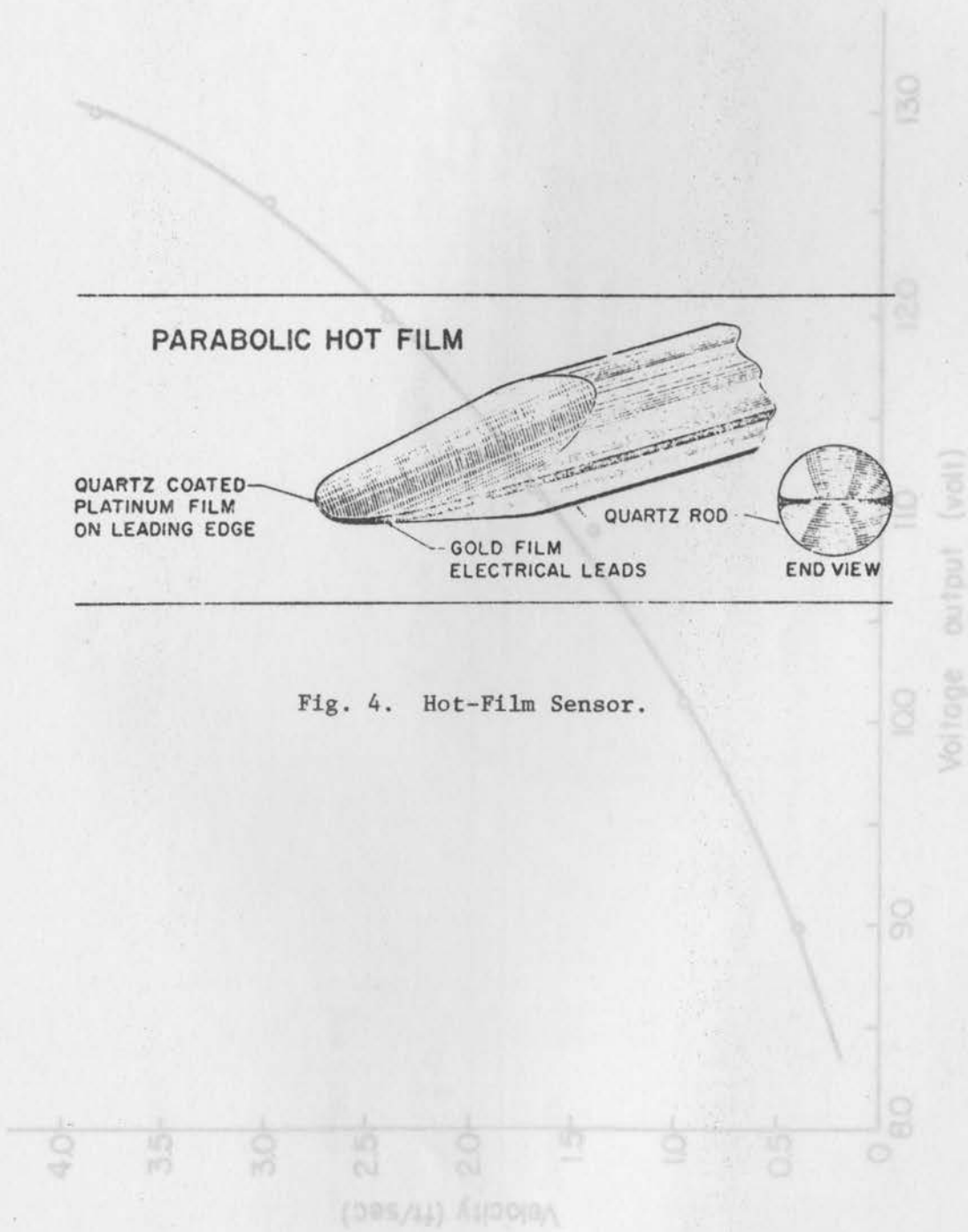


Fig. 5. Calibration Curve of Hot-Film Sensor.

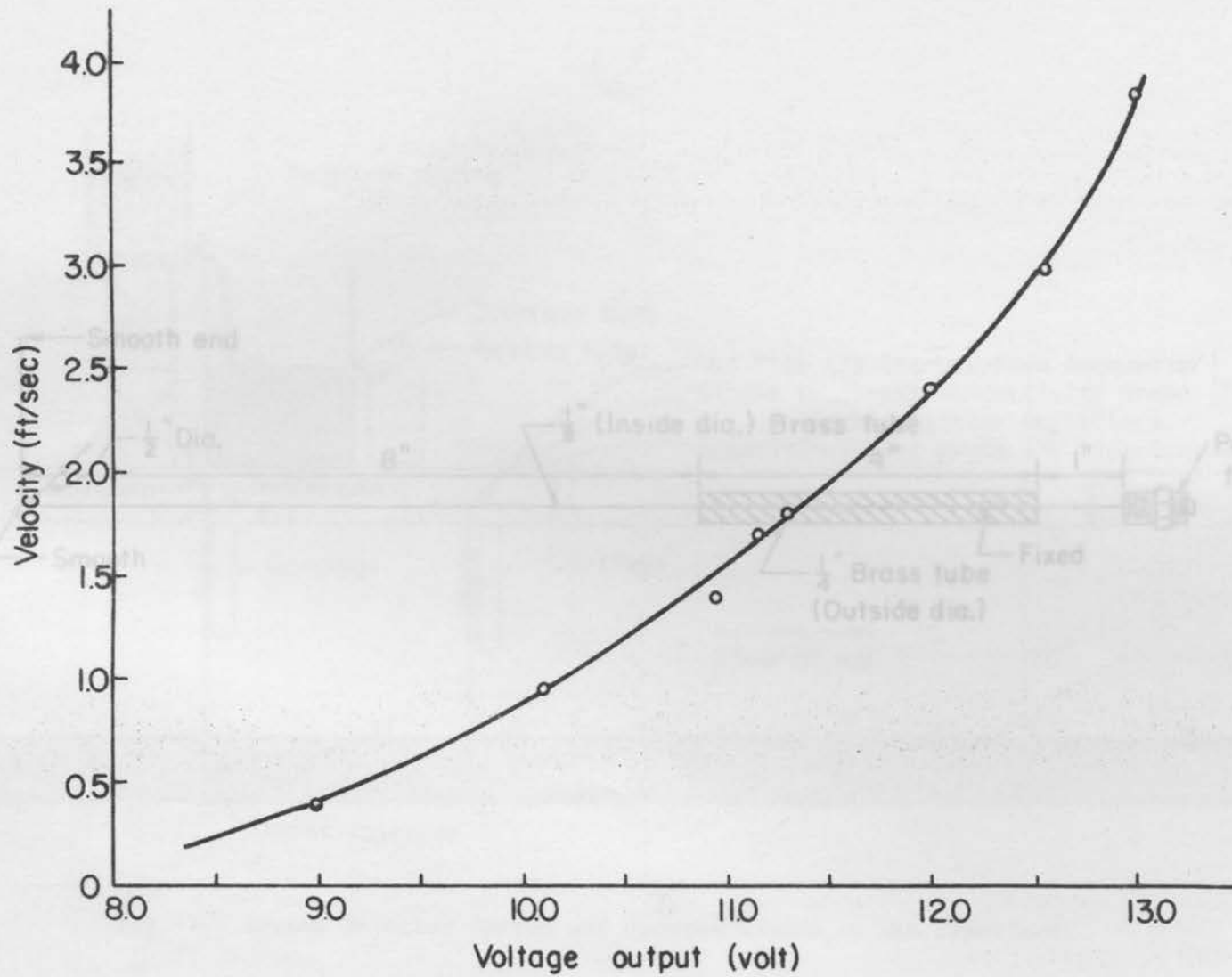


Fig. 5. Calibration Curve of Hot-Film Sensor.

Fig. 6. Tracer Injector

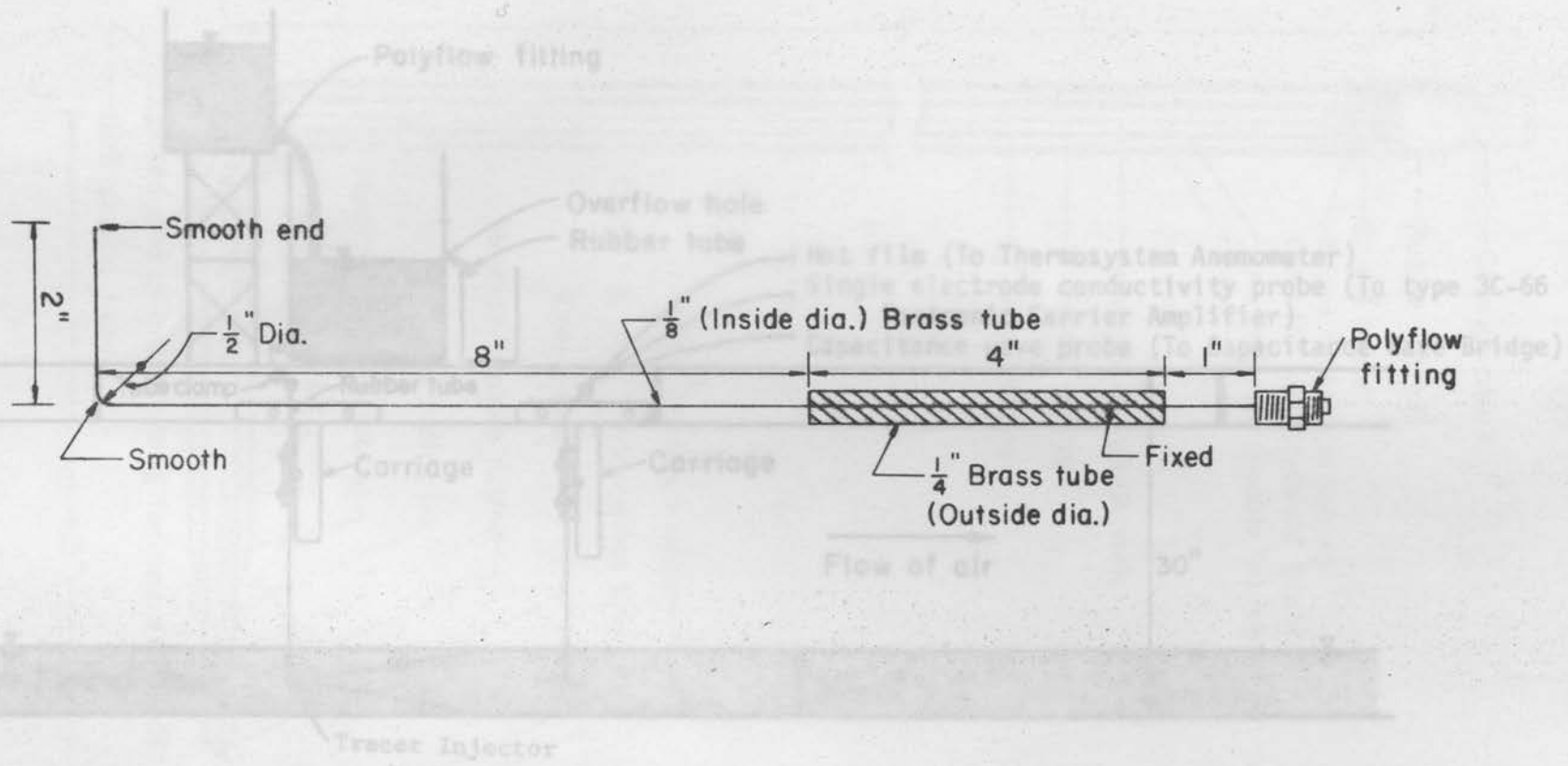


Fig. 7. Tracer Injector System and General Layout of the Experiment.

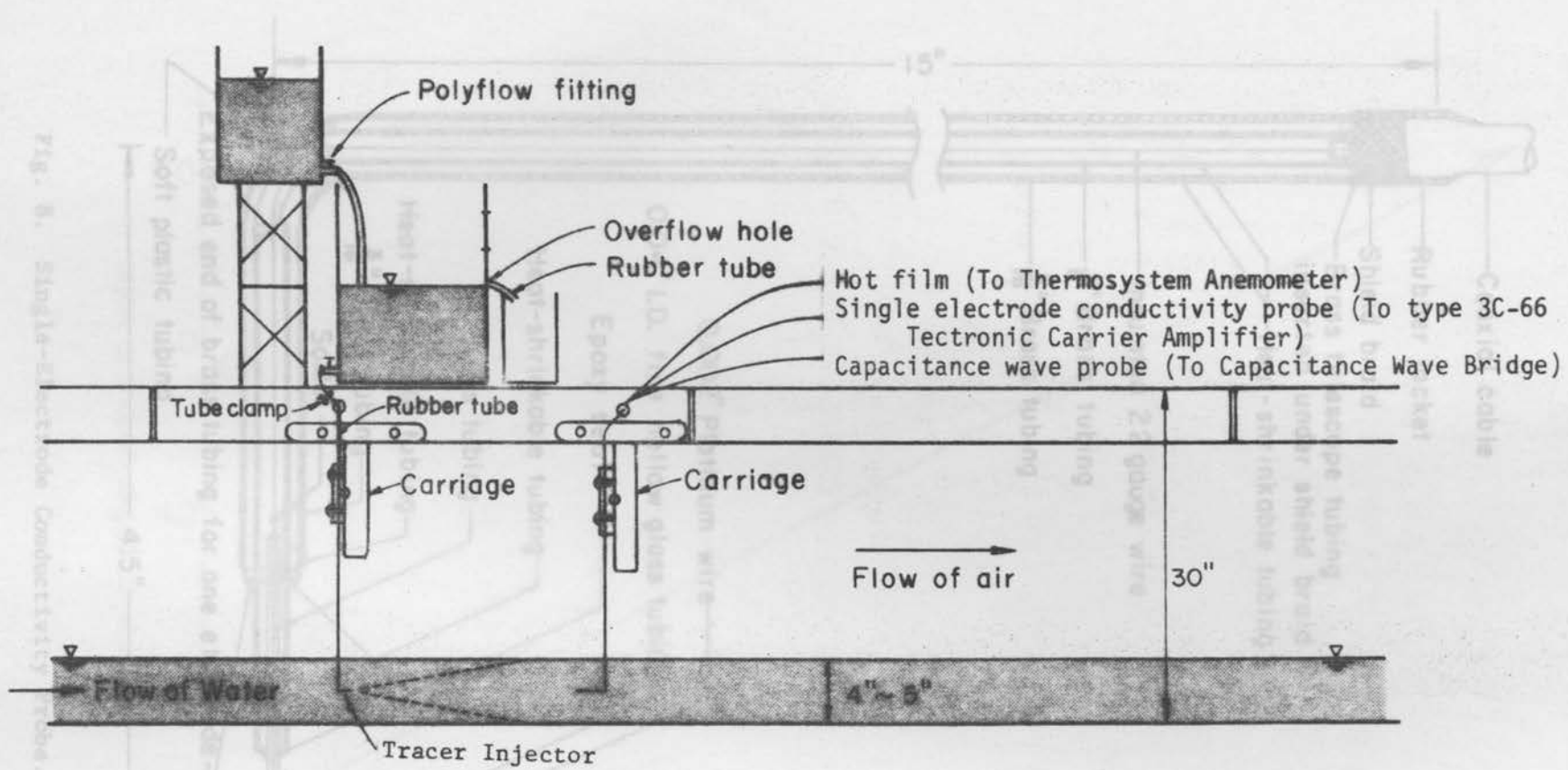


Fig. 7. Tracer Injector System and General Layout of the Experiment.

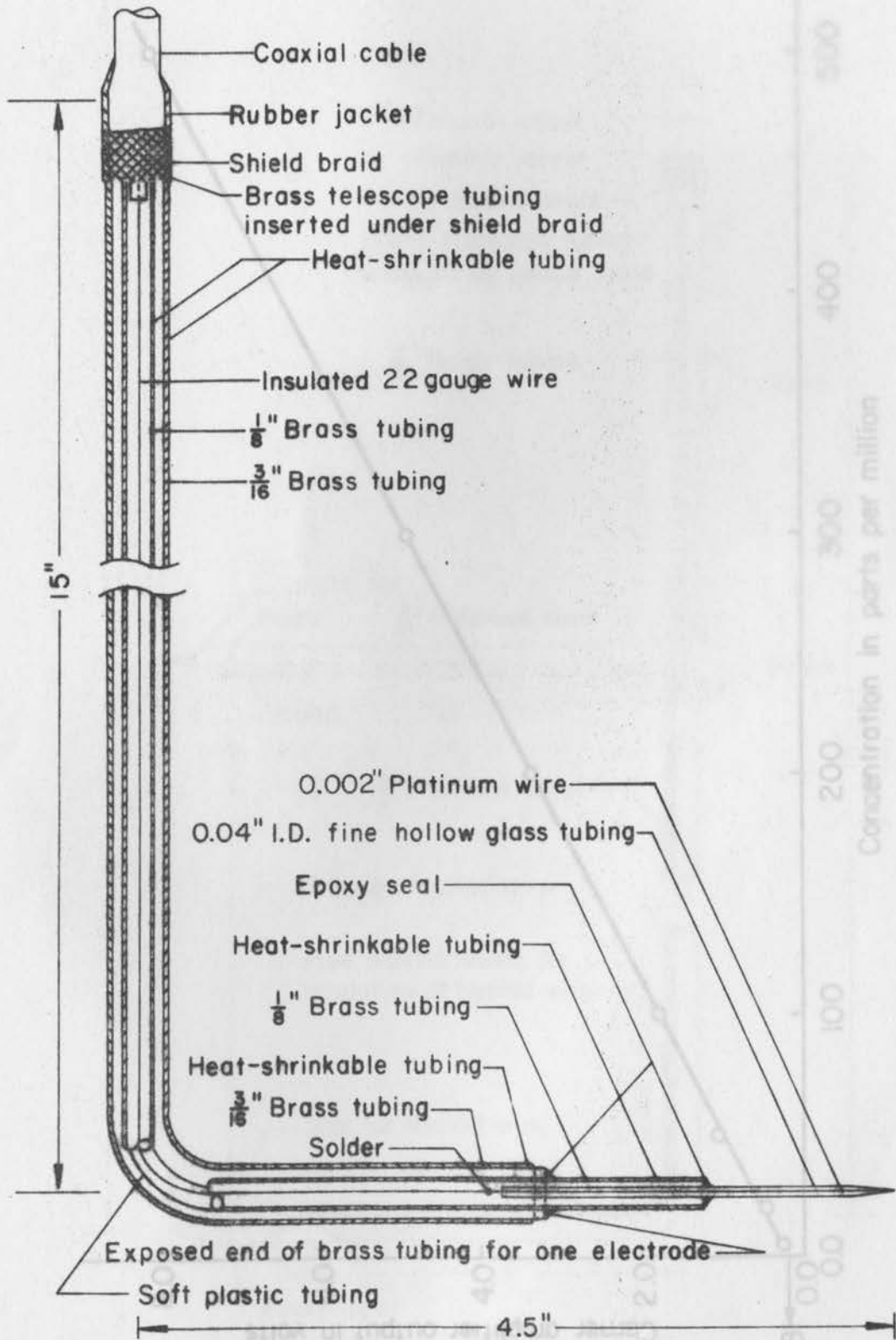


Fig. 8. Single-Electrode Conductivity Probe.

Fig. 9. Calibration Curve of Single-Electrode Conductivity Probe.

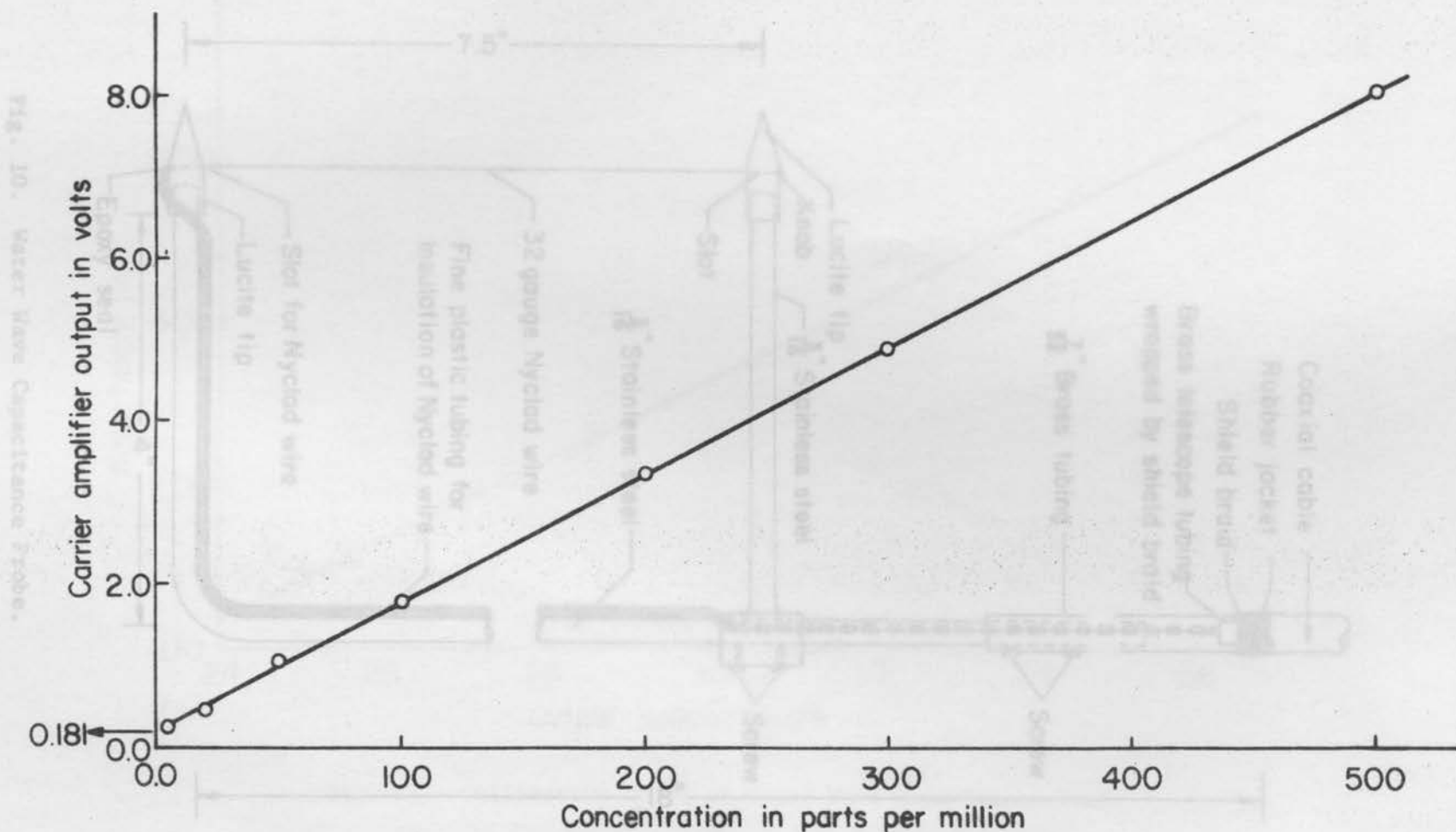


Fig. 9. Calibration Curve of Single-Electrode Conductivity Probe.

Fig. 10. Water Wave Capacitance Probe.

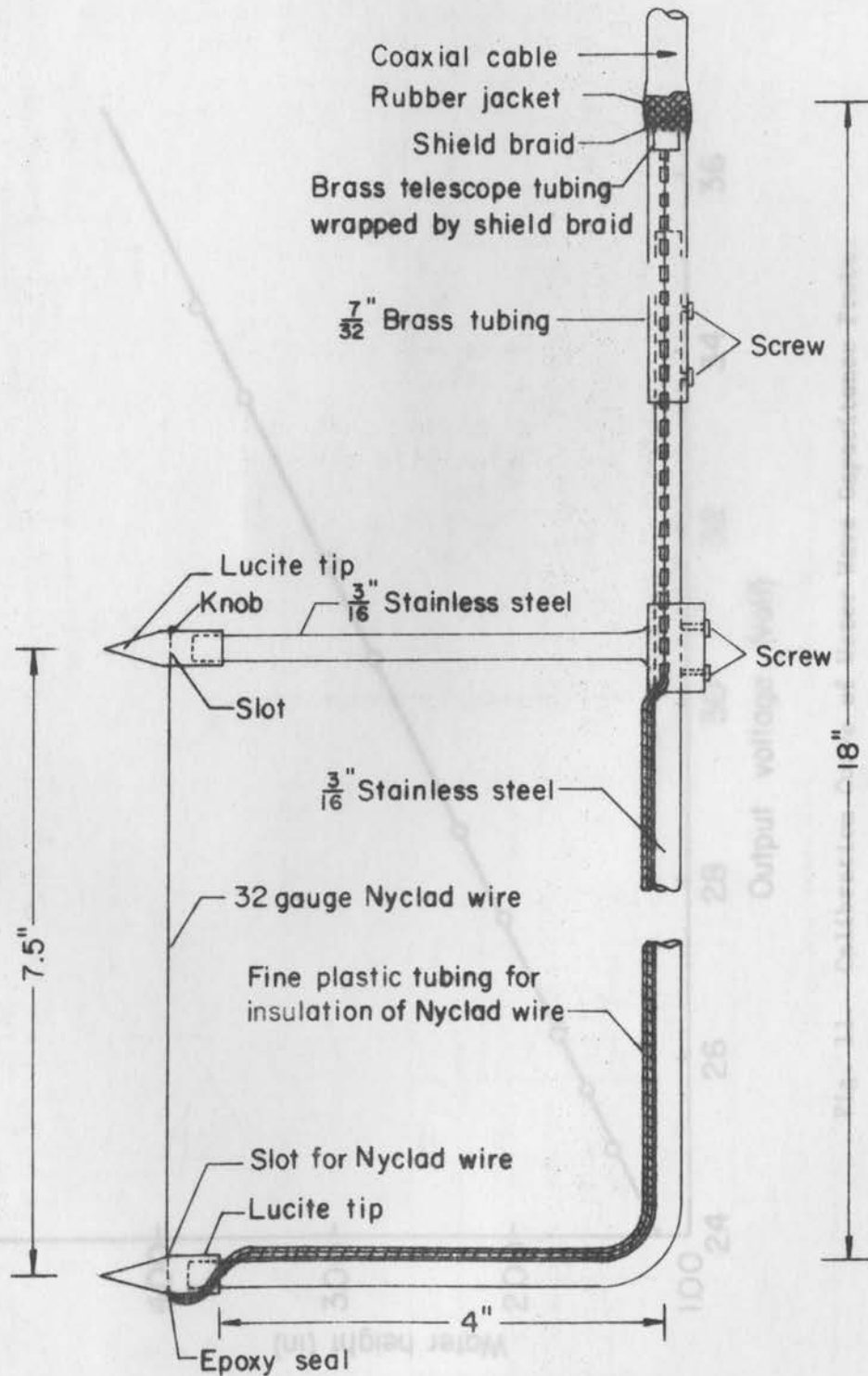


Fig. 10. Water Wave Capacitance Probe.

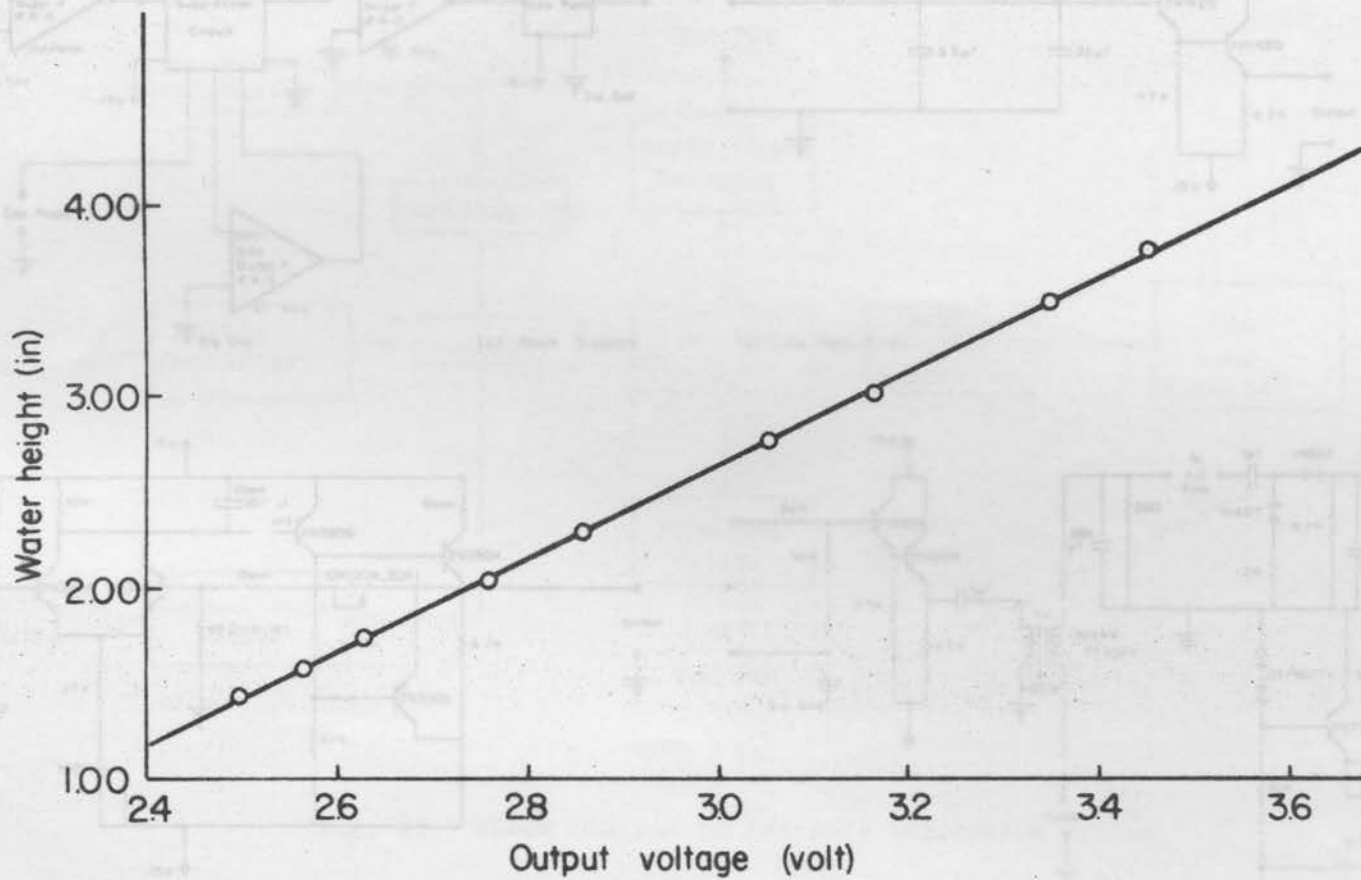
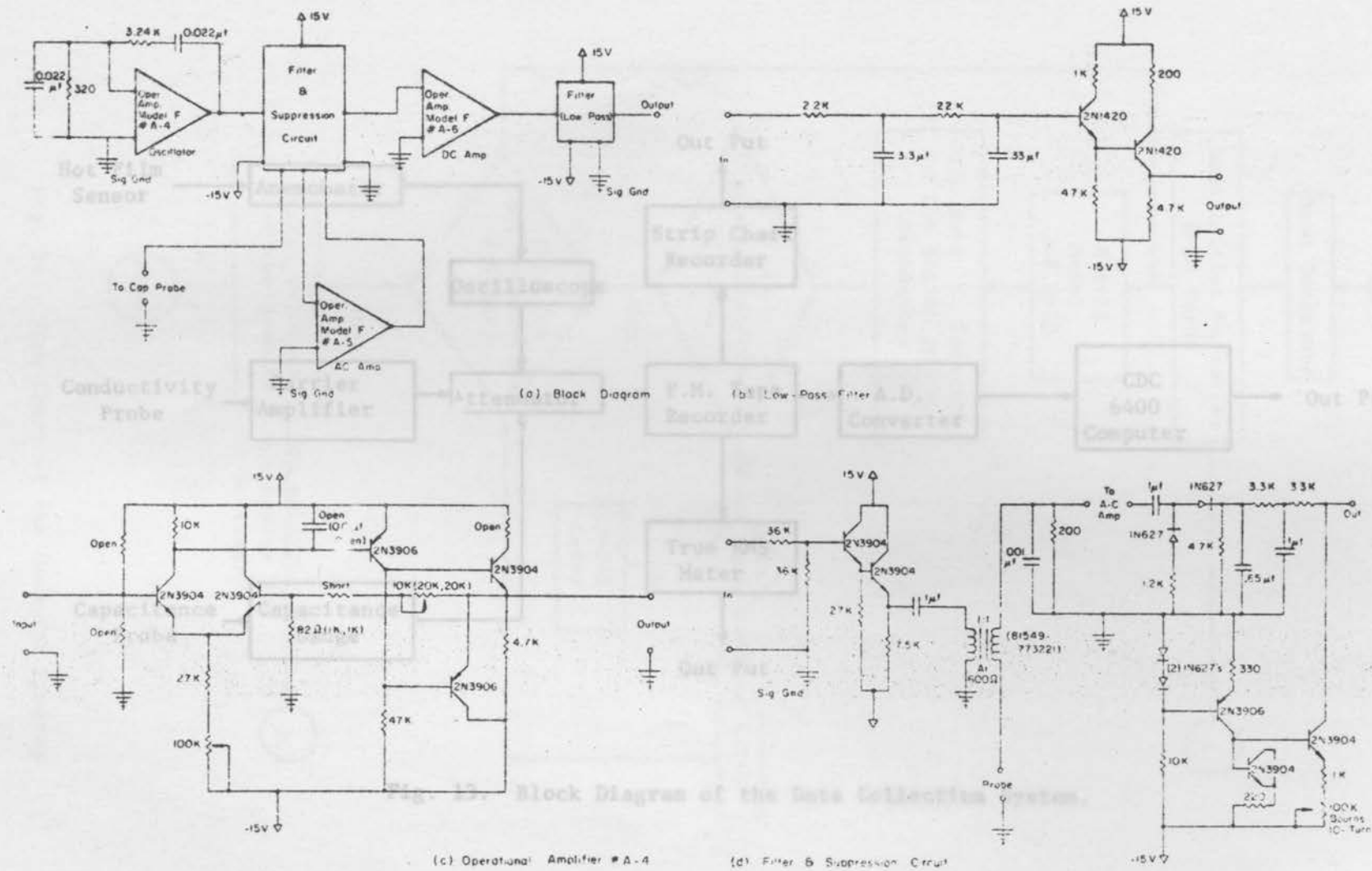


Fig. 11. Calibration Curve of Water Wave Capacitance Probe.

Fig. 12. Schematic and Block Diagram of the Capacitance Bridge.



Note: The values in parenthesis are for Models #5 B #6

Fig. 12. Schematic and Block Diagram of the Capacitance Bridge.

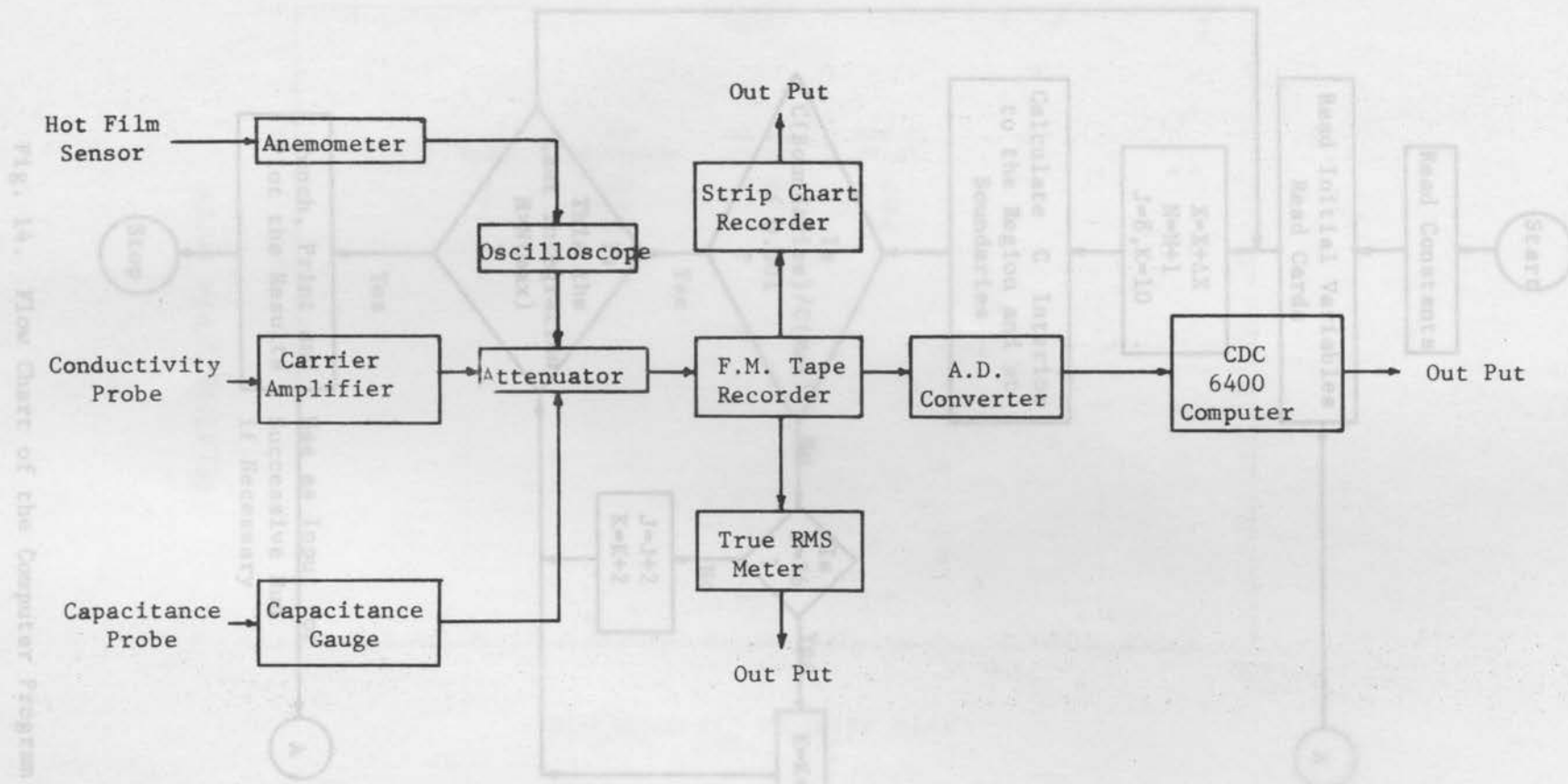


Fig. 13. Block Diagram of the Data Collection System.

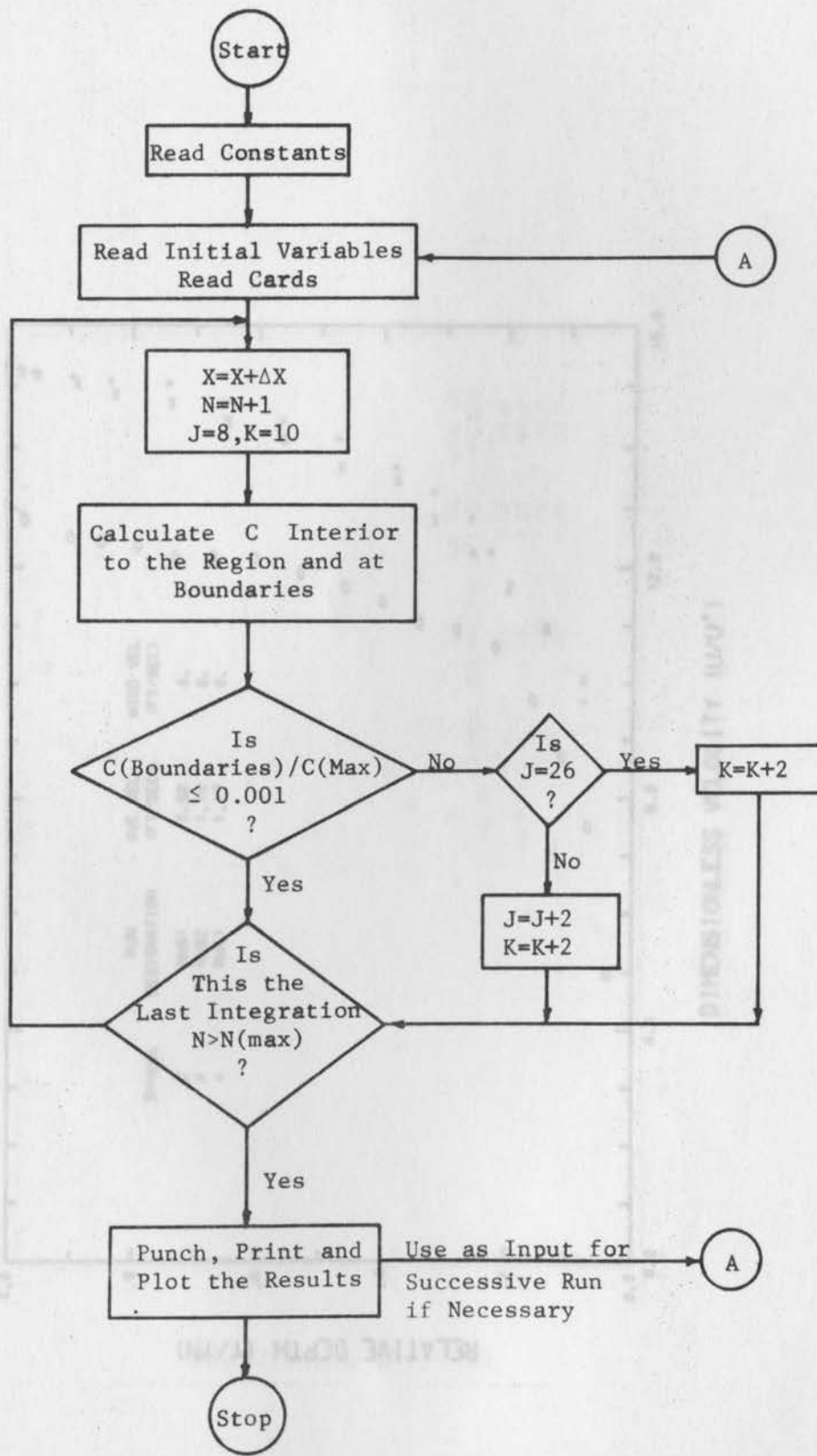


Fig. 14. Flow Chart of the Computer Program

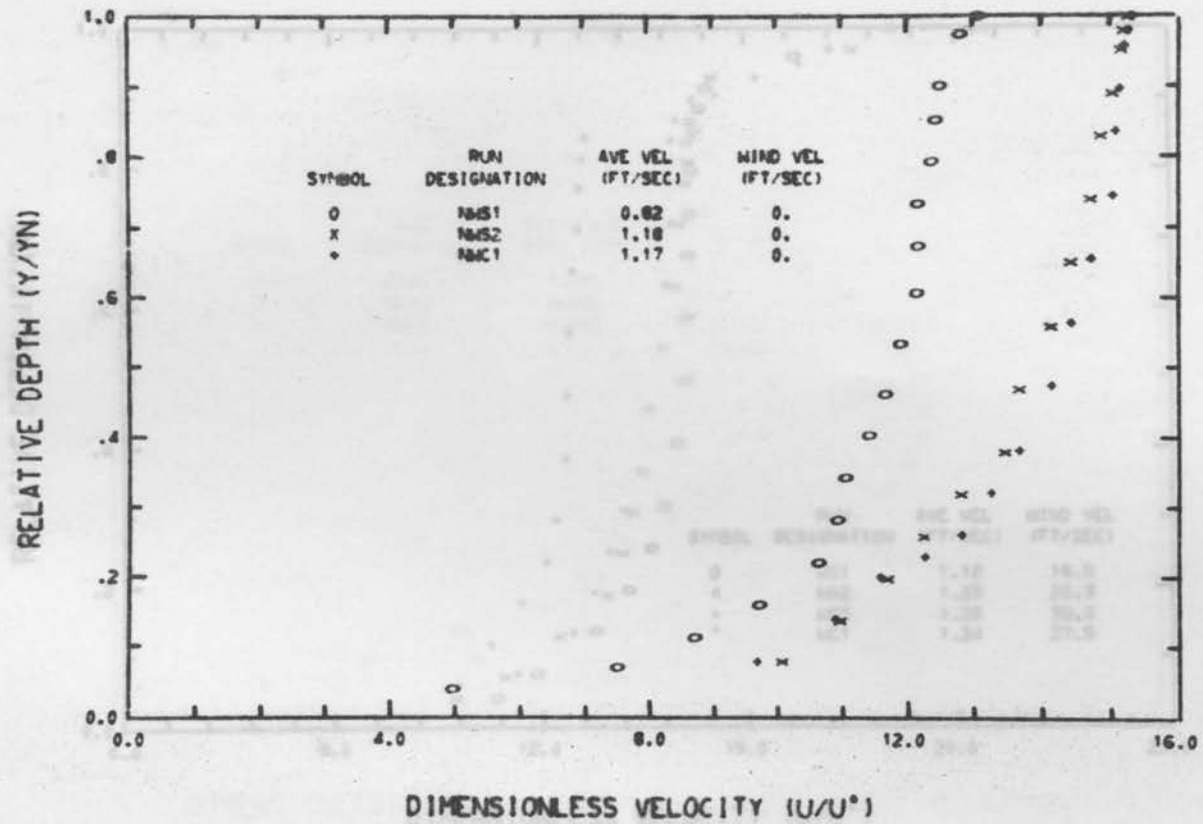


Fig. 15. Non-Dimensionalized Velocity Profile (without wind).

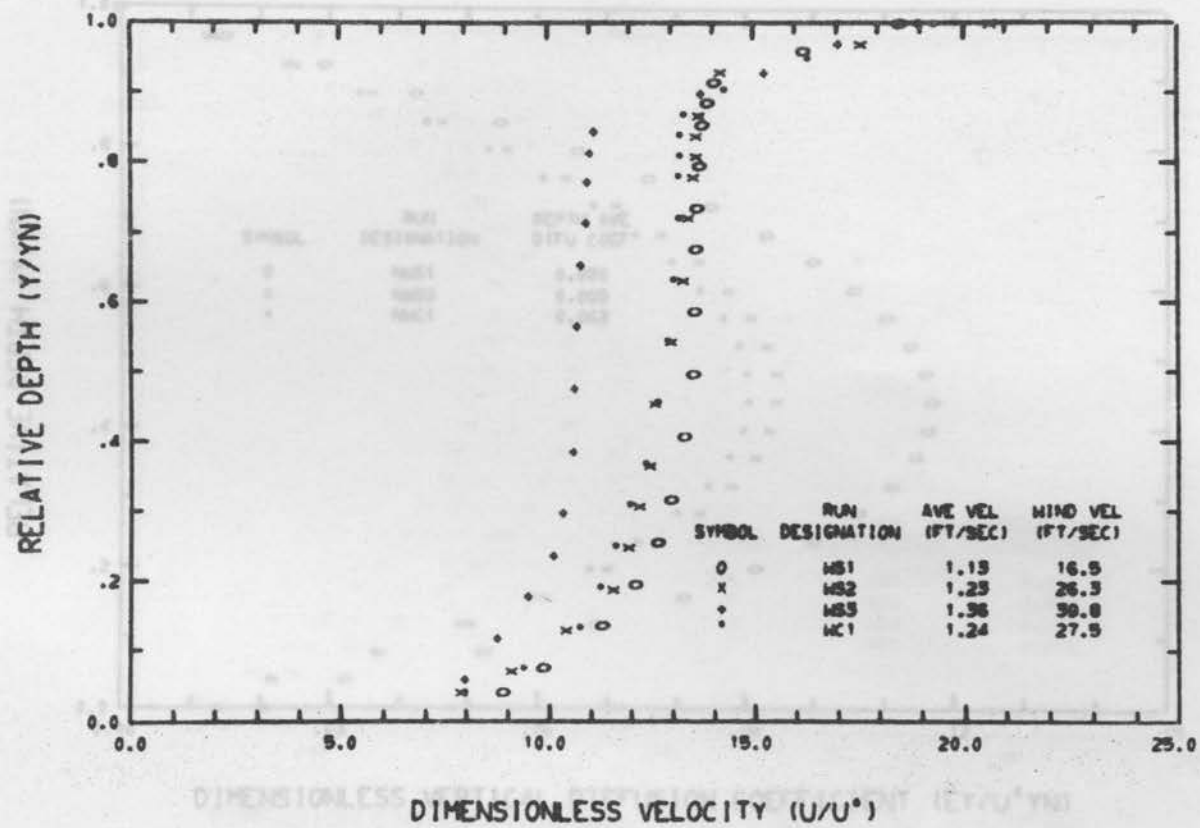


Fig. 16. Non-Dimensionalized Velocity Profile (with wind).

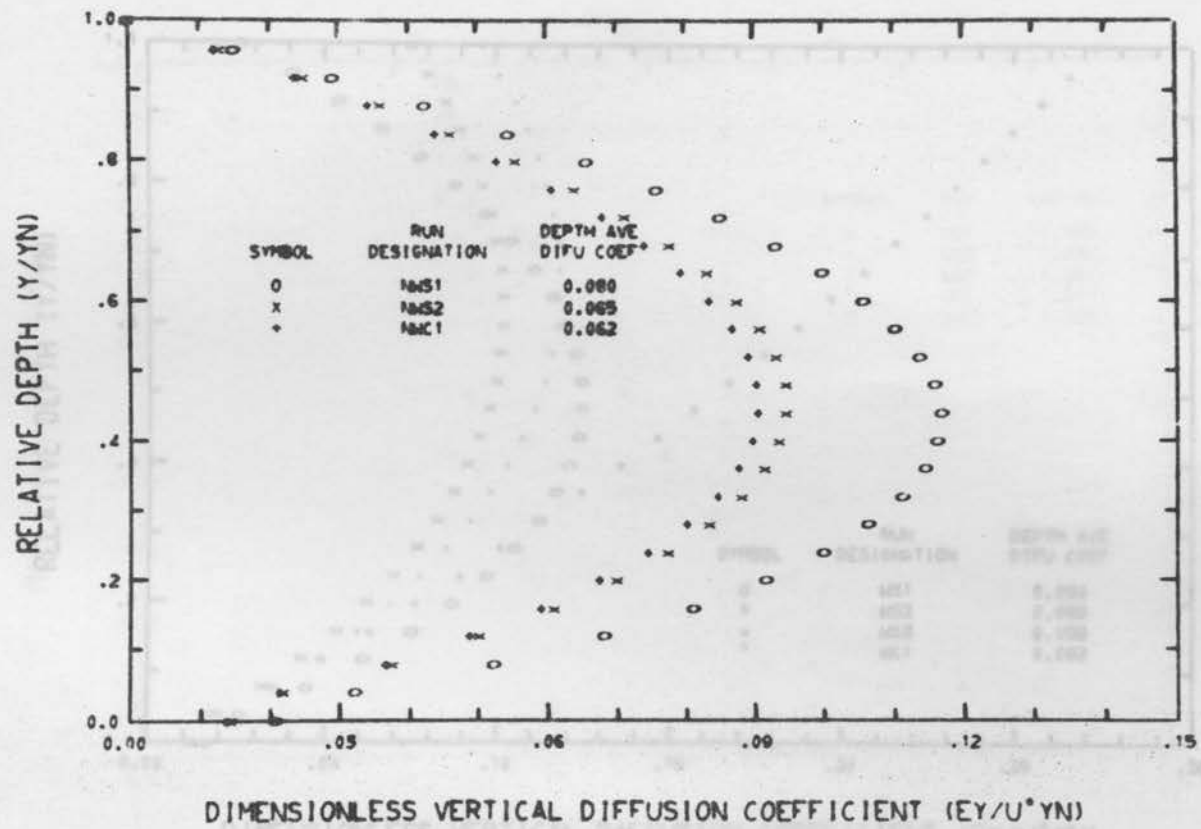


Fig. 17. Dimensionless Vertical Diffusion Coefficients (without wind).

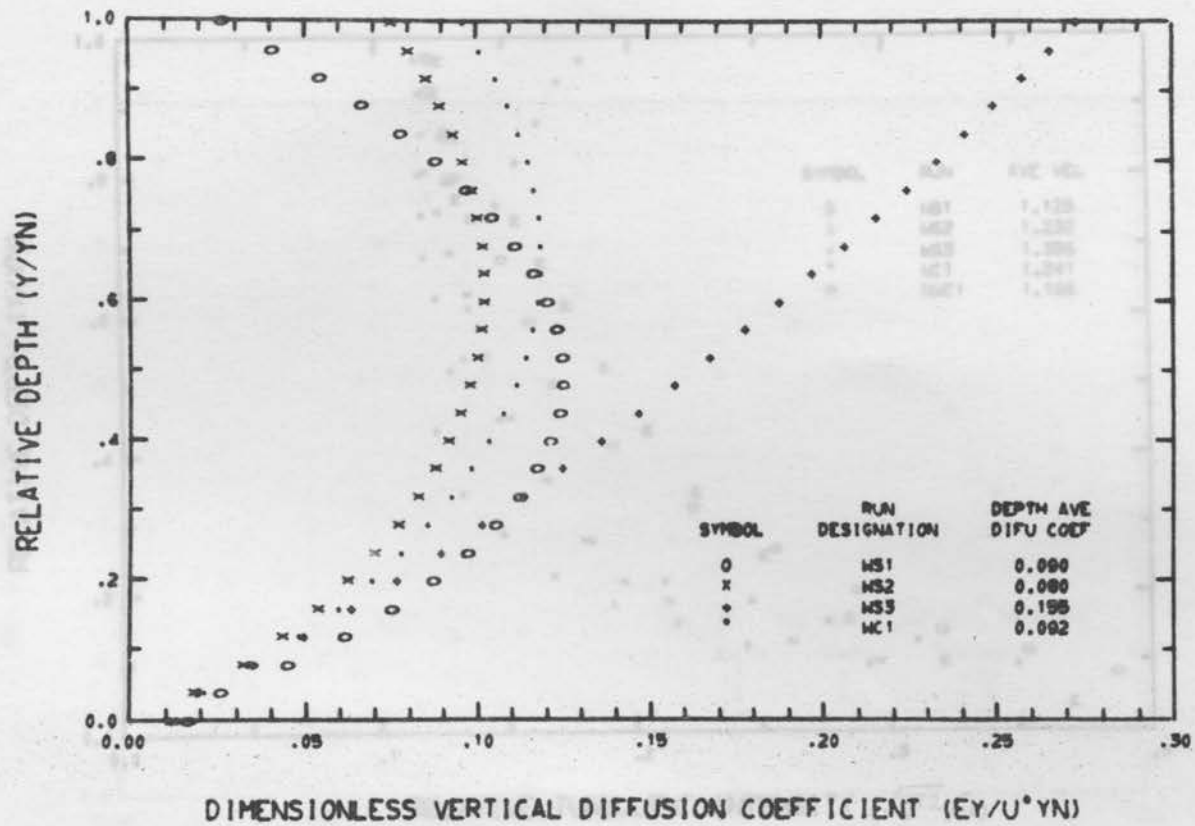


Fig. 18. Dimensionless Vertical Diffusion Coefficients (with wind).

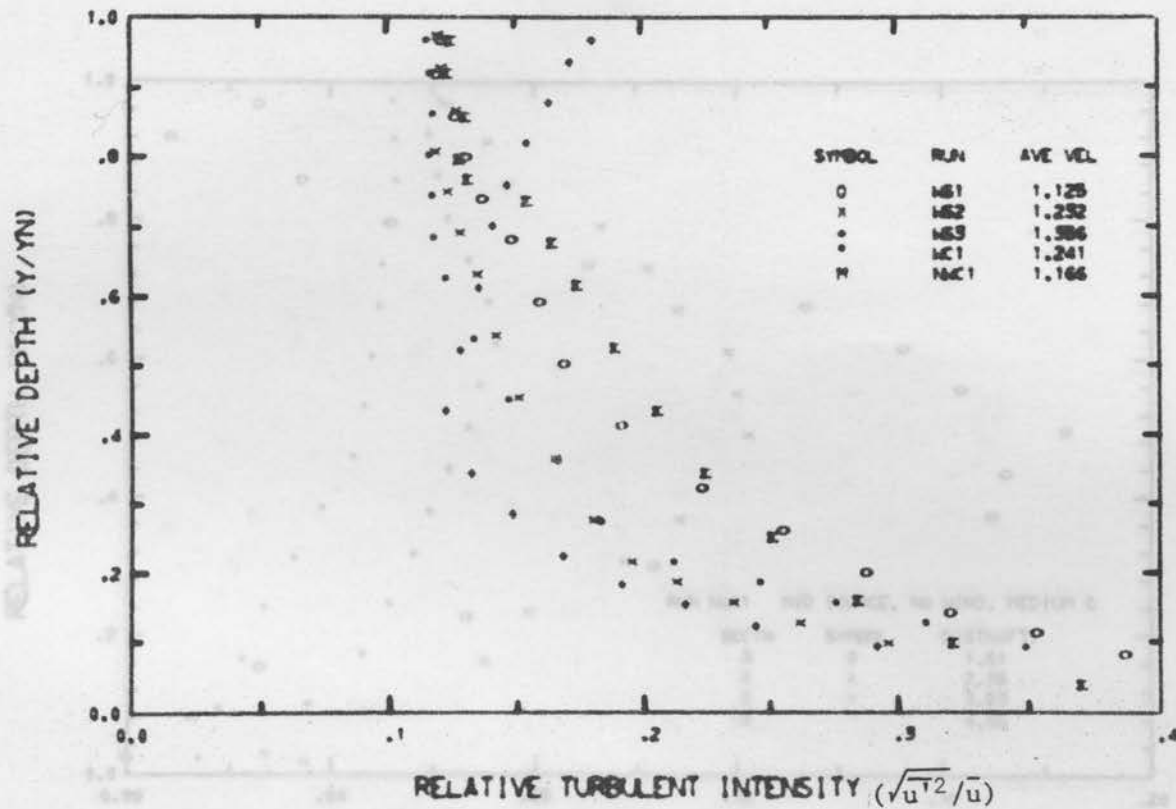


Fig. 19. Relative Turbulent-Intensity of Water Velocity.

Fig. 20. Relative Intensity of Concentration Fluctuations, Run 165 (vertically).

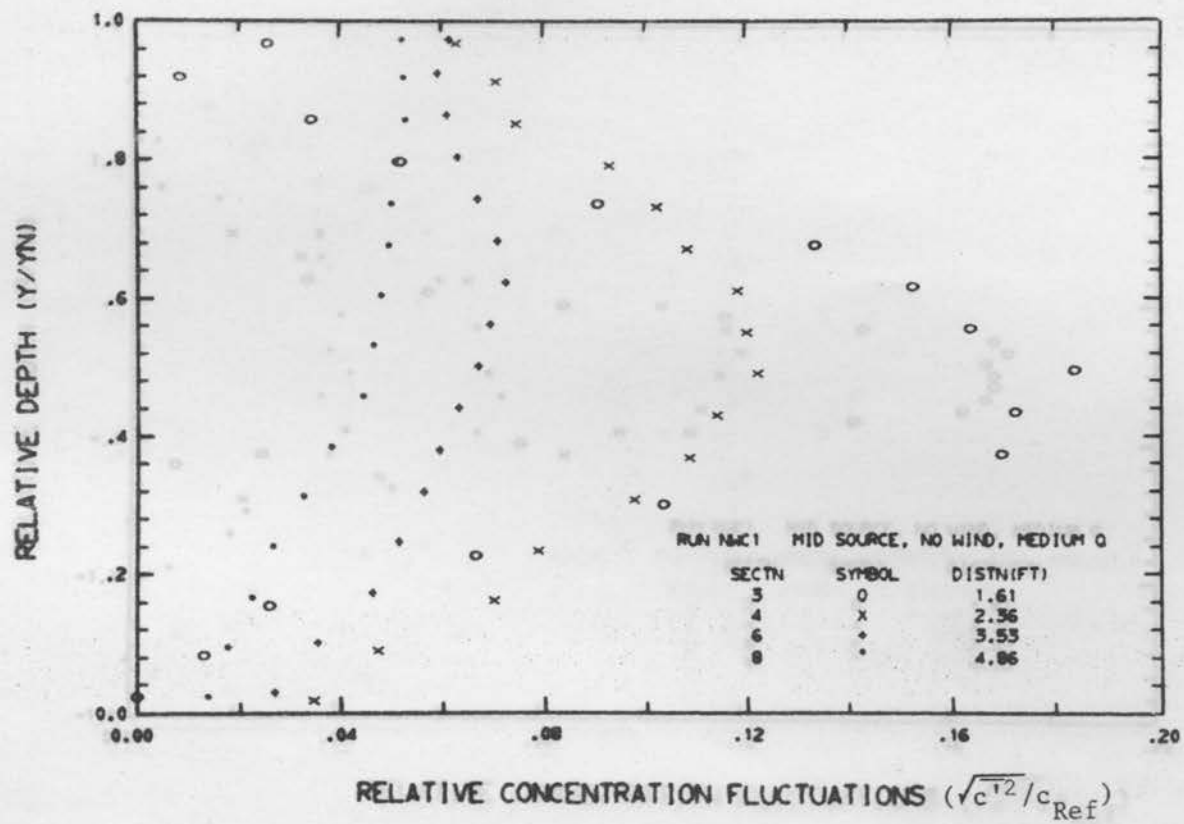


Fig. 20. Relative Intensity of Concentration Fluctuations, Run NWC1 (vertically).

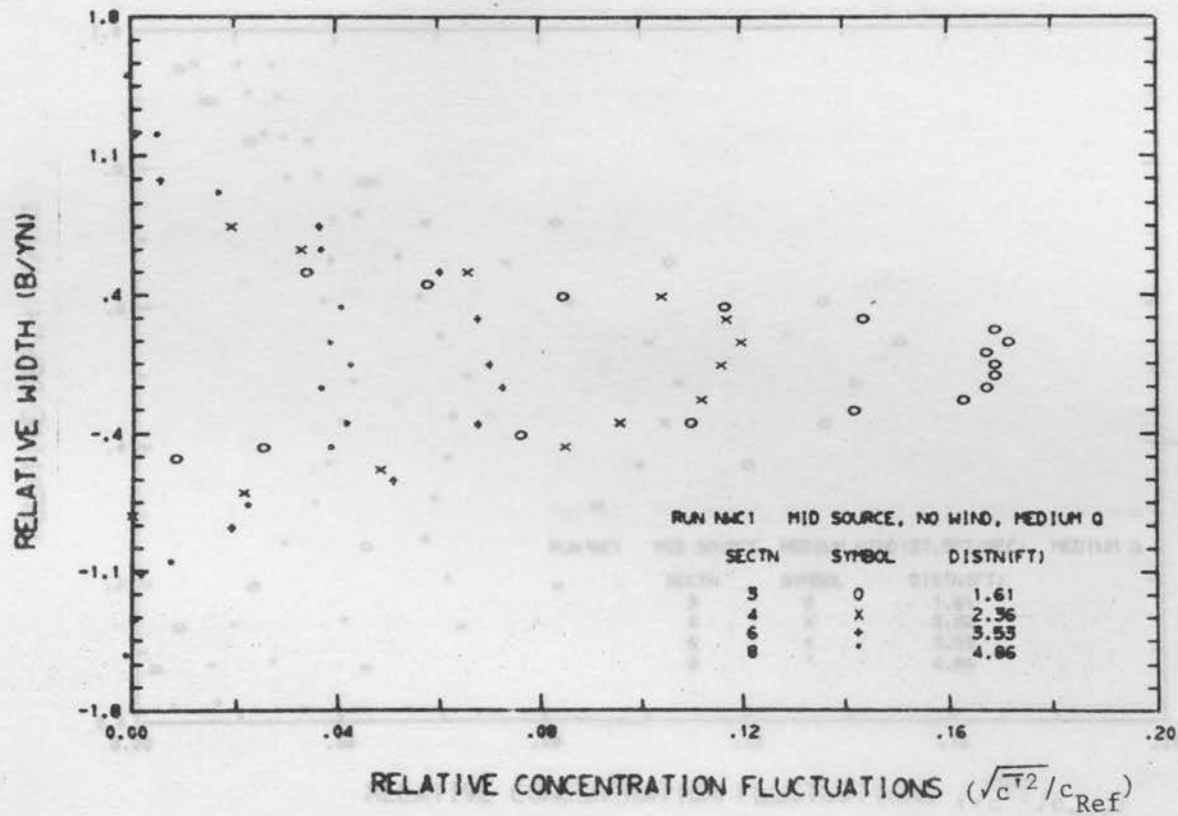


Fig. 21. Relative Intensity of Concentration Fluctuations, Run NWC1 (horizontally).

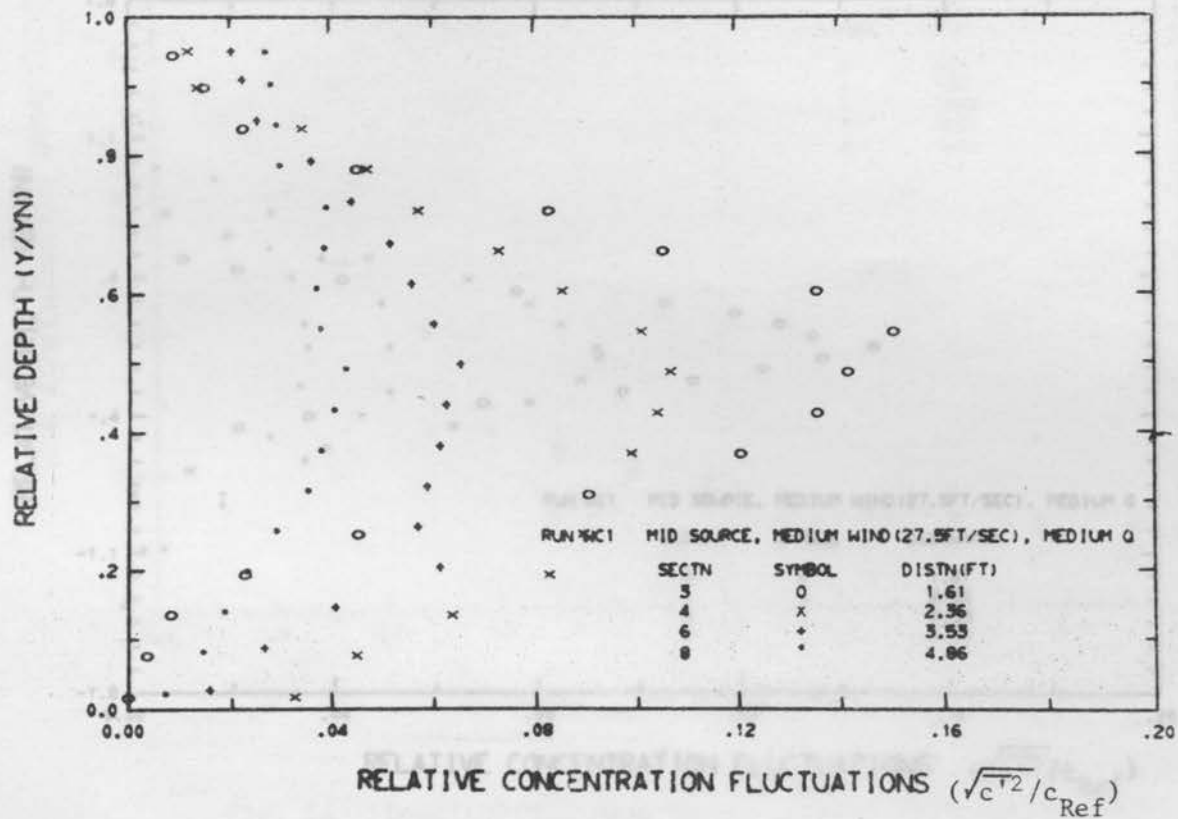


Fig. 22. Relative Intensity of Concentration Fluctuations, Run WC1 (vertically).

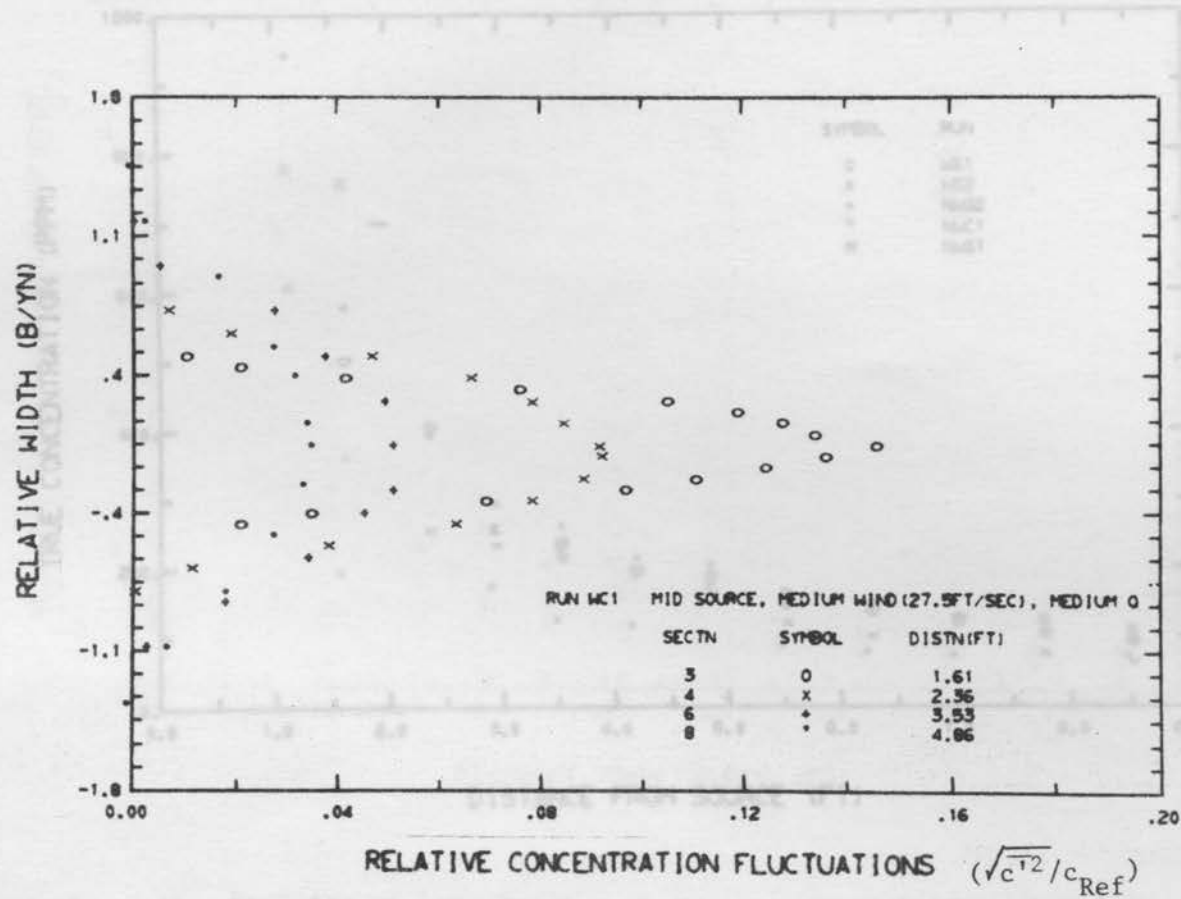


Fig. 24. Longitudinal Mean Concentration Profiles.

Fig. 23. Relative Intensity of Concentration Fluctuations, Run WC1 (horizontally).

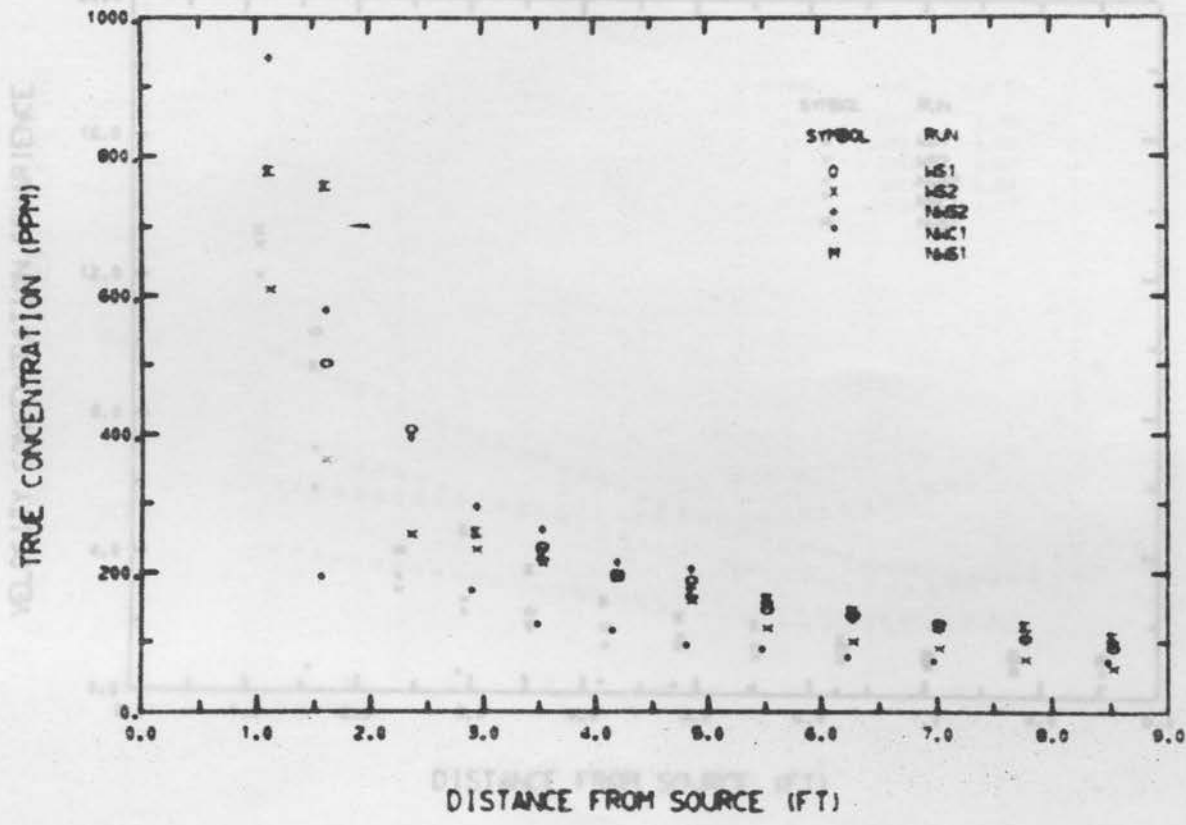


Fig. 24. Longitudinal Mean Concentration Profiles.

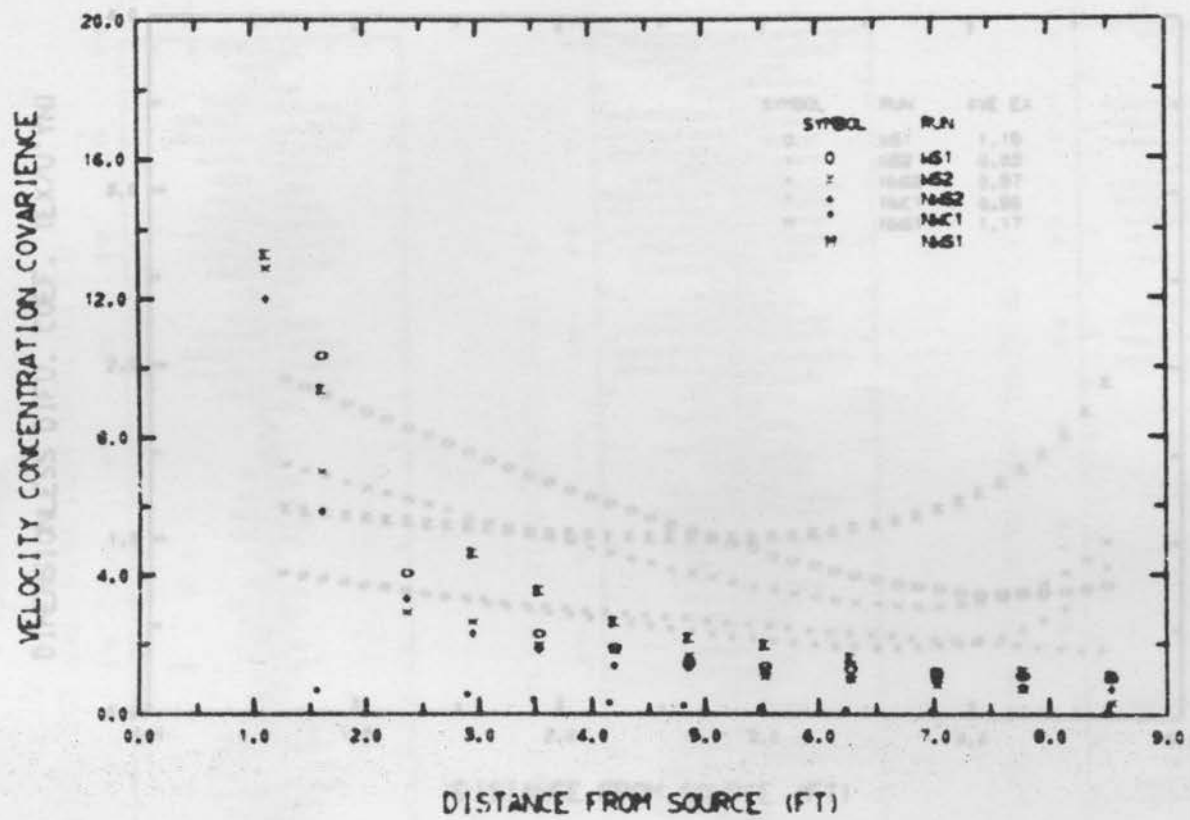


Fig. 25. Profiles of Longitudinal Velocity-Concentration Covariance.

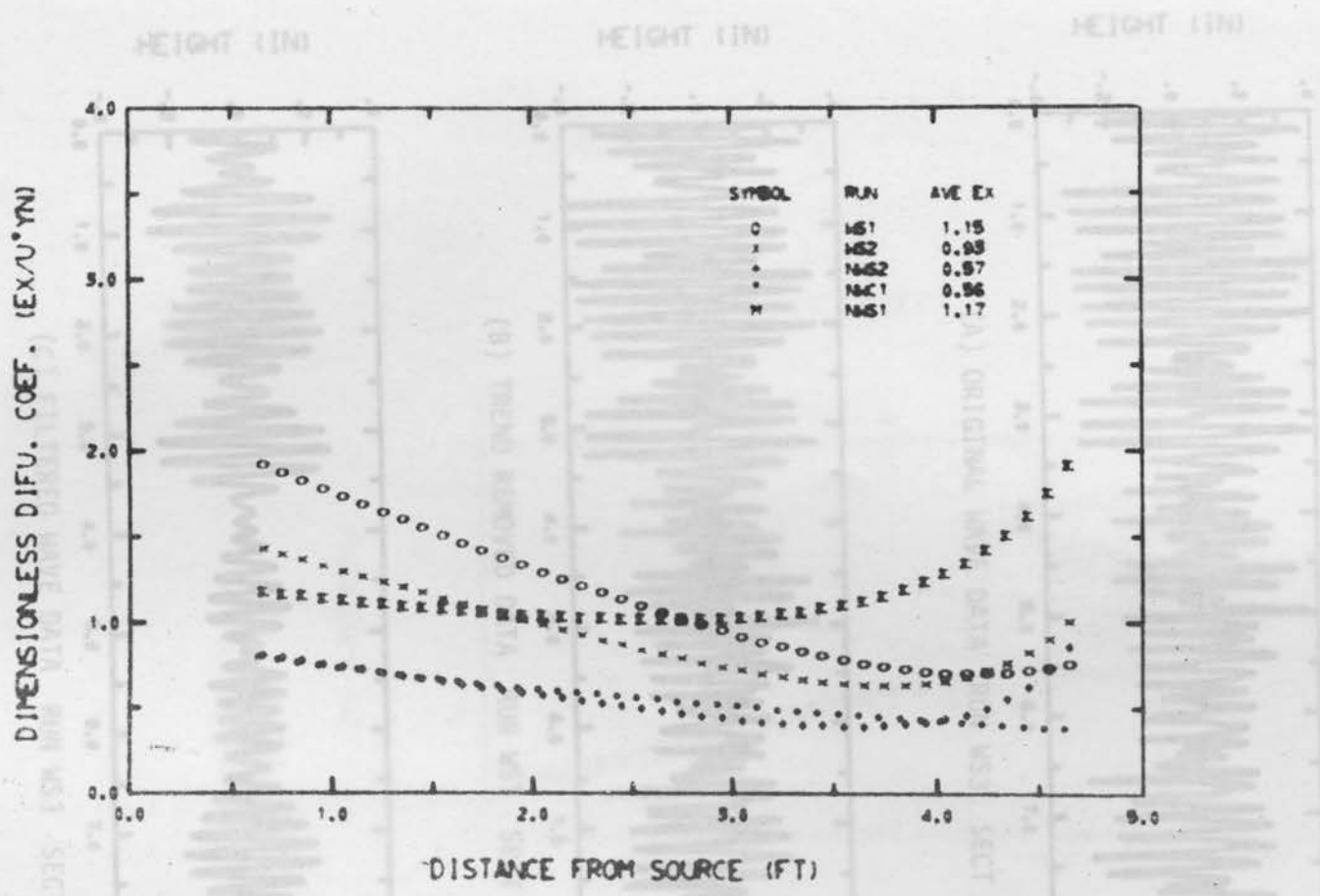
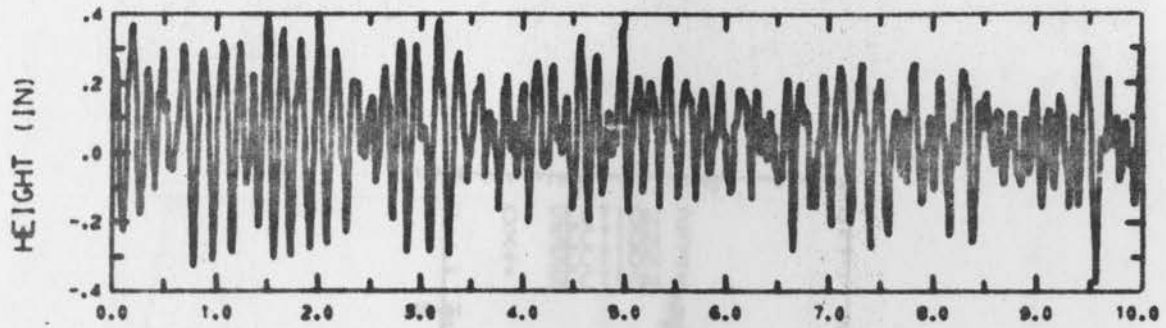
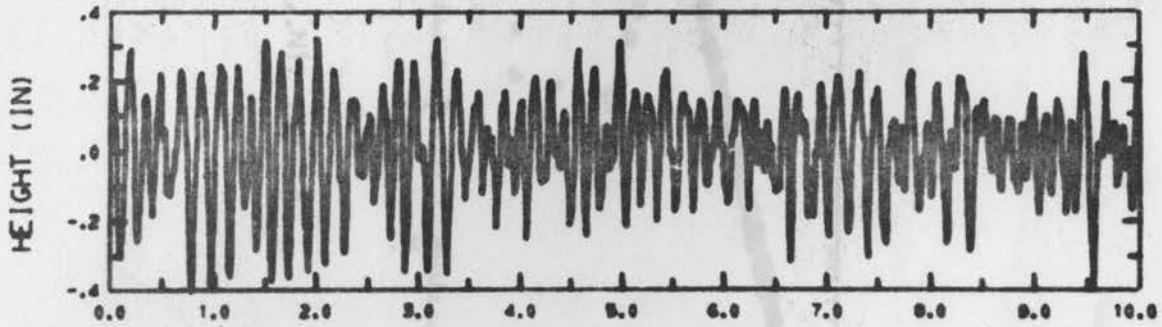


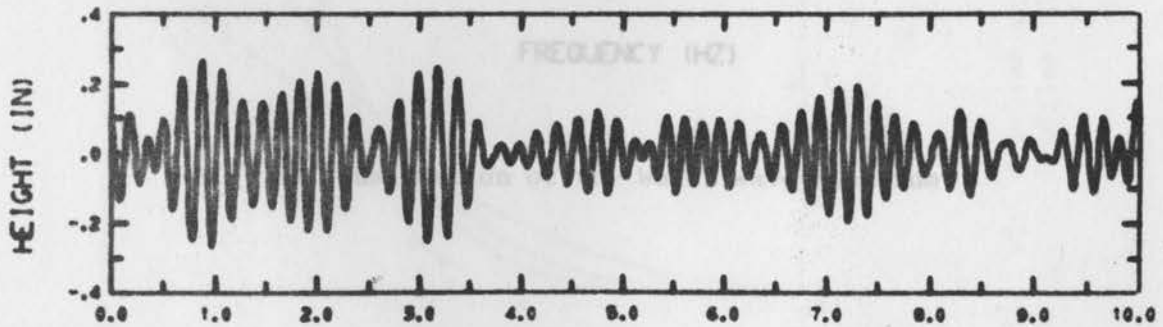
Fig. 26. Longitudinal Turbulent Diffusion Coefficients.



(A) ORIGINAL WAVE DATA RUN WS3 SECT 4



(B) TREND REMOVED DATA RUN WS3 SECT 4



(C) FILTERED WAVE DATA RUN WS3 SECT 4

TIME (SEC)

Fig. 27. Measured and Filtered Water Wave Data.

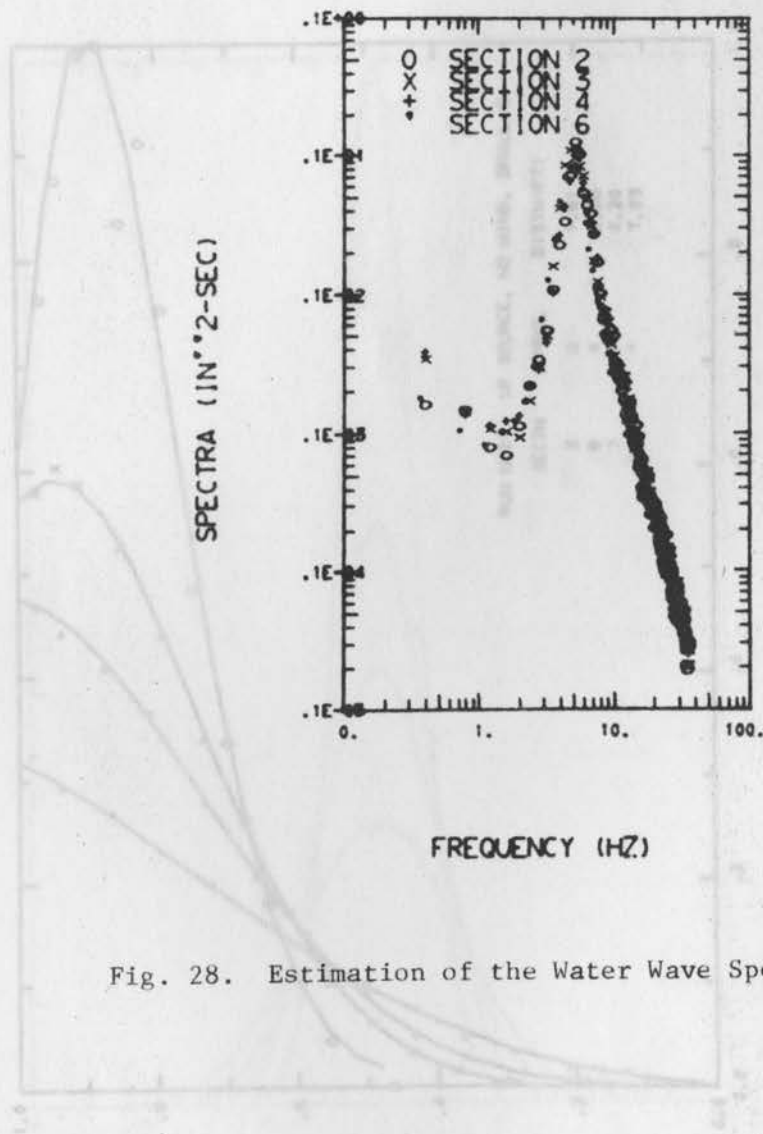


Fig. 28. Estimation of the Water Wave Spectrum.



Fig. 29. Measured and Numerical Results of Vertical Concentration Profiles, Case W51.

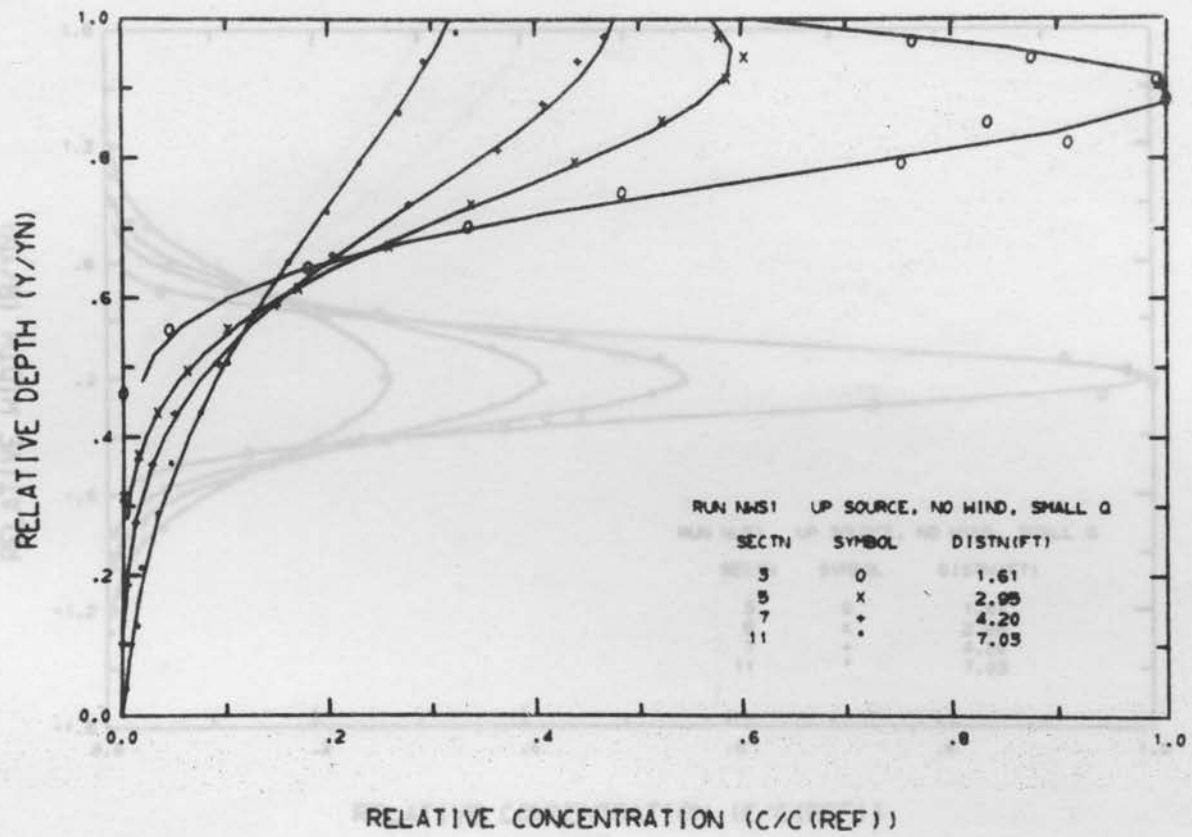


Fig. 29. Measured and Numerical Results of Vertical Concentration Profiles, Case NWS1.

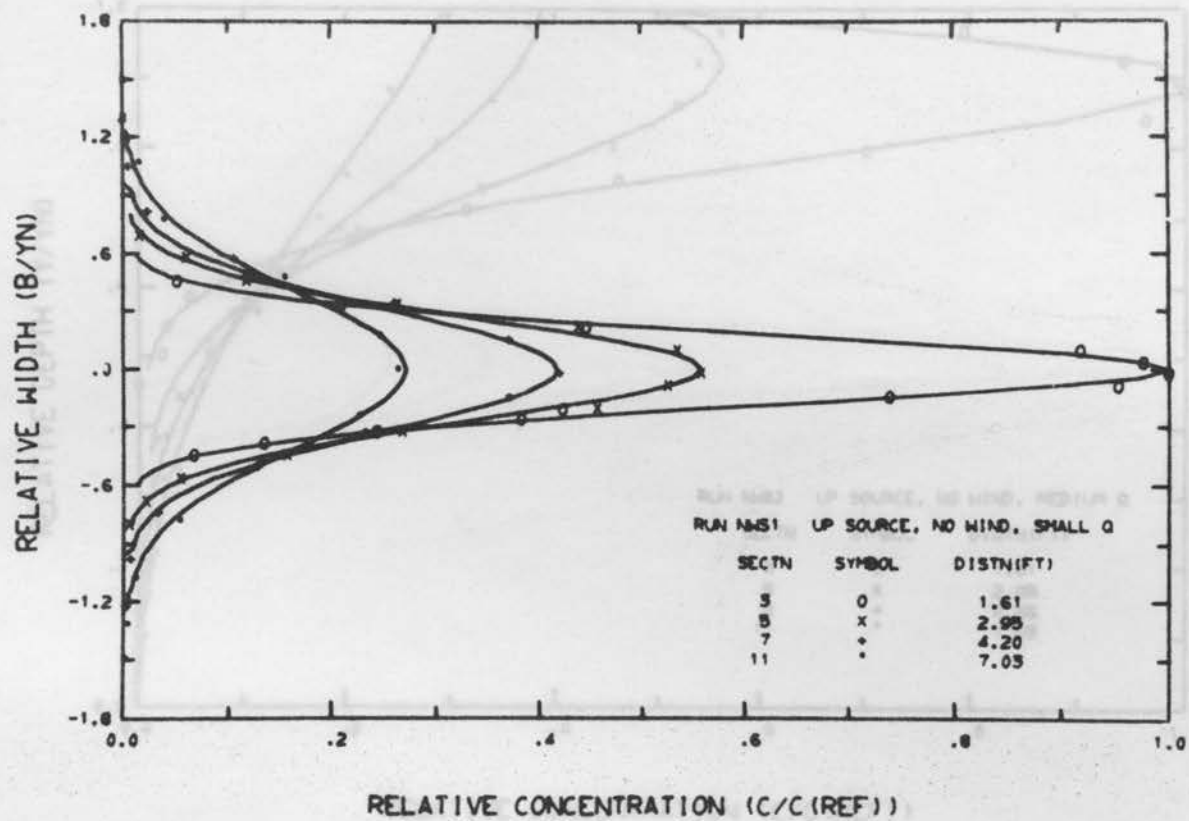


Fig. 30. Measured and Numerical Results of Horizontal Concentration Profiles, Case NWS1.

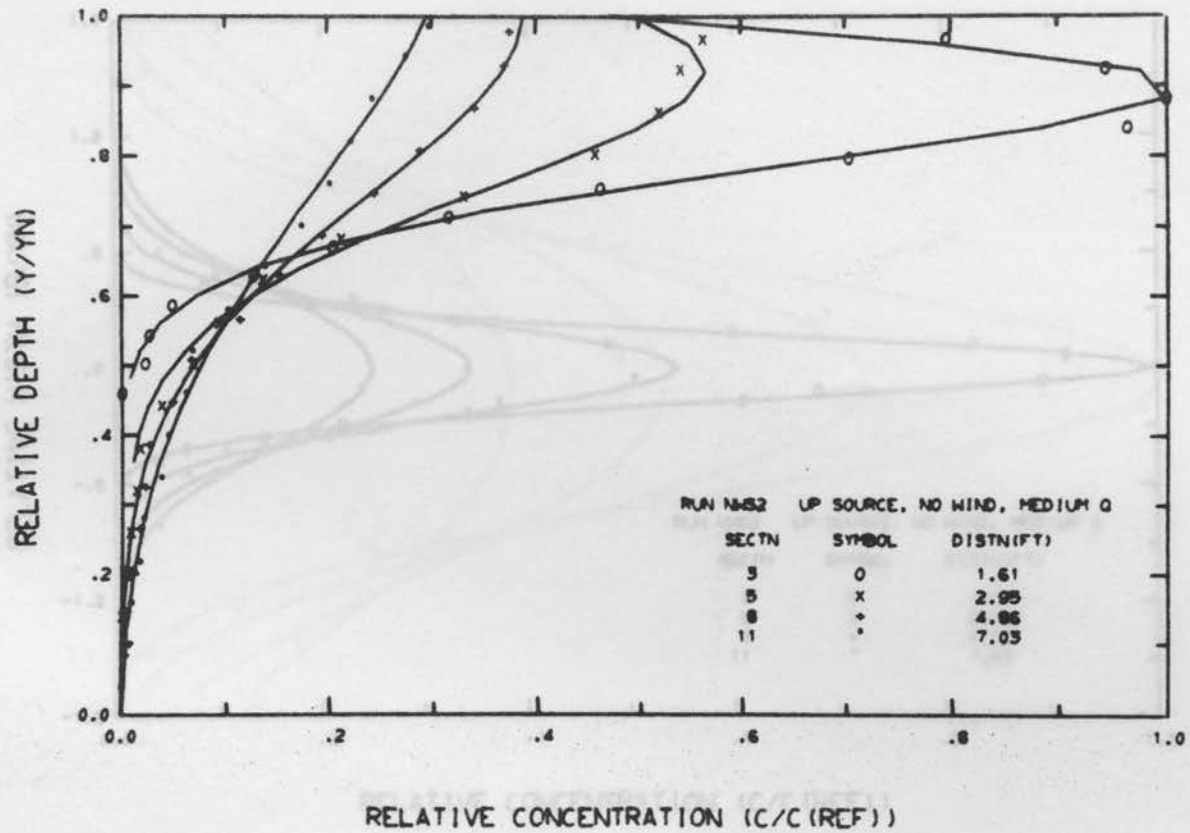


Fig. 31. Measured and Numerical Results of Vertical Concentration Profiles, Case NWS2.

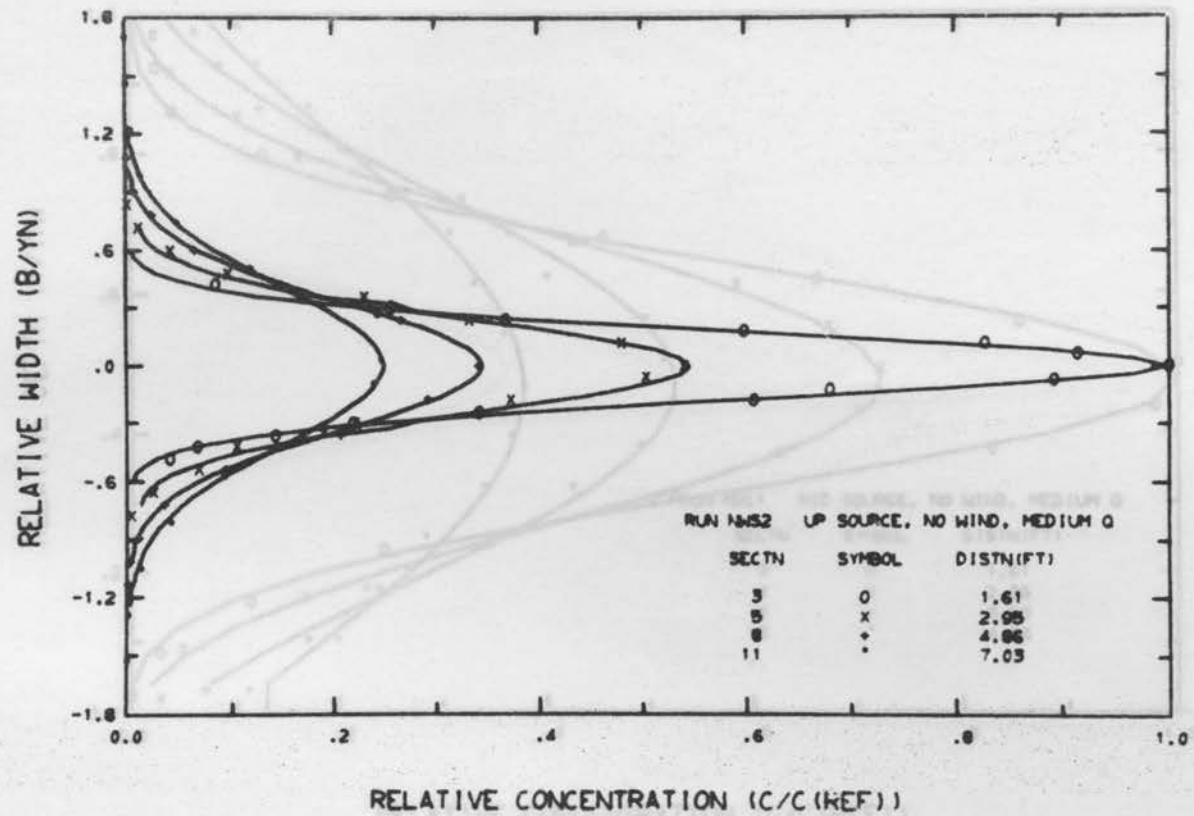


Fig. 32. Measured and Numerical Results of Horizontal Concentration Profiles, Case NWS2.

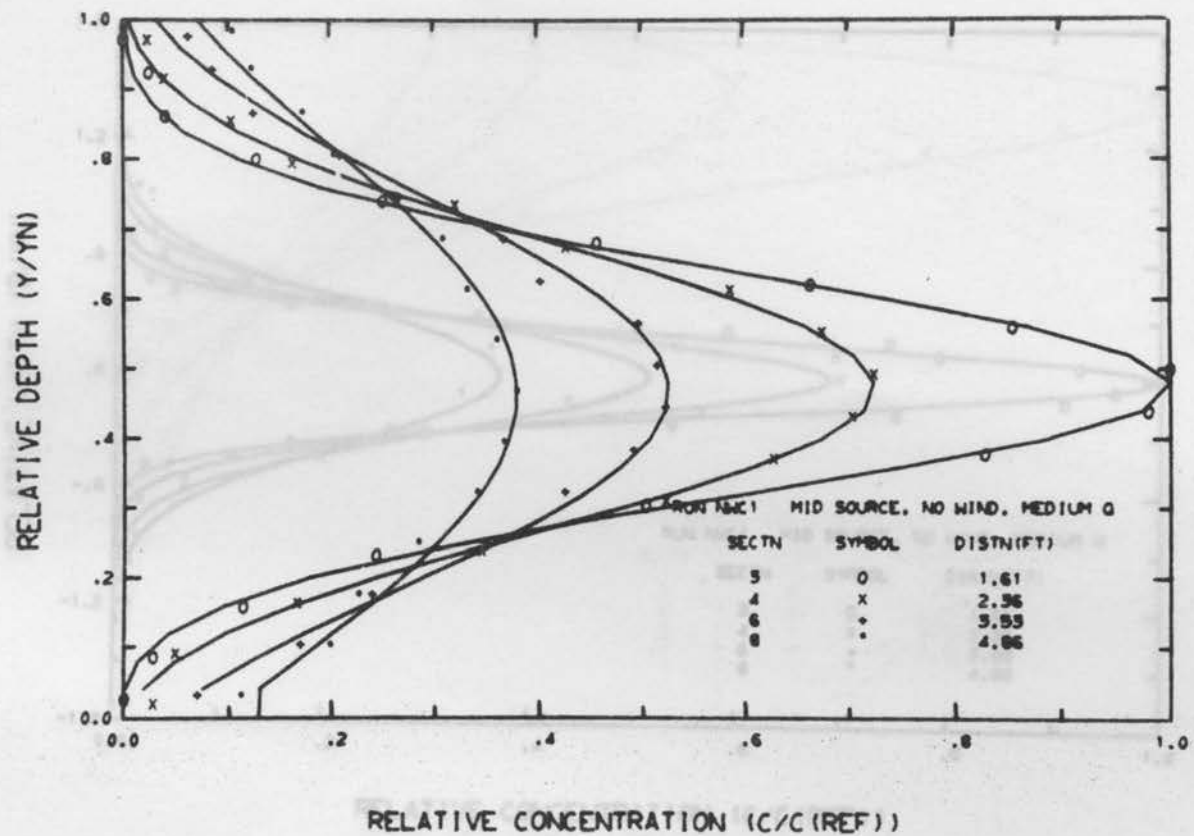


Fig. 33. Measured and Numerical Results of Vertical Concentration Profiles, Case NWCl.

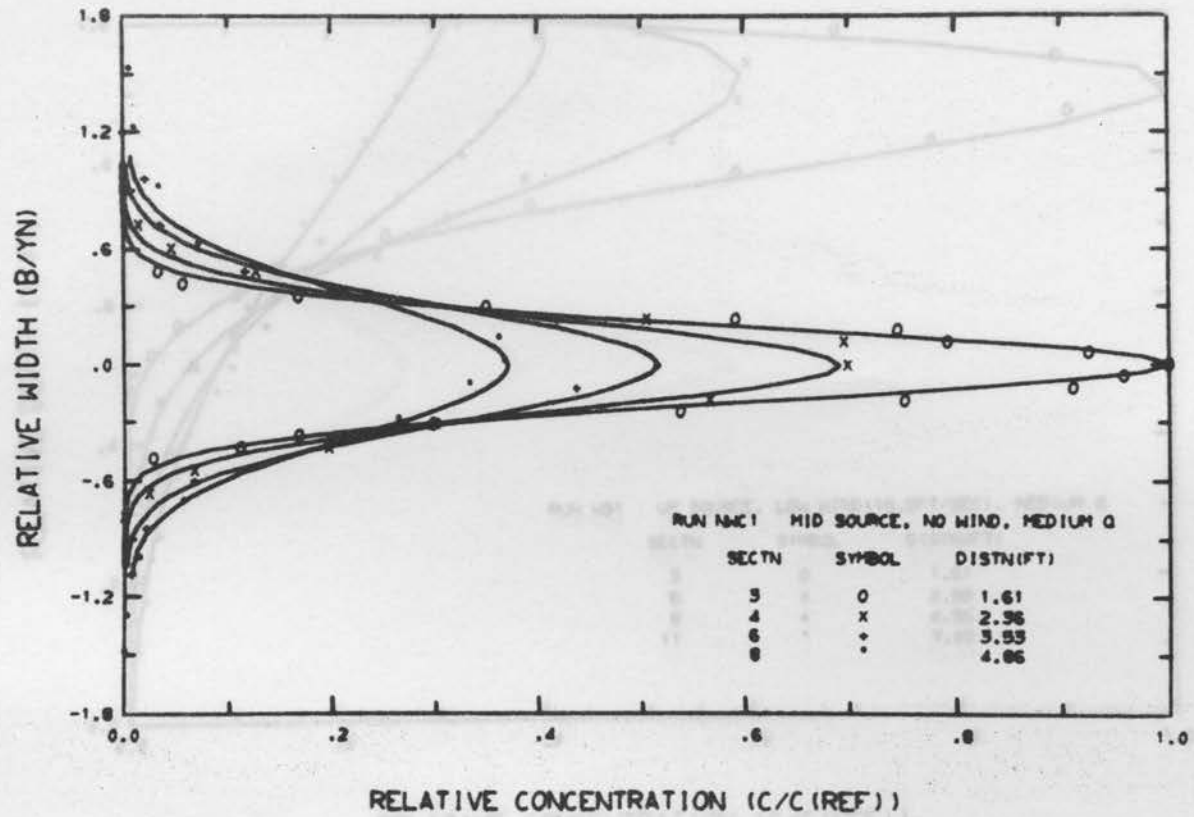


Fig. 34. Measured and Numerical Results of Horizontal Concentration Profiles, Case NW1.

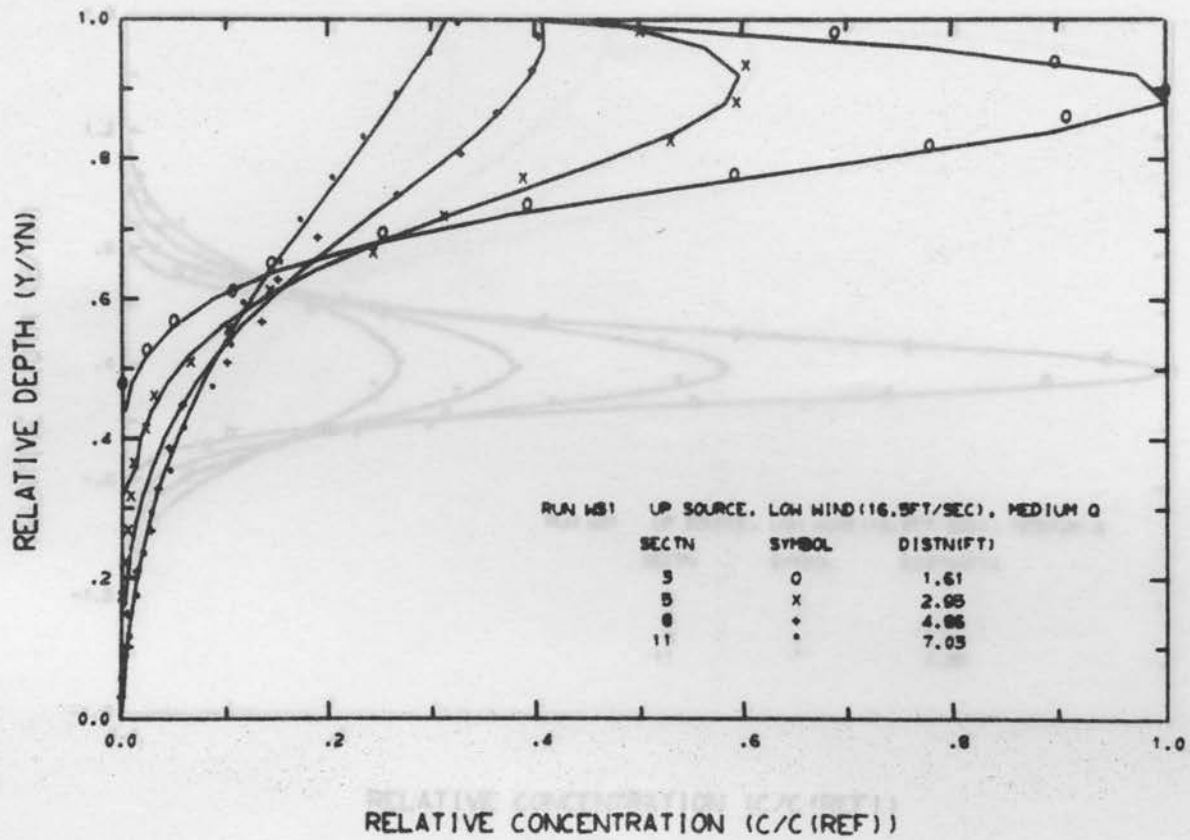


Fig. 35. Measured and Numerical Results of Vertical Concentration Profiles, Case WS1.

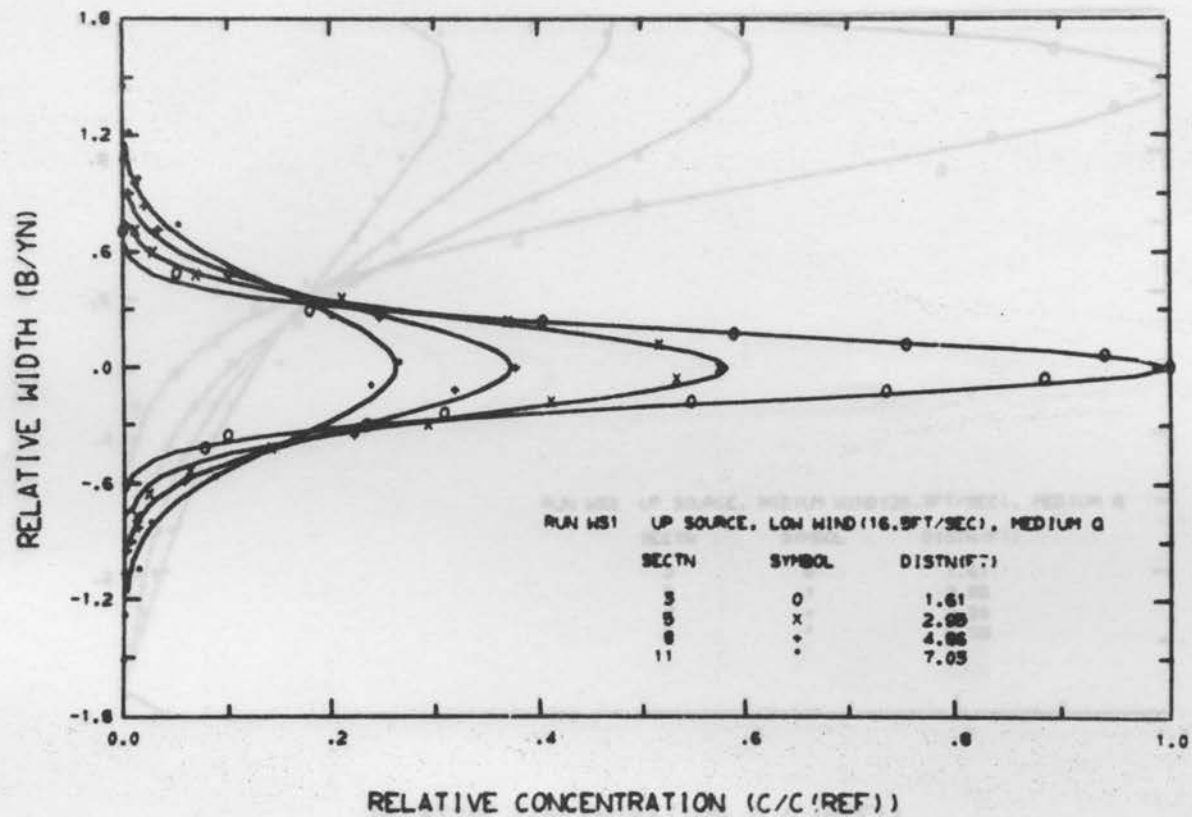


Fig. 36. Measured and Numerical Results of Horizontal Concentration Profiles, Case WS1.

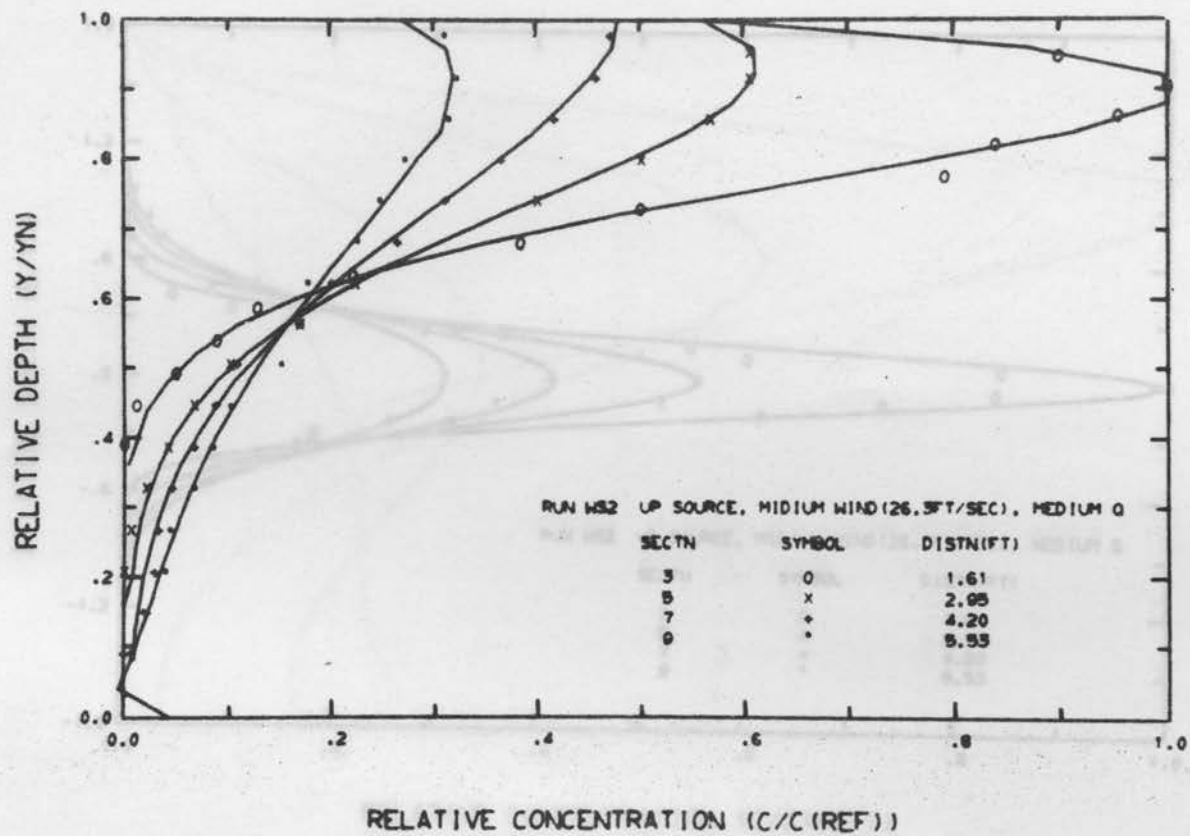


Fig. 37. Measured and Numerical Results of Vertical Concentration Profiles, Case WS2.

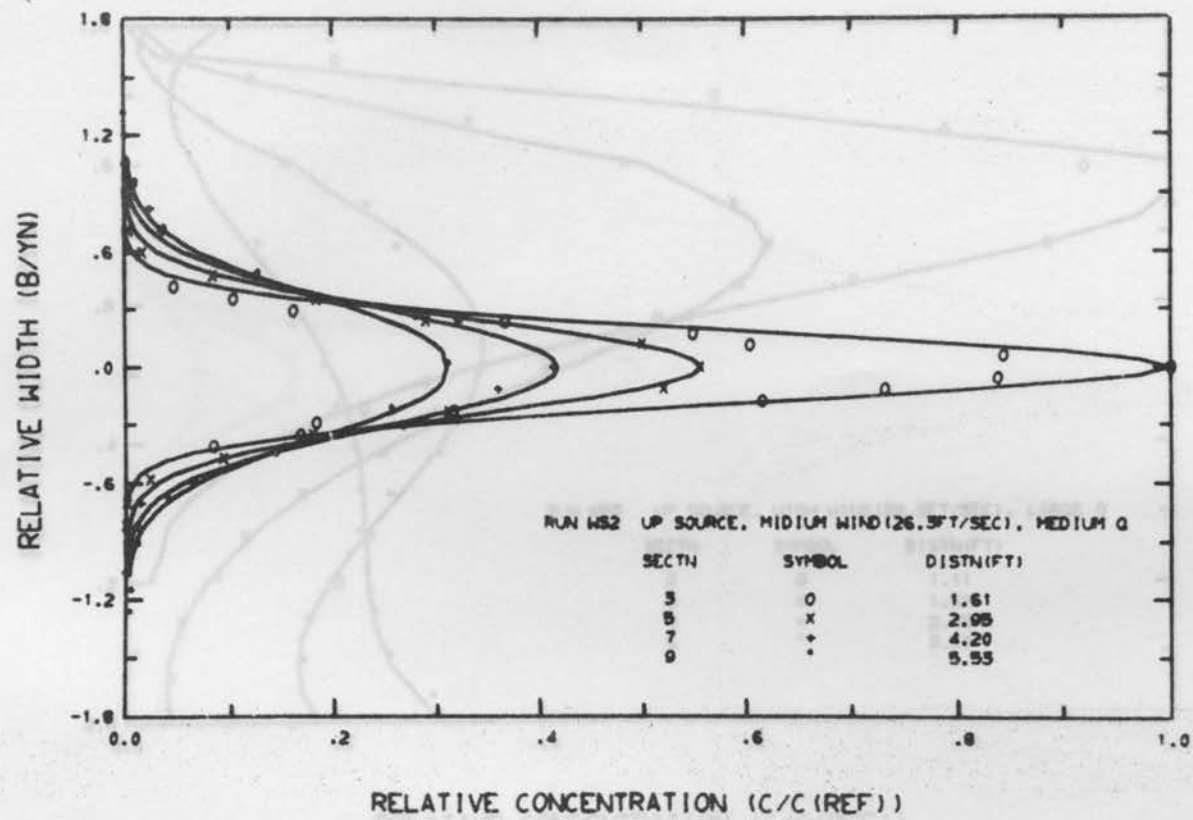


Fig. 38. Measured and Numerical Results of Horizontal Concentration Profiles, Case WS2.

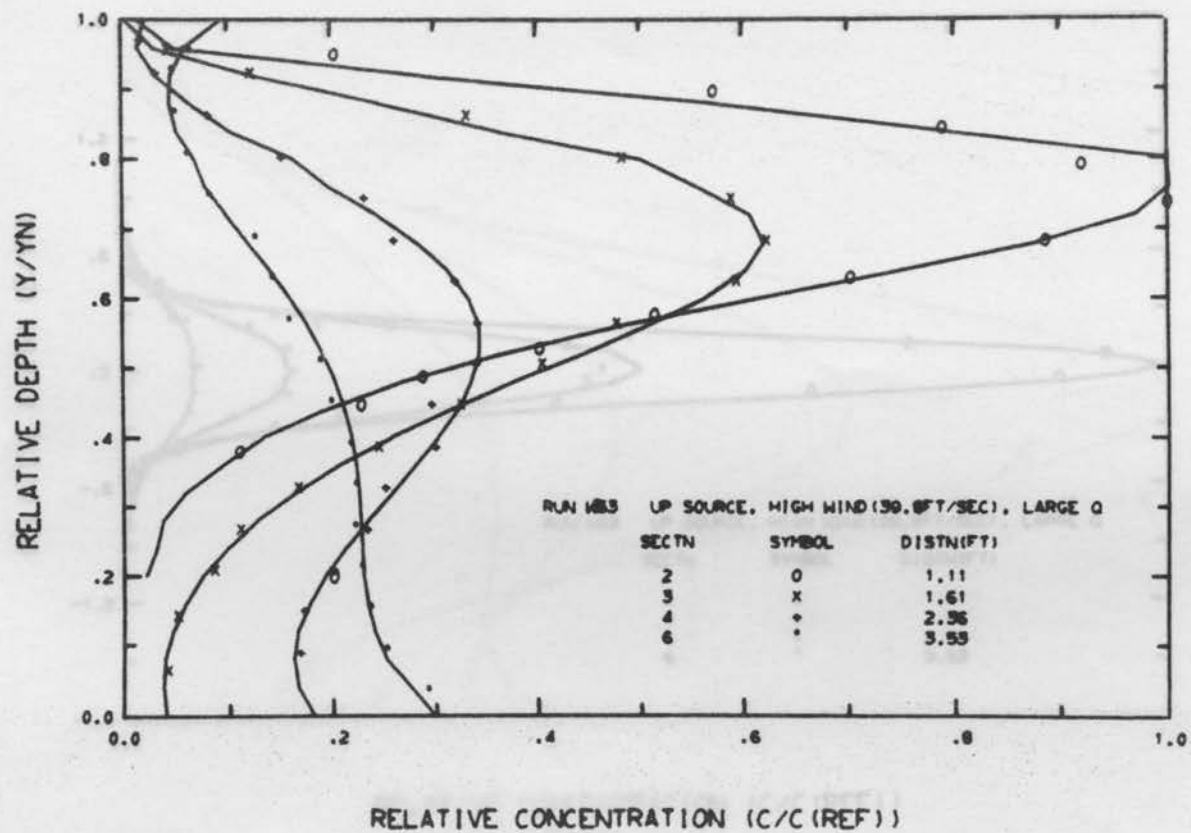


Fig. 39. Measured and Numerical Results of Vertical Concentration Profiles, Case WS3.

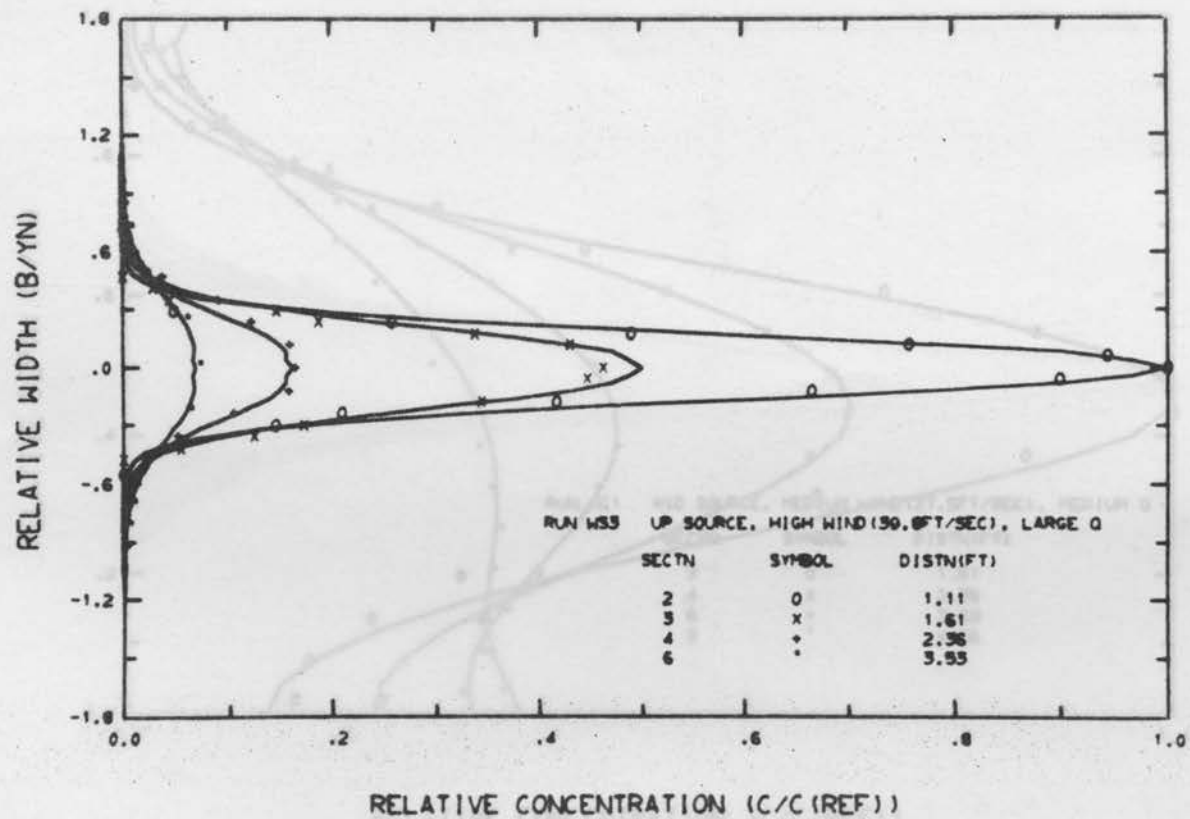


Fig. 40. Measured and Numerical Results of Horizontal Concentration Profiles, Case WS3.

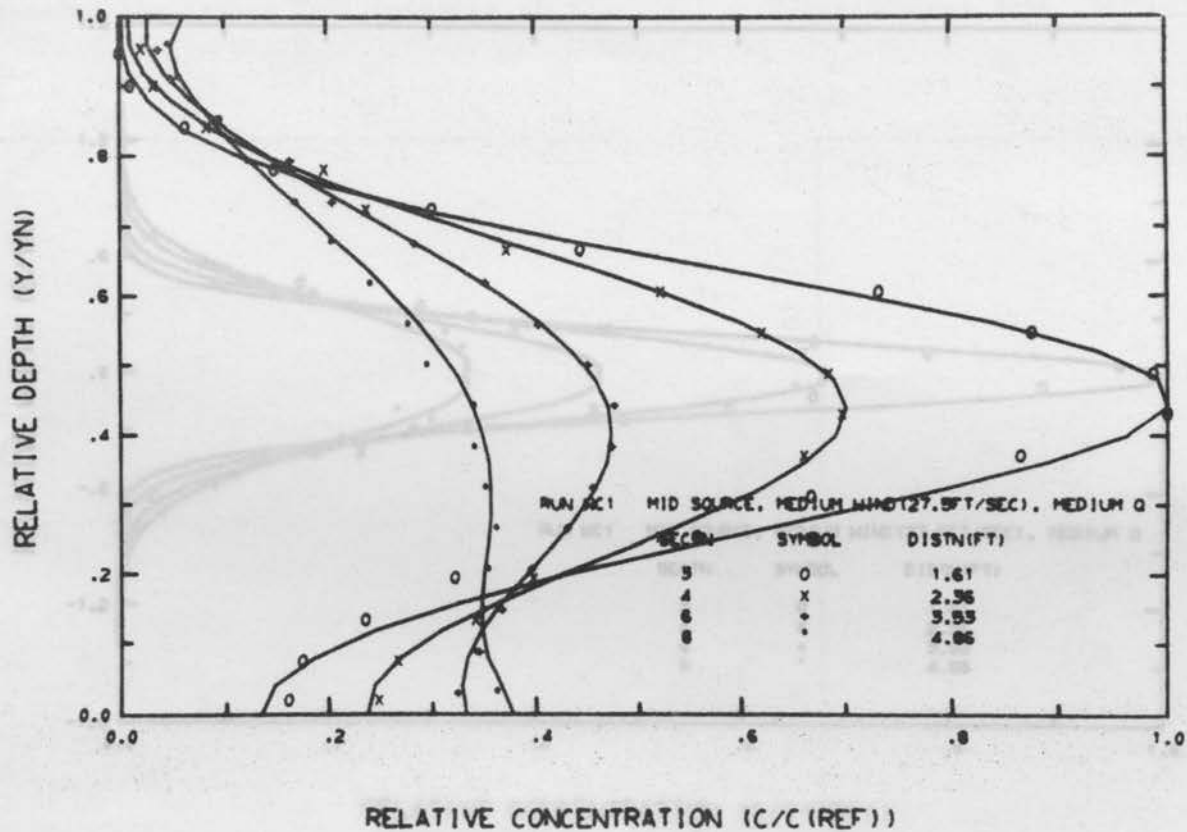


Fig. 41. Measured and Numerical Results of Vertical Concentration Profiles, Case W1.

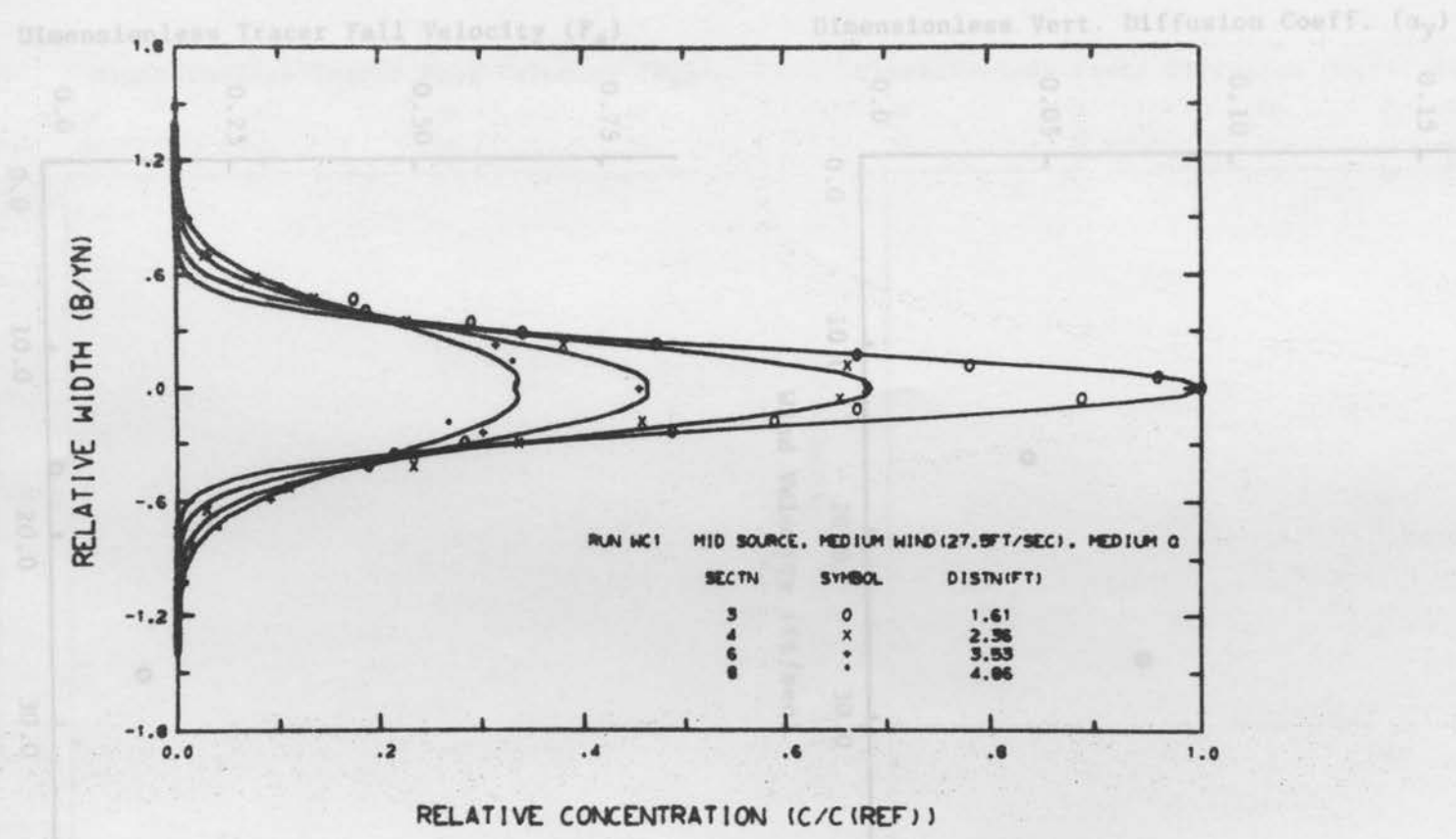


Fig. 42. Measured and Numerical Results of Horizontal Concentration Profiles, Case WCl.

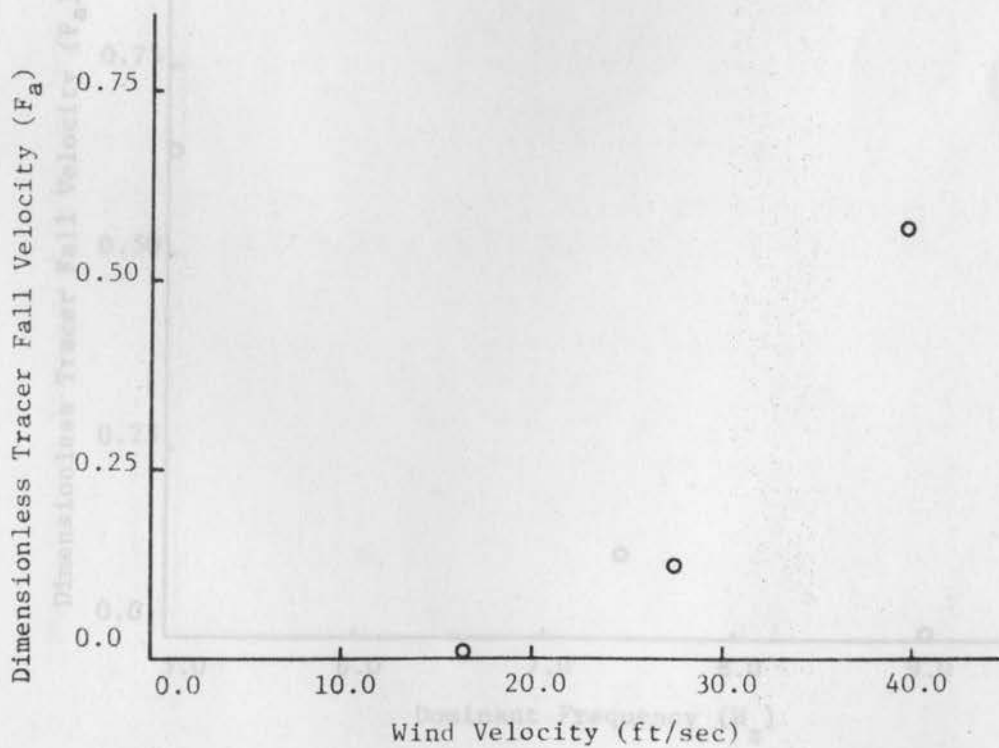
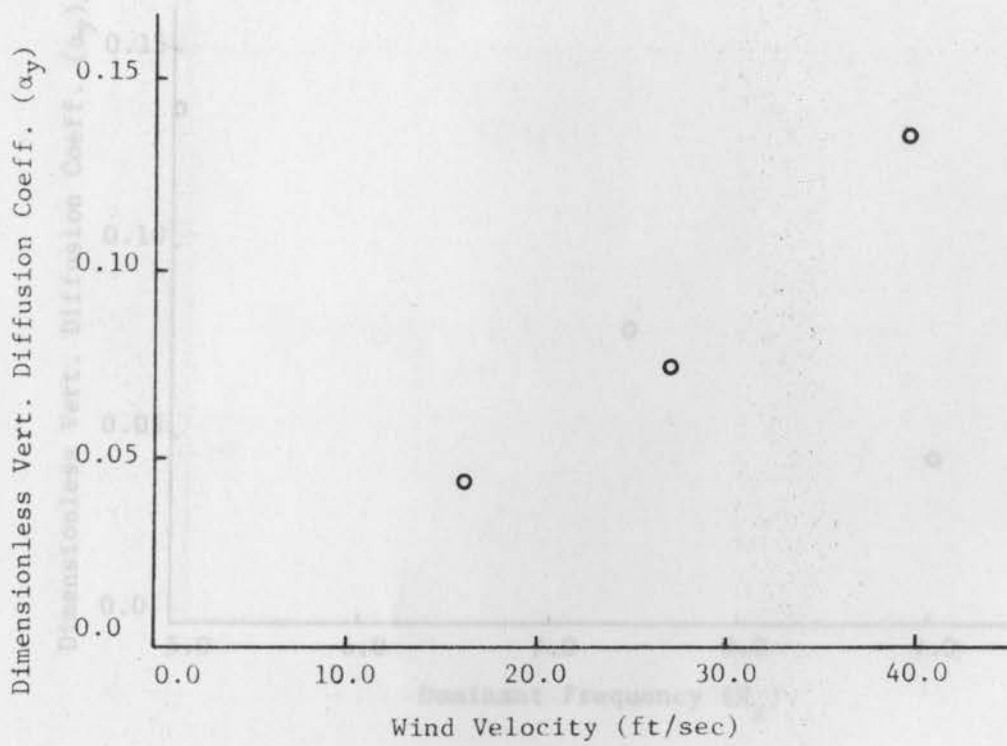


Fig. 43. Relations of the Vertical Diffusivity, Tracer Fall Velocity and Wind Velocity.

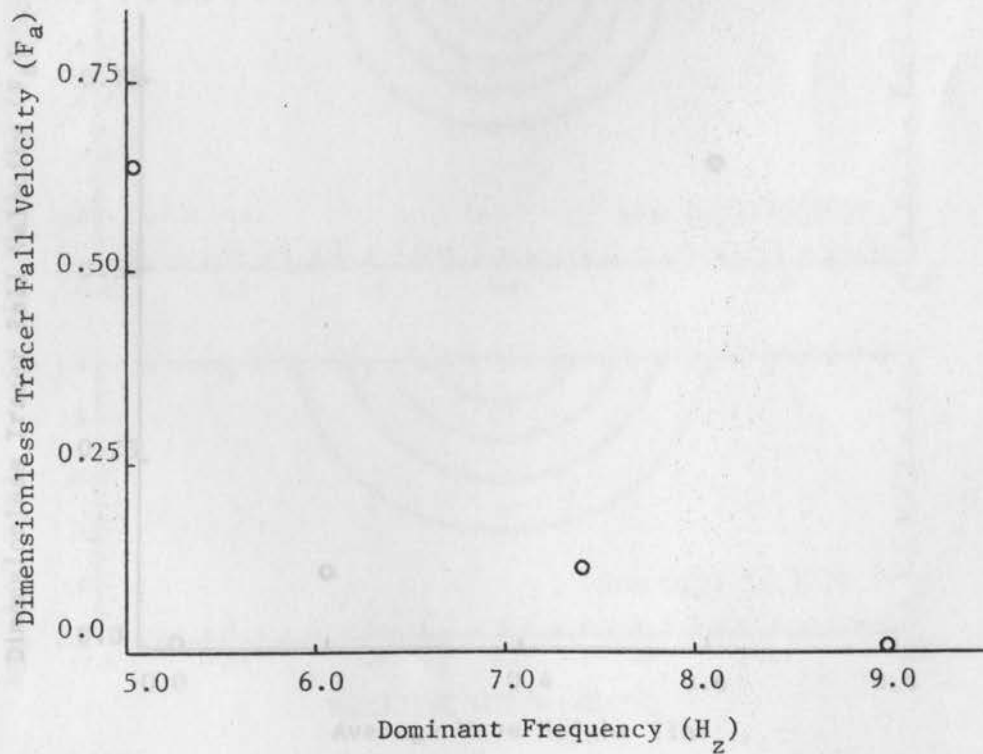
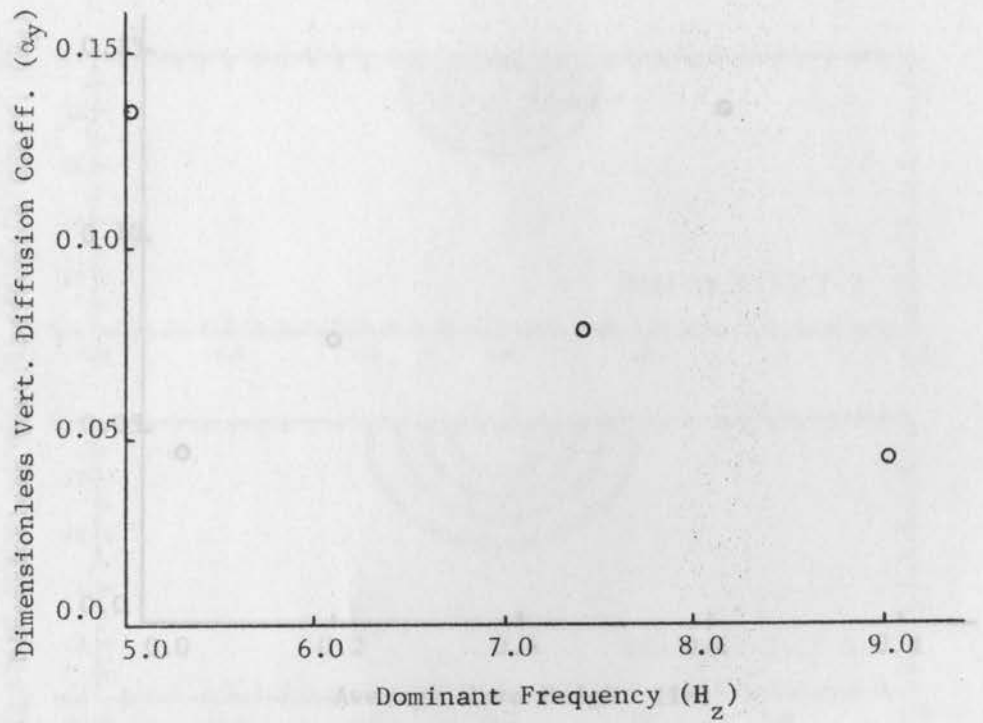


Fig. 44. Relations of the Vertical Diffusivity, Tracer Fall Velocity and Dominant Frequency.

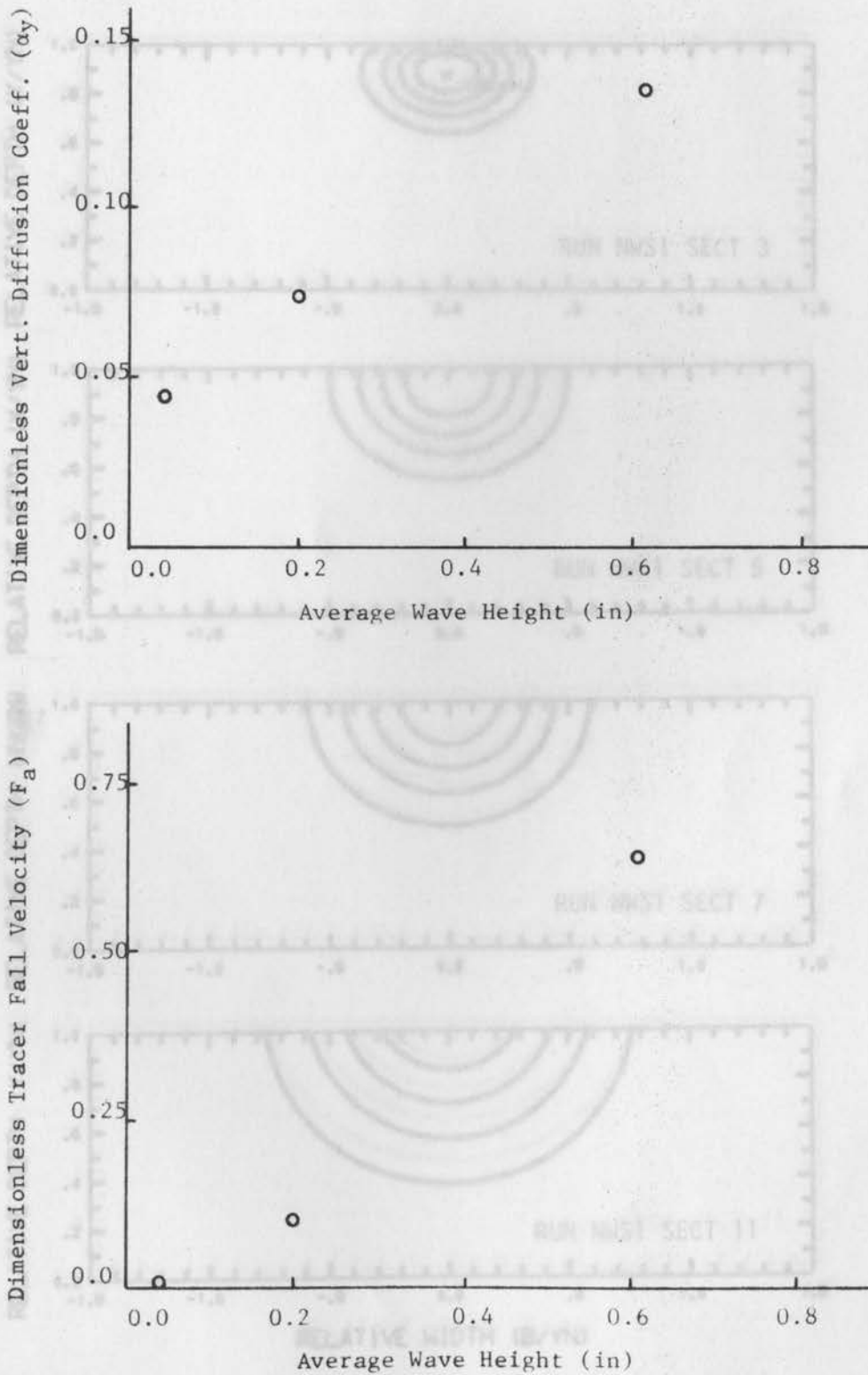


Fig. 45. Relations of the Vertical Diffusivity, Tracer Fall Velocity and Average Wave Height.

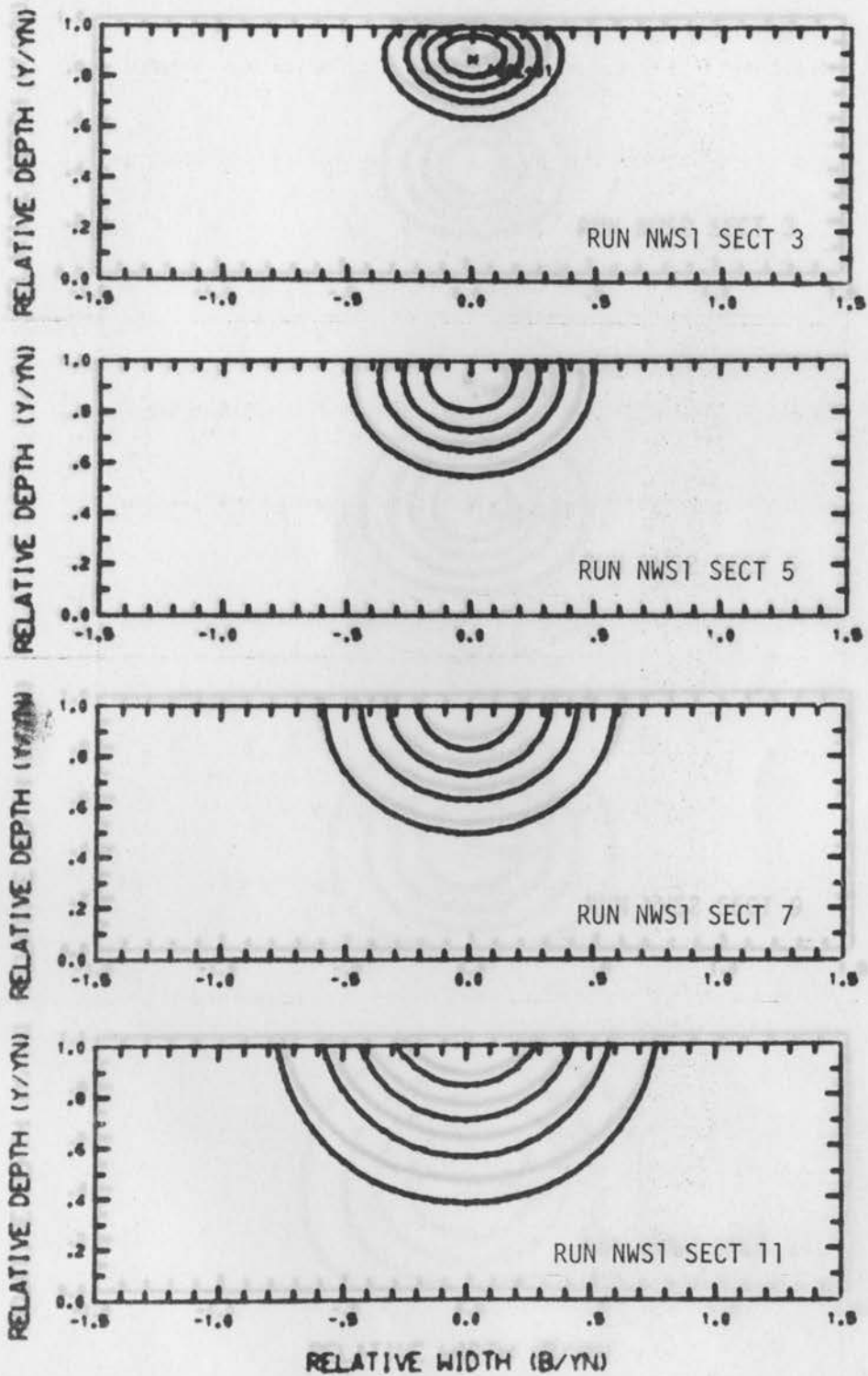


Fig. 46. Contours of Normalized Concentration of Numerical Results, Case NWS1.

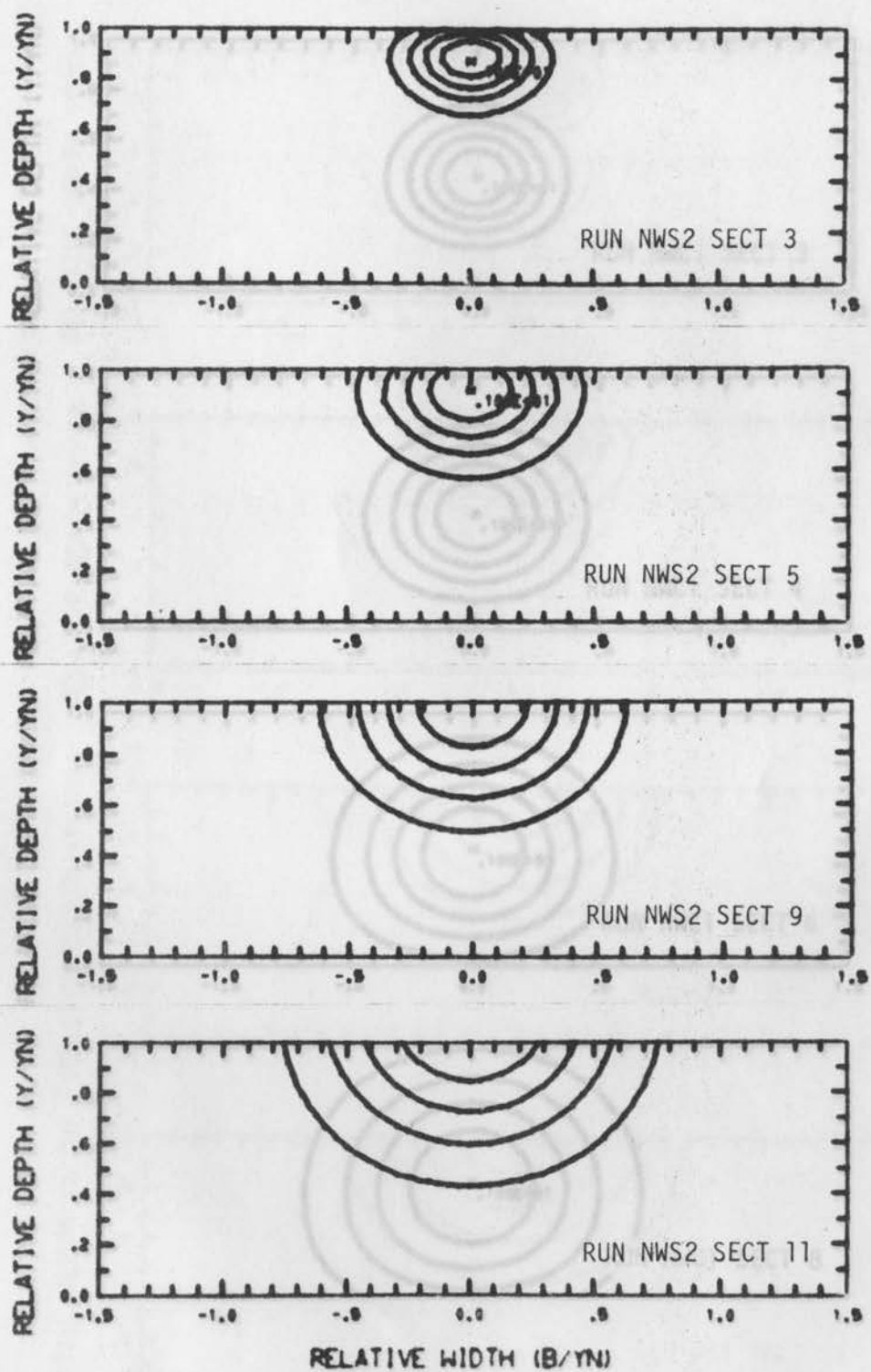


Fig. 47. Contours of Normalized Concentration of Numerical Results, Case NWS2.

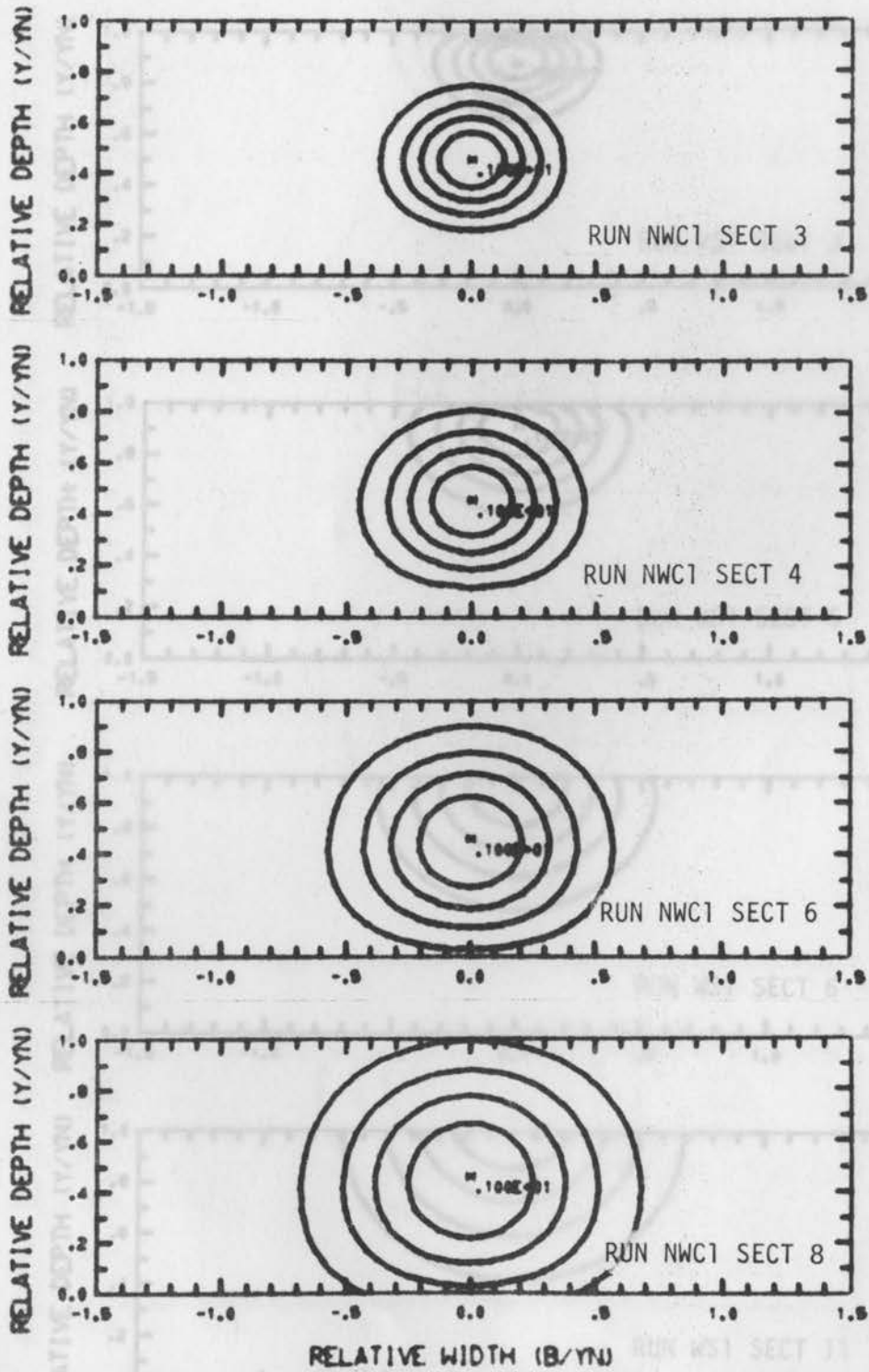


Fig. 48. Contours of Normalized Concentration of Numerical Results, Case NWC1.

Fig. 49. Contours of Normalized Concentration of Numerical Results, Case WSI.

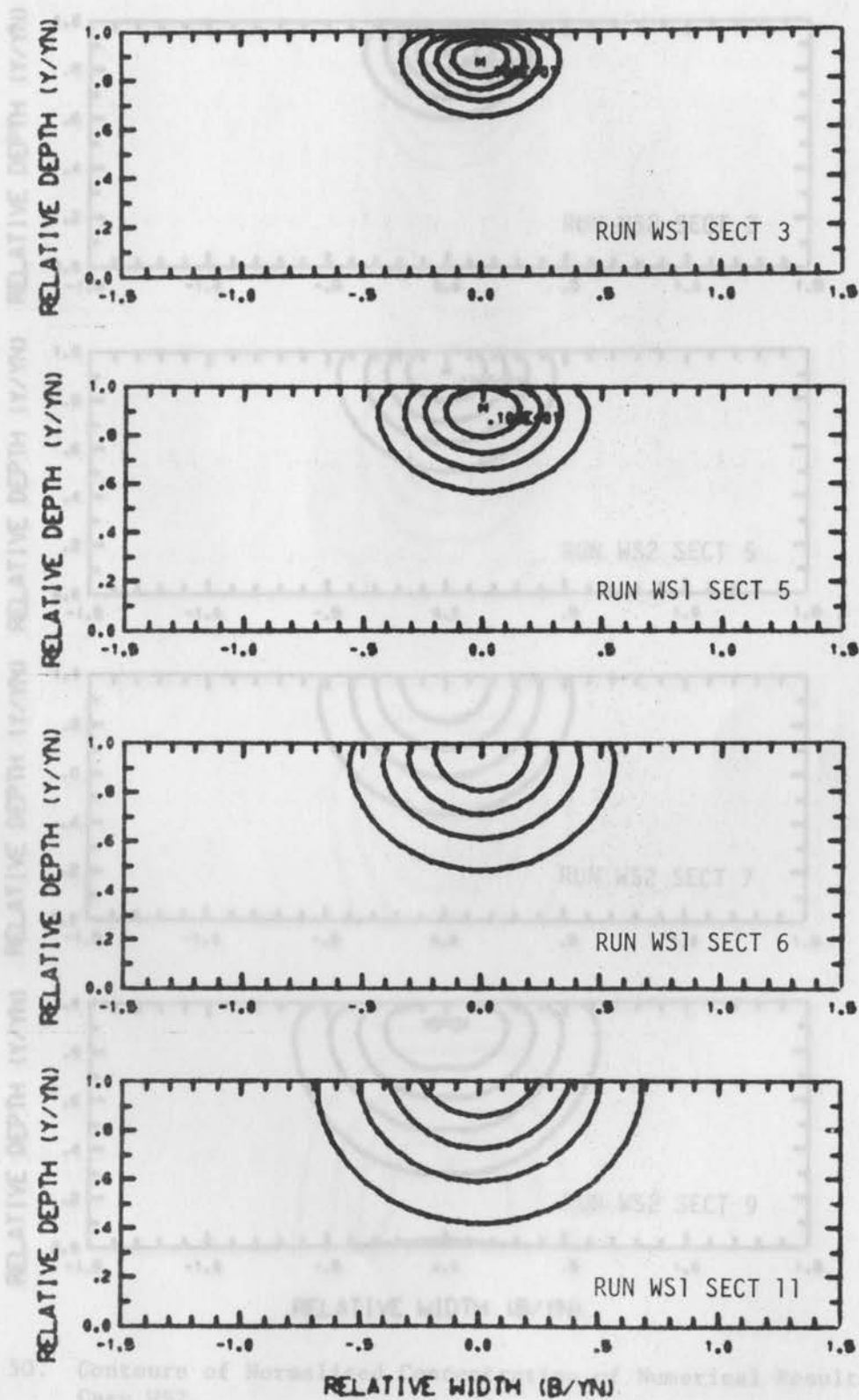


Fig. 30. Contours of Normalized Concentration of Numerical Results, Case WS2.

Fig. 49. Contours of Normalized Concentration of Numerical Results, Case WS1.

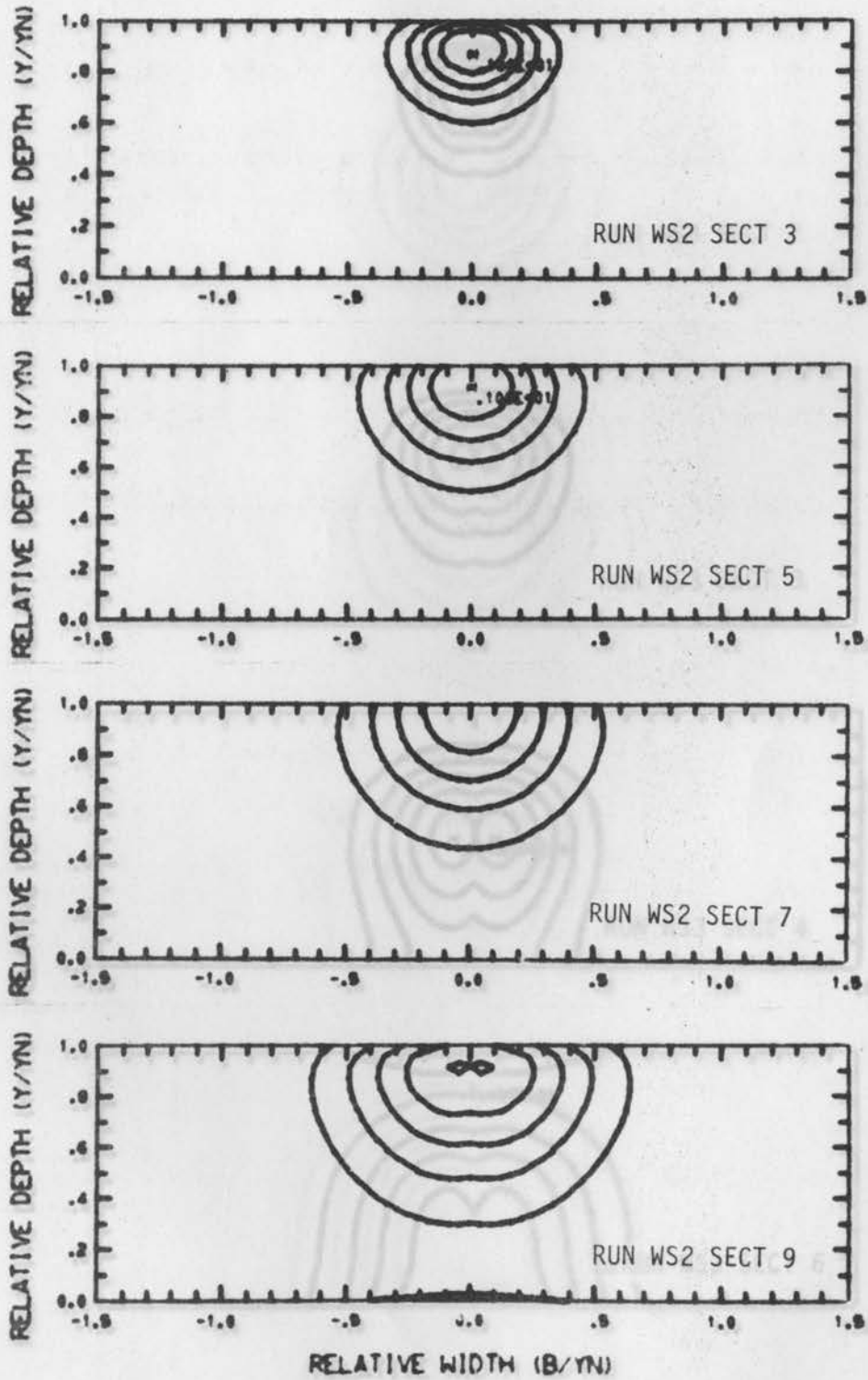


Fig. 50. Contours of Normalized Concentration of Numerical Results, Case WS2.

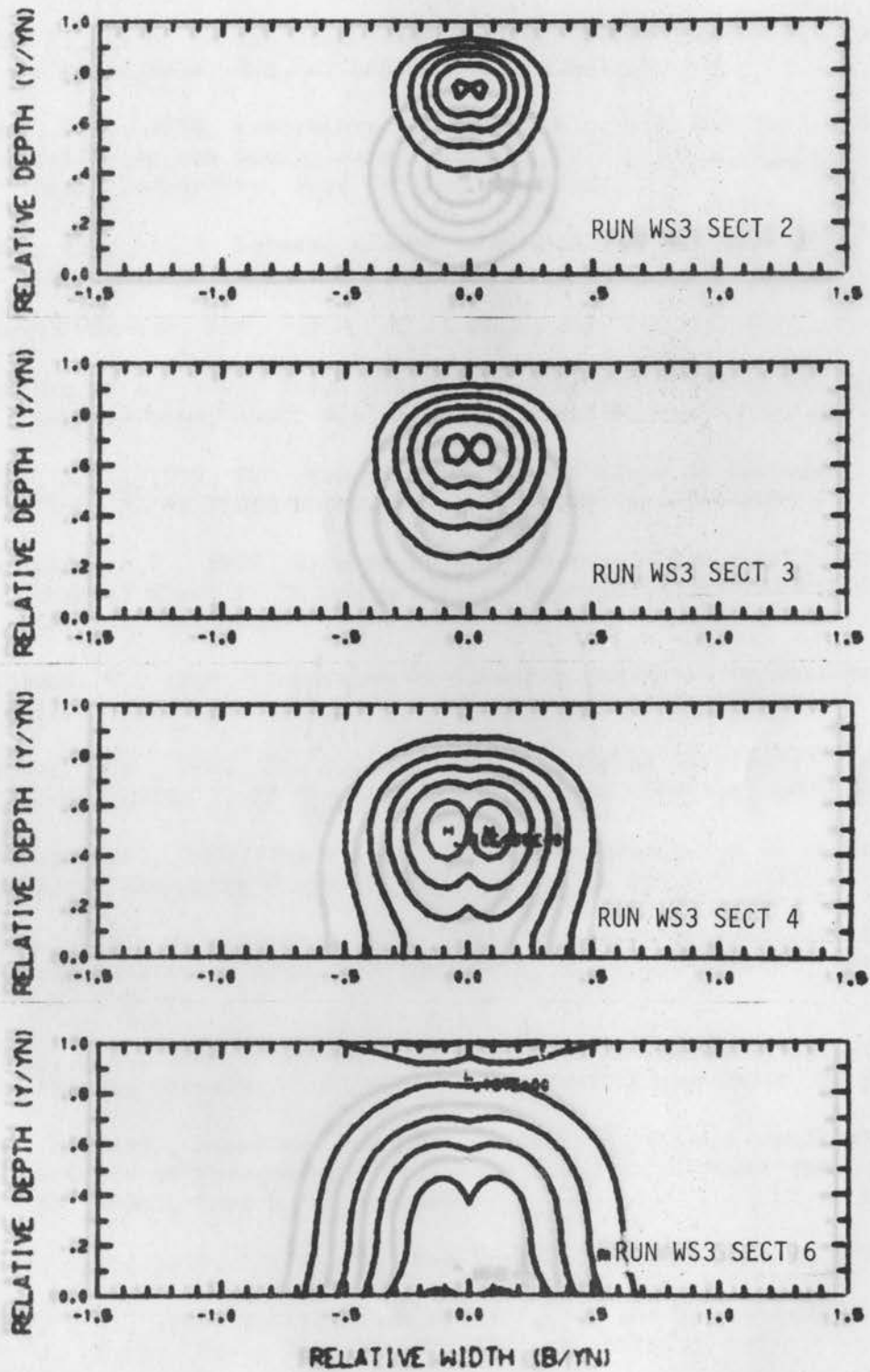


Fig. 51. Contours of Normalized Concentration of Numerical Results, Case WS3.

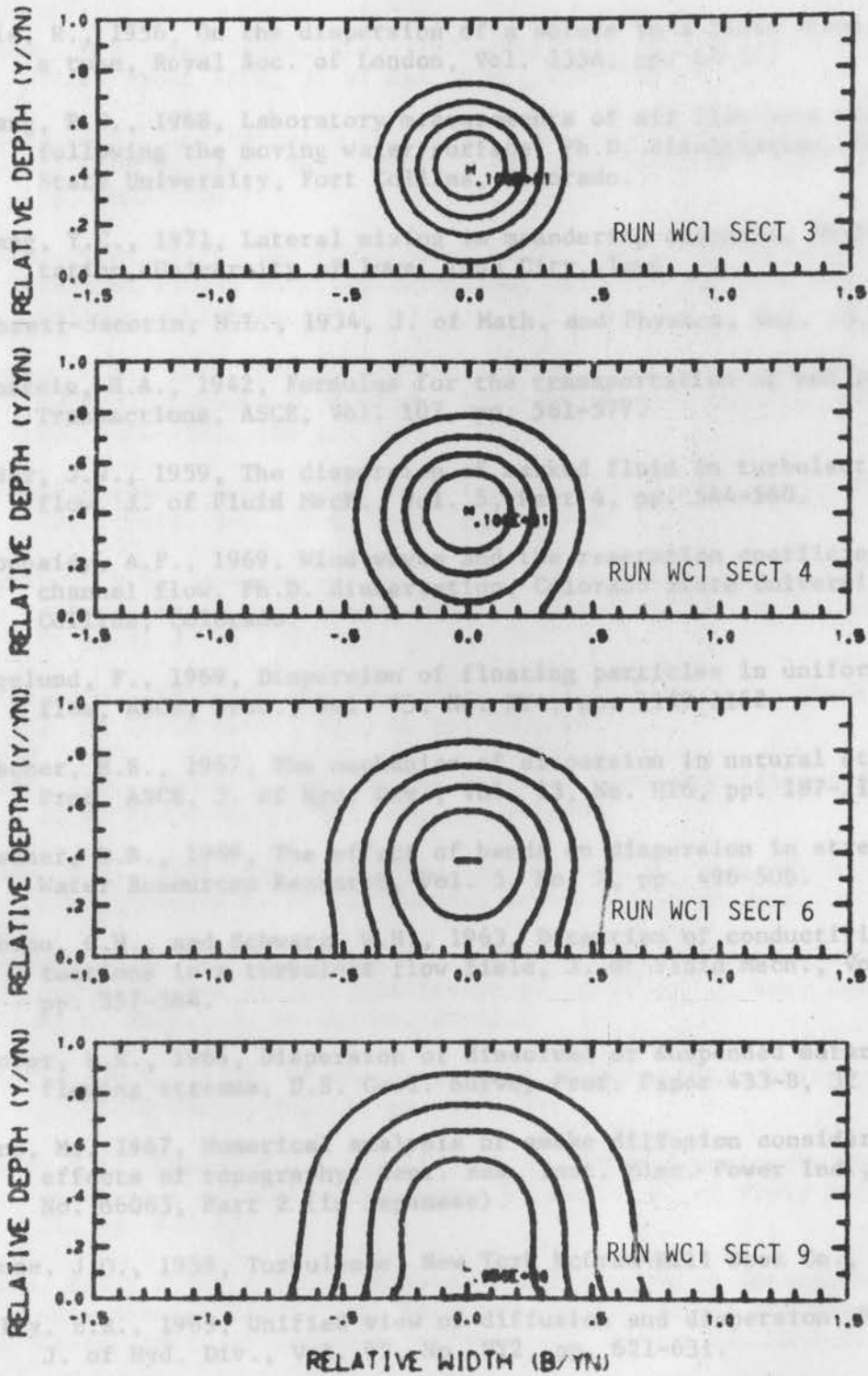


Fig. 52. Contours of Normalized Concentration of Numerical Results, Case WC1.

BIBLIOGRAPHY

- Aris, R., 1956, On the dispersion of a solute in a fluid flowing through a tube, Royal Soc. of London, Vol. 235A, pp. 67-77.
- Chang, P.C., 1968, Laboratory measurements of air flow over wind waves following the moving water surface, Ph.D. dissertation, Colorado State University, Fort Collins, Colorado.
- Chang, Y.C., 1971, Lateral mixing in meandering channels, Ph.D. dissertation, University of Iowa, Iowa City, Iowa.
- Dubreil-Jacotin, M.L., 1934, J. of Math. and Physics, Vol. 13, p. 217.
- Einstein, H.A., 1942, Formulas for the transportation of bed load, Transactions, ASCE, Vol. 107, pp. 561-577.
- Elder, J.W., 1959, The dispersion of marked fluid in turbulent shear flow, J. of Fluid Mech., Vol. 5, Part 4, pp. 544-560.
- Eloubaidy, A.F., 1969, Wind waves and the reaeration coefficient in open channel flow, Ph.D. dissertation, Colorado State University, Fort Collins, Colorado.
- Engelund, F., 1969, Dispersion of floating particles in uniform channel flow, ASCE, Proc., Vol. 95, No. HY4, pp. 1149-1162.
- Fischer, H.B., 1967, The mechanics of dispersion in natural streams, Proc. ASCE, J. of Hyd. Div., Vol. 93, No. HY6, pp. 187-216.
- Fischer, H.B., 1969, The effect of bends on dispersion in streams, Water Resources Research, Vol. 5, No. 2, pp. 496-506.
- Gibson, C.H., and Schwarz, W.H., 1963, Detection of conductivity fluctuations in a turbulent flow field, J. of Fluid Mech., Vol. 16, pp. 357-364.
- Glover, R.E., 1964, Dispersion of dissolved or suspended materials in flowing streams, U.S. Geol. Survey Prof. Paper 433-B, 32 pp.
- Hino, M., 1967, Numerical analysis of smoke diffusion considering the effects of topography, Cent. Res. Inst. Elec. Power Ind., Report No. 66063, Part 2 (in Japanese).
- Hinze, J.O., 1959, Turbulence, New York McGraw-Hill Book Co., 586 pp.
- Holly, E.R., 1969, Unified view of diffusion and dispersion, Proc. ASCE, J. of Hyd. Div., Vol. 95, No. HY2, pp. 621-631.
- Jeffreys, H., 1925, On the formation of water waves by wind, Proc. Roy. Soc. A., Vol. 107, pp. 189-206.

BIBLIOGRAPHY - Continued

- Jobson, H.E., and Sayre, W.W., 1970, Vertical transfer in open channel flow, Proc. ASCE, J. of Hyd. Div., Vol. 96, No. HY3, pp. 703-724.
- Jobson, H.E., and Sayre, W.W., 1970, Predicting concentration profiles in open channel, Proc. ASCE, J. of Hyd. Div., Vol. 96, No. HY10, pp. 1983-1996.
- Keefer, T.N., 1971, The relation of turbulence to diffusion in open channel flows, Ph.D. dissertation, Colorado State University, Fort Collins, Colorado.
- Keeler, R.N., 1964, Mixing and chemical reaction in turbulent flow reactors, Ernest O. Lawrence Lab. (Livermore, Calif.), Report No. UCRL-7852, 180 pp.
- Longuet-Higgins, M.S., 1953, Mass transport in water waves, Trans., Camb. Phil. Soc., Vol. 245A, pp. 535-581.
- McQuivey, R.S., and Keefer, T.N., 1971, Measurement of the velocity-concentration covariance, written communication, to be published in ASCE, J. of Hyd. Div.
- Miles, J.W., 1957, On the generation of surface waves by shear flow, J. of Fluid Mech., Vol. 3, pp. 185-204.
- Miles, J.W., 1962a, A note on the inviscid Orr-Sommerfeld equation, J. of Fluid Mech., Vol. 13, pp. 427-432.
- Orlob, G.T., 1958, Eddy diffusion in open channel flow, Ph.D. dissertation, University of California, Berkeley, California.
- Peaceman, D.W., and Rachford, H.H., 1955, The numerical solution of parabolic and elliptic differential equation, J. Soc. Indust. Appl. Math., 3, No. 1, pp. 28-41.
- Phillips, O.M., 1957, On the generation of waves by turbulent wind, J. of Fluid Mech., Vol. 2, pp. 417-445.
- Plate, E.J., Chang, P.C., and Hidy, G.M., 1969, Experiments on the generation of small water waves by winds, J. of Fluid Mech., Vol. 35, pp. 625-656.
- Prych, E.A., 1970, Effects of density differences on lateral mixing in open channel flows, W.M. Keck Lab. of Hydraulics and Water Resources Calif. Inst. of Technology (Pasadena), Report No. KH-R-21, 225 pp.
- Roberts, O.F.T., 1923, Proc. Roy. (London), A 104, p. 640.

BIBLIOGRAPHY - Continued

- Sayre, W.W., 1968, Dispersion of mass in open channel flow, Ph.D. dissertation, Colorado State University, Fort Collins, Colorado.
- Sayre, W.W., and Chang, F.M., 1966, A laboratory investigation of open-channel dispersion process for dissolved, suspended and floating dispersants, U.S. Geol. Survey, Water Resources Div., Open File Report, Fort Collins, Colorado, 210 pp.
- Sayre, W.W., and Chang, F.M., 1968, A laboratory investigation of open-channel dispersion process for dissolved suspended and floating dispersant, U.S. Geol. Survey, Prof. Paper, 433-E, 71 pp.
- Smith, G.D., 1965, Numerical solution of partial differential equation, Oxford University Press, New York, 179 pp.
- Stokes, G.G., 1847, On the theory of oscillatory waves, Trans., Camb. Phil. Soc., Vol. 8, p. 441.
- Su, K.S., and Chang, P.C., 1971, Design of digital low pass and band pass filter for bio-medical data series, Presented at San Diego Bio-Medical Symposium, 1971.
- Taylor, G.I., 1922, Diffusion by continuous movements, Proc. London Math. Soc., A20, pp. 196-211.
- Taylor, G.I., 1953, Dispersion of soluble matter in solvent flowing slowly through a tube, Proc. Royal Soc. London, Vol. 219A, pp. 186-203.
- Taylor, G.I., 1954a, The dispersion of matter in turbulent flow through a pipe, Proc. Royal Soc. London, Vol. 223A, pp. 446-468.
- Taylor, G.I., 1954b, Conditions under which dispersion of a solute in a stream of solvent can be used to measure molecular diffusion, Proc. Royal Soc. London, Vol. 225A, pp. 473-477.
- Varga, R.S., 1962, Matrix iterative analysis, Englewood Cliffs, N.J., Prentice-Hall, 322 pp.
- Wu, J., 1969, An estimation of wind effects on dispersion in wide channels, Water Resources Research, Vol. 5, pp. 1097-1104.
- Yotsukura, N., and Fiering, M.B., 1964, Numerical solution to a dispersion equation, Proc. ASCE, Vol. 90, No. HY5, pp. 83-104.
- Yotsukura, N., and Fiering, M.B., 1966, Closure to Numerical solution to a dispersion equation, Proc. ASCE, Vol. 92, No. HY3, pp. 67-72.
- Yotsukura, N., Fischer, H.B., and Sayre, W.W., 1970, Measurement of mixing characteristics of the Missouri River between Sioux City, Iowa and Plattsmouth, Nebraska, U.S. Geol. Survey Water Supply Paper 1899-G.